UCLA
UCLA Electronic Theses and Dissertations

Title

Mapping Brain Development with Magnetic Resonance Imaging in Clinical and Genetic Neuropsychiatric Risk Syndromes

Permalink

https://escholarship.org/uc/item/5899j1b2

Author

Schleifer, Charles H

Publication Date

2024

Peer reviewed|Thesis/dissertation

eScholarship.org Powered by the California Digital Library
University of California

UNIVERSITY OF CALIFORNIA

Los Angeles

Mapping Brain Development with Magnetic Resonance Imaging in Clinical and Genetic Neuropsychiatric Risk Syndromes

A dissertation submitted in partial satisfaction of the requirements

for the degree Doctor of Philosophy in Neuroscience

by

Charles Hamlin Schleifer

2024

© Copyright by

Charles Hamlin Schleifer

2024

ABSTRACT OF THE DISSERTATION

Mapping Brain Development with Magnetic Resonance Imaging

in Clinical and Genetic Neuropsychiatric Risk Syndromes

by

Charles Hamlin Schleifer

Doctor of Philosophy in Neuroscience

University of California, Los Angeles, 2024

Professor Carrie E. Bearden, Chair

Neurodevelopmental syndromes such as schizophrenia and autism are driven by a confluence of genetic and environmental risk factors leading to differences in brain development. Rare copy number variants (CNVs) involving deletions or duplications of multiple genes can incur high risk for neuropsychiatric illness and represent a ‘genetic-first’ model for understanding important biological pathways contributing to risk. Investigation of brain phenotypes in populations with behaviorally defined risk factors for mental illness represents a complementary ‘top down’ approach for linking clinical symptoms to brain systems and underlying biology. In this dissertation, three separate studies apply magnetic resonance imaging (MRI) in cohorts with genetic and clinical risk factors to better understand the developmental differences in brain structure and function that contribute to neuropsychiatric risk. In the first study, we assessed longitudinal development of functional connectivity between the thalamus and cortex in individuals with 22q11.2 deletion syndrome (22qDel) who are at high risk for schizophrenia and autism compared to neurotypical controls. We found altered developmental trajectories in 22qDel, with

children displaying a pattern of thalamocortical hyperconnectivity in somatomotor regions and hypoconnectivity in frontoparietal regions, which had been previously observed in studies of schizophrenia, clinical high risk (CHR) for psychosis, and a cross-sectional analysis of 22qDel. In the second study, we investigated gene dosage effects on maturation of subcortical brain volumes across 22qDel, neurotypical controls, and carriers of 22q11.2 duplications (22qDup) who are at high risk for autism but not schizophrenia. We found gene dosage effects on multiple subcortical structures and a wide range of developmental alterations across the two CNV groups, illuminating the role of the 22q11.2 locus in subcortical development. In the final study we compared resting-state functional MRI case-control phenotypes in 22qDel versus CHR for psychosis to better understand similarities between these two high-risk populations. We found broadly dissimilar effects on long-range connectivity, local connectivity, and brain signal variability in these two cohorts, and related 22qDel case-control differences to multiple established brain maps, most notably positron emission tomography maps of hemodynamics and metabolism from neurotypical adults. These three studies provide important new insights into brain development and neuropsychiatric risk.

The dissertation of Charles Hamlin Schleifer is approved.

Loes Marlein Olde Loohuis

Carlos Portera-Cailliau

Lucina Q. Uddin

Carrie E. Bearden, Committee Chair

University of California, Los Angeles

2024

DEDICATION

There are many individuals who I would like to earnestly thank for their support:

the mentors who have guided and motivated me before and during my graduate education,

the colleagues and friends who I have worked alongside and learned from,

the mentees who I have been fortunate enough to work with and who have taught me so much,

the many research participants and their families who made this work possible,

and lastly, my family and friends who have supported and encouraged me throughout my life.

TABLE OF CONTENTS

ACKNOWLEDGEMENTS

Chapter one is a version of: Schleifer, C., O'Hora, K., Jalbrzikowski, M., Bondy, E., Kushan-Wells, L., Lin, A., Uddin, L., Bearden, C. (2023). Longitudinal development of thalamocortical functional connectivity in 22q11.2 deletion syndrome. Biological Psychiatry: CNNI, S2451-9022(23)00239-2. https://doi.org/10.1016/j.bpsc.2023.09.001

Chapter two is a version of: Schleifer, C., O'Hora, K., Fung, H., Xu, J., Robinson, T., Wu, A., Kushan-Wells, L., Lin, A., Ching, C., Bearden, C. (2024). Effects of Gene Dosage and Development on Subcortical Nuclei Volumes in Individuals with 22q11.2 Copy Number Variations. Neuropsychopharmacology. https://doi.org/10.1038/s41386-024-01832-3

Chapter three is a version of: Schleifer, C., Chang, S., Amir, C., O'Hora, K. Fung, H. Kang, JW., Kushan-Wells, L., Daly, E., Di Fabio, F., Frascarelli, M. Gudbrandsen, M., Kates, W., Murphy, D., Addington, J., Anticevic, A., Cadenhead, K., Cannon, T., Cornblatt, B., Keshavan, M., Mathalon, D., Perkins, D., Stone, W., Tsuang, M., Walker, E., Woods, S., Uddin, L., Kumar, K., Hoftman, G., Bearden, C. (2024). Unique functional neuroimaging signatures of genetic versus clinical high risk for psychosis. (https://doi.org/10.1101/2024.04.03.587988, pre-print under review)

Funding for this work was provided to Charles H. Schleifer by the National Institute of Mental Health grant F31MH133326, the UCLA Neurobehavioral Genetics Training Program T32NS048004, and the UCLA Medical Scientist Training Program T32GM008042.

Thank you to the many mentors, peers, friends, family, and research participants who made this work possible. Specific contributions of each co-author are noted in the acknowledgements sections at the end of each chapter.

VITA / BIOGRAPHICAL SKETCH

Education

David Geffen School of Medicine at UCLA, MD, 2018-2026 (in progress)

Yale University, B.S., Psychology, 2012-2016

Research/Employment

Graduate Student Researcher, Semel Institute, UCLA, 2020-2024

Research Assistant, Department of Psychiatry, Yale School of Medicine, 2014-2018

Research Assistant (part time), Department of Neuroscience, McLean Hospital, 2013-2016

First-author Publications

Schleifer, C., Chang, S., Amir, C., O'Hora, K. Fung, H. Kang, JW., Kushan-Wells, L., Daly, E., Di Fabio, F., Frascarelli, M. Gudbrandsen, M., Kates, W., Murphy, D., Addington, J., Anticevic, A., Cadenhead, K., Cannon, T., Cornblatt, B., Keshavan, M., Mathalon, D., Perkins, D., Stone, W., Tsuang, M., Walker, E., Woods, S., Uddin, L., Kumar, K., Hoftman, G., Bearden, C. (2024). Unique functional neuroimaging signatures of genetic versus clinical high risk for psychosis. (https://doi.org/10.1101/2024.04.03.587988, pre-print under review)

Schleifer, C., O'Hora, K., Fung, H., et al. (2024). Effects of Gene Dosage and Development on Subcortical Nuclei Volumes in Individuals with 22q11.2 Copy Number Variations. Neuropsychopharmacology

Schleifer, C. (2024). Brainwide Risk Scores: an example of psychiatric risk prediction from resting-state functional magnetic resonance imaging. Biological Psychiatry

Schleifer, C., O'Hora, K., Jalbrzikowski, M., et al. (2023). Longitudinal development of thalamocortical functional connectivity in 22q11.2 deletion syndrome. Biological Psychiatry: CNNI

Schleifer, C., Lin, A., Kushan, et al. (2019). Dissociable Disruptions in Thalamic and Hippocampal Resting-State Functional Connectivity in Youth with 22q11.2 Deletions. Journal of Neuroscience

INTRODUCTION

BACKGROUND

Neurodevelopmental syndromes such as schizophrenia and autism are driven by a confluence of genetic and environmental risk factors (1,2). These conditions are highly heritable (3), and the landscape of genetic risk includes hundreds of common variants of individually small effects (4), as well as several rare copy number variants (CNVs) in which deletions or duplications of multiple genes incur high risk for neuropsychiatric disorders (5). Risk for neuropsychiatric syndromes can also be assessed based on clinical symptoms. Individuals with sub-threshold psychosis symptoms are deemed at Clinical High Risk (CHR) for developing a psychosis spectrum disorder, and these adolescents and young adults have been shown to convert to a threshold diagnosis at a rate of 20-30% in the 2-3 years following ascertainment (6,7). There is a need for improved early diagnosis and treatment for these at-risk individuals, which informs the need for research refining brain biomarkers and modeling pathophysiological mechanisms of clinical and genetic risk factors for psychosis and other neurodevelopmental disorders. Investigating both genetic and clinical high-risk groups provides complementary frameworks for understanding the biology underlying neuropsychiatric disorders, in which rare genetic syndromes provide a genetics-first ‘bottom up’ approach to linking genes to brain phenotypes, and clinically ascertained groups provide a ‘top down’ approach for connecting clinical symptoms to brain systems.

22q11.2 Deletion Syndrome (22qDel), also known as DiGeorge or Velocardiofacial syndrome (OMIM #188400, #192430), is a genetic condition caused by a recurrent CNV in which a short segment of one copy of chromosome 22 is lost. This segment contains ~2.6 Mb of DNA spanning ~46 protein-coding genes (8) which are hemizygously deleted in ~1 in every 4,000 people. 22qDel is one of the strongest genetic risk factors for schizophrenia, with 10-25 times the base rate of psychotic disorders observed in the general population (9–12). The neuropsychiatric phenotype in 22qDel also includes increased rates of autism, intellectual disability, Attention

Deficit Hyperactivity Disorder (ADHD), and mood and anxiety disorders (12). The reciprocal duplication of this same genetic locus leads to 22q11.2 Duplication Syndrome (22qDup) (OMIM #608363). Individuals with 22qDup experience elevated rates of neurodevelopmental disorders, including intellectual disability and autism, compared to the general population; however, the duplication generally has a milder impact on neurodevelopment compared to 22qDel (13,14). In contrast to 22qDel, 22qDup is *less* common in individuals with schizophrenia compared to the general population, highlighting the importance of these genes for psychosis risk (15–17). The genes within the human 22q11.2 locus are highly conserved, allowing for animal models that can generate specific neurobiological hypotheses relevant to human conditions such as schizophrenia and autism (18). Study of individuals with 22q11.2 CNVs thus provides a powerful framework for linking specific genetic disruptions to brain circuits and systems in the context of developmental neuropsychiatric conditions.

Abnormal structural and functional connections in neural circuits are hypothesized to underlie many of the symptoms of severe neuropsychiatric disorders such as schizophrenia (19–22). Information processing in the brain arises from activity in populations of neurons with complex local and long-range anatomical connectivity. This gives rise to functional brain networks, which can be observed as intrinsic patterns of functional connectivity measured as correlations in activity across brain regions (23,24). Resting-state functional Magnetic Resonance Imaging (rs-fMRI), measuring the Blood Oxygen Level-Dependent (BOLD) signal as a proxy for neuronal activity, is a useful tool for evaluating functional connectivity at the scale of these networks. Structural MRI (sMRI) measurements of regional morphology can also inform our understanding of systems-level brain alterations across patient groups. Human neuroimaging in populations with specific genetic conditions like 22qDel and 22qDup is particularly valuable because it provides a genetics-first approach for characterizing neuropsychiatric risk biology.

A growing body of literature suggests that functional network-level disruptions play an important role in 22qDel. Independent Components Analysis (ICA) approaches have supported

large-scale network dysconnectivity in 22qDel (25,26), as has an atlas-based study of cortical connectivity (27). Subcortical brain structures are also of particular interest as they play important roles in cognitive and sensory processes and have been found to exhibit wide ranging alterations in conditions such as autism and schizophrenia (28–30). In a cross-sectional case-control analysis of thalamic and hippocampal functional connectivity in 22qDel, we found a pattern of dysconnectivity that maps onto large-scale sensory and executive networks (31). Relative to typically developing controls, 22qDel carriers exhibit thalamic hyper-connectivity and hippocampal hypo-connectivity to a set of somatomotor regions, and a reciprocal pattern of dysconnectivity to a network of frontal and parietal regions. This novel finding in 22qDel patients extended the relevance of a thalamocortical functional connectivity biomarker previously observed in both patients with schizophrenia (32–34) and CHR individuals who subsequently convert to overt psychosis (35).

There are several key knowledge gaps related to 22q11.2 CNVs and CHR that will be addressed in this dissertation. In terms of thalamocortical functional connectivity, we have previously found alterations in 22qDel that resemble findings in schizophrenia and CHR; however, these analyses were cross-sectional and controlled for age without directly investigating maturational trajectories (31). Longitudinal development of thalamocortical functional connectivity has not been previously studied in 22qDel compared to typically developing (TD) controls. Characterizing development of thalamocortical systems in 22qDel from childhood to early adulthood is particularly important because psychosis symptoms generally first emerge during this key developmental window.

Additionally, to better understand the effects of gene dosage at the 22q11.2 locus on the development of subcortical nuclei including the thalamus, we use structural MRI to map for the first time cross-sectional and longitudinal effects on thalamus, hippocampus, and amygdala subregional volumes across 22qDel, TD, and 22qDup cohorts. A study from another group has found bi-directional effects on thalamic subregional volumes in 22qDel, with larger and smaller

volumes relative to controls in nuclei associated with sensory and cognitive functions, respectively (36), and prior cross-sectional work from our group in reciprocal 22q11.2 CNV carriers has shown local alterations to subcortical structure shape that suggest some subregional specificity of effects (37). The inclusion of a longitudinal 22qDup sample in our analysis is particularly novel and provides a framework for investigating the effects of gene dosage (i.e., variation in copy number) and maturation beyond simple case-control analyses. Only in recent years have neuroimaging samples of 22qDup carriers been collected that allow for evaluation of 22q11.2 gene dosage effects on developmental brain phenotypes. A recent study by our group of longitudinal development of cortical phenotypes across 22qDel and 22qDup showed a broad cortical pattern of flattened development across both CNV groups relative to typically developing controls (38).

Finally, while we have previously observed similar thalamocortical functional connectivity phenotypes in separate studies of 22qDel and CHR, no study has investigated cortical rs-fMRI phenotypes using directly comparable methods in these two groups which are both associated with high psychosis risk. To address this, we compile an unprecedented multi-site sample of rs-fMRI from 22qDel, CHR, and demographically matched TD controls, all processed using the same analytic pipelines. In this dataset we measure case-control differences in global functional connectivity, local functional connectivity, and the temporal variability of brain signals. Using spatial permutation approaches (39), we compare the patterns of these case-control effects between 22qDel and CHR to illuminate convergence and divergence in rs-fMRI phenotypes. We also use these same spatial permutation approaches to compare cortical maps of 22qDel and CHR rs-fMRI effects to previously established brain maps from multiple sources including positron emission tomography (PET) studies of brain metabolism, multi-modal MRI, magnetoencephalography (MEG), and spatial patterns of gene expression across the cortex from the Allen Human Brain Atlas (40,41). This exploratory analysis will facilitate generation of hypotheses regarding the biological underpinnings of observed rs-fMRI alterations in 22qDel and CHR.

This dissertation is structured as three chapters, each corresponding to a separate manuscript, followed by an overall conclusion. The aims of these three manuscripts, and initial hypotheses are outlined below.

AIMS

Aim 1: Characterize differential age-related changes in network-level functional connectivity between the thalamus and cortex in 22qDel carriers and TD controls from childhood to early adulthood using resting-state fMRI.

Hypothesis: We predict that 22qDel carriers will exhibit age-related disruptions in thalamocortical functional connectivity, primarily in frontoparietal and sensorimotor networks. Specifically, we expect that the transition from childhood to adolescence will be associated with the emergence of a psychosis-like phenotype (31,35,42) of frontoparietal hyperconnectivity and somatomotor hypoconnectivity in 22qDel but not TD controls.

Aim 2: Investigate the effects of genomic copy number variation at the 22q11.2 locus and age-related changes in subcortical subregional volumes using structural MRI in individuals with 22q11.2 deletions, duplications, and TD controls.

Hypothesis: We predict that gene dosage (i.e., 22q11.2 locus copy number) will show linear relationships to subcortical volumes in a bi-directional fashion, with positive relationships for nuclei involved primarily in executive function and negative relationships for sensory nuclei. Additionally, we expect to find flattened patterns of maturation in both 22qDel and 22qDup relative to TD controls, similar to patterns observed for cortical development (38).

Aim 3: Compare cortical rs-fMRI phenotypes in 22qDel and CHR and map these phenotypes to underlying biology via comparisons to established brain maps from sources including PET, multi-modal MRI, MEG, and spatial patterns of gene expression.

Hypothesis: We predict that, relative to demographically matched TD controls, 22qDel and CHR individuals will show both convergent and divergent alterations in global functional connectivity, local functional connectivity, and temporal variability of brain signals. Additionally, we expect that spatial patterns of case-control differences will map onto multiple biologically relevant signals. Given animal model findings of disrupted parvalbumin expressing interneurons in 22qDel (43–45), and spatial transcriptomic findings of brain signal variability associations with a cortical gradient of parvalbumin versus somatostatin expressing interneurons in neurotypical adults (46), we hypothesize that this parvalbumin-somatostatin gradient may predict regions of disrupted brain signal variability in 22qDel and potentially CHR as well. We also expect these exploratory multi-modal brain map comparisons to provide additional insight into diverse biological systems such as brain metabolism or sensory/executive hierarchies that may be altered in these clinical groups.

INTRODUCTION REFERENCES

1. Seidman LJ, Mirsky AF (2017): Evolving Notions of Schizophrenia as a Developmental Neurocognitive Disorder. *J Int Neuropsychol Soc JINS* 23: 881–892.

2. Insel TR (2010): Rethinking schizophrenia [no. 7321]. *Nature* 468: 187–193.

3. Hilker R, Helenius D, Fagerlund B, Skytthe A, Christensen K, Werge TM, *et al.* (2018): Heritability of Schizophrenia and Schizophrenia Spectrum Based on the Nationwide Danish Twin Register. *Biol Psychiatry* 83: 492–498.

4. Pardiñas AF, Holmans P, Pocklington AJ, Escott-Price V, Ripke S, Carrera N, *et al.* (2018): Common schizophrenia alleles are enriched in mutation-intolerant genes and in regions under strong background selection [no. 3]. *Nat Genet* 50: 381–389.

5. Marshall CR, Howrigan DP, Merico D, Thiruvahindrapuram B, Wu W, Greer DS, *et al.* (2017): Contribution of copy number variants to schizophrenia from a genome-wide study of 41,321 subjects. *Nat Genet* 49: 27–35.

6. Fusar-Poli P, Borgwardt S, Bechdolf A, Addington J, Riecher-Rössler A, Schultze-Lutter F, *et al.* (2013): The psychosis high-risk state: a comprehensive state-of-the-art review. *JAMA Psychiatry* 70: 107–120.

7. Fusar-Poli P, Salazar de Pablo G, Correll CU, Meyer-Lindenberg A, Millan MJ, Borgwardt S, *et al.* (2020): Prevention of Psychosis: Advances in Detection, Prognosis, and Intervention. *JAMA Psychiatry* 77: 755–765.

8. Jonas RK, Montojo CA, Bearden CE (2014): The 22q11.2 deletion syndrome as a window into complex neuropsychiatric disorders over the lifespan. *Biol Psychiatry* 75: 351–360.

9. Green T, Gothelf D, Glaser B, Debbane M, Frisch A, Kotler M, *et al.* (2009): Psychiatric disorders and intellectual functioning throughout development in velocardiofacial (22q11.2 deletion) syndrome. *J Am Acad Child Adolesc Psychiatry* 48: 1060–1068.

10. Bassett AS, Chow EWC (2008): Schizophrenia and 22q11.2 deletion syndrome. *Curr Psychiatry Rep* 10: 148–157.

11. Provenzani U, Damiani S, Bersano I, Singh S, Moschillo A, Accinni T, *et al.* (2022): Prevalence and incidence of psychotic disorders in 22q11.2 deletion syndrome: a meta-analysis. *Int Rev Psychiatry Abingdon Engl* 34: 676–688.

12. Schneider M, Debbané M, Bassett AS, Chow EWC, Fung WLA, van den Bree M, *et al.* (2014): Psychiatric disorders from childhood to adulthood in 22q11.2 deletion syndrome: results from the International Consortium on Brain and Behavior in 22q11.2 Deletion Syndrome. *Am J Psychiatry* 171: 627–639.

13. Hoeffding LK, Trabjerg BB, Olsen L, Mazin W, Sparsø T, Vangkilde A, *et al.* (2017): Risk of Psychiatric Disorders Among Individuals With the 22q11.2 Deletion or Duplication: A Danish Nationwide, Register-Based Study. *JAMA Psychiatry* 74: 282–290.

14. Lin A, Vajdi A, Kushan-Wells L, Helleman G, Hansen LP, Jonas RK, *et al.* (2020): Reciprocal Copy Number Variations at 22q11.2 Produce Distinct and Convergent Neurobehavioral Impairments Relevant for Schizophrenia and Autism Spectrum Disorder. *Biol Psychiatry* 88: 260–272.

15. Marshall CR, Howrigan DP, Merico D, Thiruvahindrapuram B, Wu W, Greer DS, *et al.* (2017): Contribution of copy number variants to schizophrenia from a genome-wide study of 41,321 subjects. *Nat Genet* 49: 27–35.

16. Rees E, Kirov G, Sanders A, Walters JTR, Chambert KD, Shi J, *et al.* (2014): Evidence that duplications of 22q11.2 protect against schizophrenia. *Mol Psychiatry* 19: 37–40.

17. Rees E, Walters JTR, Georgieva L, Isles AR, Chambert KD, Richards AL, *et al.* (2014): Analysis of copy number variations at 15 schizophrenia-associated loci. *Br J Psychiatry J Ment Sci* 204: 108–114.

18. Ellegood J, Markx S, Lerch JP, Steadman PE, Genç C, Provenzano F, *et al.* (2014): Neuroanatomical Phenotypes in a Mouse Model of the 22q11.2 Microdeletion. *Mol Psychiatry* 19: 99–107.

19. Uddin LQ, Dajani DR, Voorhies W, Bednarz H, Kana RK (2017): Progress and roadblocks in the search for brain-based biomarkers of autism and attention-deficit/hyperactivity disorder. *Transl Psychiatry* 7: e1218.

20. Satterthwaite TD, Baker JT (2015): How Can Studies of Resting-state Functional Connectivity Help Us Understand Psychosis as a Disorder of Brain Development? *Curr Opin Neurobiol* 0: 85–91.

21. van den Heuvel MP, Fornito A (2014): Brain networks in schizophrenia. *Neuropsychol Rev* 24: 32–48.

22. Park S, Haak KV, Cho HB, Valk SL, Bethlehem RAI, Milham MP, *et al.* (2021): Atypical Integration of Sensory-to-Transmodal Functional Systems Mediates Symptom Severity in Autism. *Front Psychiatry* 12: 699813.

23. Choi EY, Yeo BTT, Buckner RL (2012): The organization of the human striatum estimated by intrinsic functional connectivity. *J Neurophysiol* 108: 2242–2263.

24. Fox MD, Snyder AZ, Vincent JL, Corbetta M, Van Essen DC, Raichle ME (2005): The human brain is intrinsically organized into dynamic, anticorrelated functional networks. *Proc Natl Acad Sci* 102: 9673–9678.

25. Debbané M, Lazouret M, Lagioia A, Schneider M, Van De Ville D, Eliez S (2012): Resting-state networks in adolescents with 22q11.2 deletion syndrome: associations with prodromal symptoms and executive functions. *Schizophr Res* 139: 33–39.

26. Mattiaccio LM, Coman IL, Schreiner MJ, Antshel KM, Fremont WP, Bearden CE, Kates WR (2016): Atypical functional connectivity in resting-state networks of individuals with 22q11.2 deletion syndrome: associations with neurocognitive and psychiatric functioning. *J Neurodev Disord* 8: 2.

27. Mattiaccio LM, Coman IL, Thompson CA, Fremont WP, Antshel KM, Kates WR (2018): Frontal dysconnectivity in 22q11.2 deletion syndrome: an atlas-based functional connectivity analysis. *Behav Brain Funct* 14: 2.

28. Kumar K, Modenato C, Moreau C, Ching CRK, Harvey A, Martin-Brevet S, *et al.* (2023): Subcortical Brain Alterations in Carriers of Genomic Copy Number Variants. *Am J Psychiatry* appi.ajp.20220304.

29. Woodward ND, Giraldo-Chica M, Rogers B, Cascio CJ (2017): Thalamocortical Dysconnectivity in Autism Spectrum Disorder: An Analysis of the Autism Brain Imaging Data Exchange. *Biol Psychiatry Cogn Neurosci Neuroimaging* 2: 76–84.

30. Giraldo-Chica M, Woodward ND (2017): Review of thalamocortical resting-state fMRI studies in schizophrenia. *Schizophr Res* 180: 58–63.

31. Schleifer C, Lin A, Kushan L, Ji JL, Yang G, Bearden CE, Anticevic A (2019): Dissociable Disruptions in Thalamic and Hippocampal Resting-State Functional Connectivity in Youth with 22q11.2 Deletions. *J Neurosci* 39: 1301–1319.

32. Welsh RC, Chen AC, Taylor SF (2010): Low-frequency BOLD fluctuations demonstrate altered thalamocortical connectivity in schizophrenia. *Schizophr Bull* 36: 713–722.

33. Anticevic A, Cole MW, Repovs G, Murray JD, Brumbaugh MS, Winkler AM, *et al.* (2014): Characterizing thalamo-cortical disturbances in schizophrenia and bipolar illness. *Cereb Cortex N Y N 1991* 24: 3116–3130.

34. Woodward ND, Karbasforoushan H, Heckers S (2012): Thalamocortical dysconnectivity in schizophrenia. *Am J Psychiatry* 169: 1092–1099.

35. Anticevic A, Haut K, Murray JD, Repovs G, Yang GJ, Diehl C, *et al.* (2015): Association of Thalamic Dysconnectivity and Conversion to Psychosis in Youth and Young Adults at Elevated Clinical Risk. *JAMA Psychiatry* 72: 882–891.

36. Mancini V, Zöller D, Schneider M, Schaer M, Eliez S (2020): Abnormal Development and Dysconnectivity of Distinct Thalamic Nuclei in Patients With 22q11.2 Deletion Syndrome Experiencing Auditory Hallucinations. *Biol Psychiatry Cogn Neurosci Neuroimaging* 5: 875–890.

37. Lin A, Ching CRK, Vajdi A, Sun D, Jonas RK, Jalbrzikowski M, *et al.* (2017): Mapping 22q11.2 Gene Dosage Effects on Brain Morphometry. *J Neurosci* 37: 6183–6199.

38. Jalbrzikowski M (n.d.): Longitudinal trajectories of cortical development in 22q11.2 copy number variants and typically developing controls. *Mol Psychiatry* 10.

39. Burt JB, Helmer M, Shinn M, Anticevic A, Murray JD (2020): Generative modeling of brain maps with spatial autocorrelation. *NeuroImage* 220: 117038.

40. Markello RD, Hansen JY, Liu Z-Q, Bazinet V, Shafiei G, Suárez LE, *et al.* (2022): neuromaps: structural and functional interpretation of brain maps [no. 11]. *Nat Methods* 19: 1472–1479.

41. Hawrylycz MJ, Lein ES, Guillozet-Bongaarts AL, Shen EH, Ng L, Miller JA, *et al.* (2012): An anatomically comprehensive atlas of the adult human brain transcriptome [no. 7416]. *Nature* 489: 391–399.

42. Anticevic A, Cole MW, Repovs G, Murray JD, Brumbaugh MS, Winkler AM, *et al.* (2014): Characterizing Thalamo-Cortical Disturbances in Schizophrenia and Bipolar Illness. *Cereb Cortex N Y NY* 24: 3116–3130.

43. Piskorowski RA, Nasrallah K, Diamantopoulou A, Mukai J, Hassan SI, Siegelbaum SA, *et al.* (2016): Age-Dependent Specific Changes in Area CA2 of the Hippocampus and Social Memory Deficit in a Mouse Model of the 22q11.2 Deletion Syndrome. *Neuron* 89: 163–176.

44. Choi SJ, Mukai J, Kvajo M, Xu B, Diamantopoulou A, Pitychoutis PM, *et al.* (2018): A Schizophrenia-Related Deletion Leads to KCNQ2-Dependent Abnormal Dopaminergic Modulation of Prefrontal Cortical Interneuron Activity. *Cereb Cortex N Y N 1991* 28: 2175–2191.

45. Al-Absi A-R, Qvist P, Okujeni S, Khan AR, Glerup S, Sanchez C, Nyengaard JR (2020): Layers II/III of Prefrontal Cortex in Df(h22q11)/+ Mouse Model of the 22q11.2 Deletion Display

Loss of Parvalbumin Interneurons and Modulation of Neuronal Morphology and Excitability. *Mol Neurobiol* 57: 4978–4988.

46. Anderson KM, Collins MA, Chin R, Ge T, Rosenberg MD, Holmes AJ (2020): Transcriptional and imaging-genetic association of cortical interneurons, brain function, and schizophrenia risk. *Nat Commun* 11: 2889.

CHAPTER ONE

Longitudinal development of thalamocortical functional connectivity in 22q11.2 deletion syndrome

Charles H. Schleifer[1,2], Kathleen P. O'Hora[1], Maria Jalbrzikowski[3,4], Elizabeth Bondy[1], Leila Kushan-Wells[1], Amy Lin[1], Lucina Q. Uddin[1,5], Carrie E. Bearden[1,5]

1. Department of Psychiatry and Biobehavioral Sciences, Semel Institute for Neuroscience and Human Behavior, University of California, Los Angeles, CA, USA.
2. David Geffen School of Medicine, University of California, Los Angeles, CA, USA.
3. Department of Psychiatry and Behavioral Sciences, Boston Children's Hospital, Boston, MA, USA.
4. Department of Psychiatry, Harvard Medical School, Boston, MA, USA.
5. Department of Psychology, University of California, Los Angeles, CA, USA.

ABSTRACT

Background: 22q11.2 Deletion Syndrome (22qDel) is a genetic Copy Number Variant (CNV) that strongly increases risk for schizophrenia and other neurodevelopmental disorders. Disrupted functional connectivity between the thalamus and somatomotor/frontoparietal cortex has been implicated in cross-sectional studies of 22qDel, idiopathic schizophrenia, and youth at clinical high risk (CHR) for psychosis. Here, we use a novel functional atlas approach to investigate longitudinal age-related changes in network-specific thalamocortical functional connectivity (TCC) in 22qDel and typically developing (TD) controls.

Methods: TCC was calculated for nine functional networks derived from resting-state functional magnetic resonance imaging (rs-fMRI) scans collected from n=65 22qDel participants (63.1% female) and n=69 demographically matched TD controls (49.3% female), ages 6 to 23 years. Analyses included 86 longitudinal follow-up scans. Non-linear age trajectories were characterized with generalized additive mixed models (GAMMs).

Results: In 22qDel, TCC in the frontoparietal network increases until approximately age 13, while somatomotor and cingulo-opercular TCC decrease from age 6 to 23. In contrast, no significant relationships between TCC and age were found in TD controls. Somatomotor connectivity in 22qDel is significantly higher than TD in childhood, but lower in late adolescence. Frontoparietal TCC shows the opposite pattern.

Conclusions: 22qDel is associated with aberrant development of functional network connectivity between the thalamus and cortex. Younger individuals with 22qDel have lower frontoparietal connectivity and higher somatomotor connectivity than controls, but this phenotype may normalize or partially reverse by early adulthood. Altered maturation of this circuitry may underlie elevated neuropsychiatric disease risk in this syndrome.

INTRODUCTION

22q11.2 Deletion Syndrome (22qDel), also known as DiGeorge or Velocardiofacial syndrome (OMIM #188400, #192430), is a genetic disorder that occurs in approximately 1 in 4000 live births (1). This syndrome is one of the greatest genetic risk factors for schizophrenia, with at least 1 in 10 individuals with 22qDel having a comorbid psychotic disorder, and even higher rates after adolescence (2,3). Individuals with 22qDel also have high rates of autism and an increased incidence of intellectual disability (ID), attentional deficits, and anxiety disorders (4–6). 22qDel is caused by a copy number variant (CNV) consisting of a hemizygous deletion of 1.5-2.6 Mb of genetic material (~46 protein-coding genes) from chromosome 22q (7). This provides a genetics-first framework for studying the biology underlying neurodevelopmental psychiatric disorders like schizophrenia (8,9).

Functional neuroimaging studies of psychosis spectrum disorders have consistently identified alterations in the functional connectivity (FC) of the thalamus, specifically, increased connectivity to somatomotor brain regions and decreased connectivity to frontoparietal associative regions compared to healthy controls (10–13). This marker is associated with conversion to psychosis in youth at clinical high risk (CHR) for the illness (14). In a cross-sectional study comparing individuals (ages 7-26) with 22qDel to typically developing (TD) controls, we observed a similar pattern of thalamic hyper-connectivity to the somatomotor network and hypo-connectivity to frontoparietal regions (15). This convergence of findings in idiopathic schizophrenia, CHR, and 22qDel may represent a shared phenotype relevant to psychosis risk. Interestingly, animal models of 22qDel implicate haploinsufficiency of the Dgcr8 gene (deleted in 22qDel) in elevation of thalamic dopamine D2 receptors and age-related disruptions in thalamocortical synchrony (16,17) and may indicate an underlying neurobiological mechanism driving this dysfunction in 22qDel.

Thalamic dysconnectivity has additional cross-diagnostic relevance. Functional neuroimaging studies in autistic individuals have consistently observed altered thalamocortical

FC (18–21). Many of these findings converge on increased connectivity within sensory networks. Furthermore, a broad convergence on disrupted thalamic connectivity has been identified in the functional connectomes from multiple idiopathic psychiatric conditions and neurodevelopmental CNVs (22,23).

The thalamus is a heterogeneous structure with dense reciprocal connections across the cortex (24). Structural and functional connectivity with the cortex across sensory and associative networks is thus a core organizational feature of the thalamus (25,26). Thalamocortical FC patterns specific to sensory and associative networks emerge early in development and have been identified in infancy (27). Recent studies of the relationship between age and thalamic FC have observed subtle developmental changes in sensory and associative network connectivity (28,29). Adolescence represents an important developmental window during which interactions between the thalamus and cortex have been hypothesized to shape prefrontal development, which may be disrupted in disorders like schizophrenia (30). One prior study of 22qDel has shown altered development of thalamic nuclei volumes, along with cross-sectional disruptions in FC (31).

In this longitudinal resting-state functional magnetic resonance imaging (rs-fMRI) study, we map age-related changes in thalamocortical FC in 22qDel and demographically matched TD control subjects, from childhood to early adulthood. To our knowledge, this is the first analysis of age-related changes in thalamic FC in 22qDel, and one of the first longitudinal analyses of thalamocortical FC in any population. Here, we use a novel functional atlas approach to compute network-specific thalamocortical functional connectivity (TCC) and generate non-linear mixed models of the relationship between age and TCC to test the prediction that development of frontoparietal and somatomotor TCC is altered in 22qDel. By examining the developmental trajectory of TCC in 22qDel, this study aims to shed light on the neurobiological mechanisms underlying the increased risk of psychosis and other neurodevelopmental disorders in this population.

METHODS

Participants

The total longitudinal sample consisted of 220 scans from 135 participants (6–23 years of age; 65 22qDel baseline; 69 TD controls baseline; see Figure 1), recruited from an ongoing longitudinal study at the University of California, Los Angeles (UCLA). 22qDel and TD participants were statistically matched based on baseline age, sex, dominant hand, fMRI movement (percent frames flagged based on displacement/intensity thresholds recommended by Power et al. 2012 (32)), as well as mean number of longitudinal visits and interval between visits, using appropriate tests (ANOVA or chi-squared; see Table 1). See Supplemental Methods for details on inclusion/exclusion criteria and clinical assessment procedures. After study procedures were fully explained, adult participants provided written consent, while participants under the age of 18 years provided written assent with the written consent of their parent or guardian. The UCLA Institutional Review Board approved all study procedures and informed consent documents.

	Control	22qDel	*p*-value
n	69	65	
Age, mean (SD)	13.44 (4.76)	14.39 (4.56)	0.242
Sex, n (%) Female	34 (49.3)	41 (63.1)	0.151
Handedness, n (%) Right	31 (44.9)	34 (52.3)	0.561
fMRI % movement, mean (SD)	6.86 (9.93)	9.84 (13.12)	0.139
Siemens Trio Scanner, n (%)	50 (73)	48 (74)	0.857
WASI Full Scale IQ, mean (SD)	112.15 (20.53)	79.00 (12.70)	<0.001
SIPS Positive total, mean (SD)	1.18 (2.16)	5.44 (5.61)	<0.001
Psychosis Risk Symptoms, n (%)	4 (5.8)	20 (30.8)	0.001
Psychotic Disorder, n (%)	0 (0.0)	5 (7.7)	0.058
ADHD, n (%)	5 (7.2)	30 (46.2)	<0.001
Autism, n (%)	0 (0.0)	36 (55.4)	<0.001
Antipsychotic med, n (%)	0 (0.0)	5 (7.7)	0.004
Visit count, mean (SD)	1.57 (0.85)	1.72 (0.96)	0.314
Days between visits, mean (SD)	653.21 (425.56)	787.04 (549.92)	0.296

Table 1-1. Baseline demographics. 22qDel and TD controls with p-values for between group comparisons (based on ANOVA for continuous variables and chi-squared tests for categorical variables). Baseline cohorts are statistically matched based on age, sex, dominant hand, and fMRI % movement (percentage of frames removed per subject for exceeding displacement and/or signal change thresholds), as well as mean number of longitudinal visits and interval between visits, and proportion of the cohort acquired on each of two scanner types (Siemens Trio or Siemens Prisma). Cognition was measured with the Wechsler Abbreviated Scale of Intelligence-2 (WASI-2). Prodromal (psychosis-risk) symptoms were assessed with the Structured Interview for Psychosis-Risk Syndromes (SIPS). Psychosis Risk Symptoms are operationalized here as having any score of 3 or greater (i.e., prodromal range) on any SIPS positive symptom item. Psychotic disorder diagnosis is based on structured clinical interview (SCID) for DSM-IV/V and includes schizophrenia, schizoaffective disorder, brief psychotic disorder, and psychotic disorder not otherwise specified.

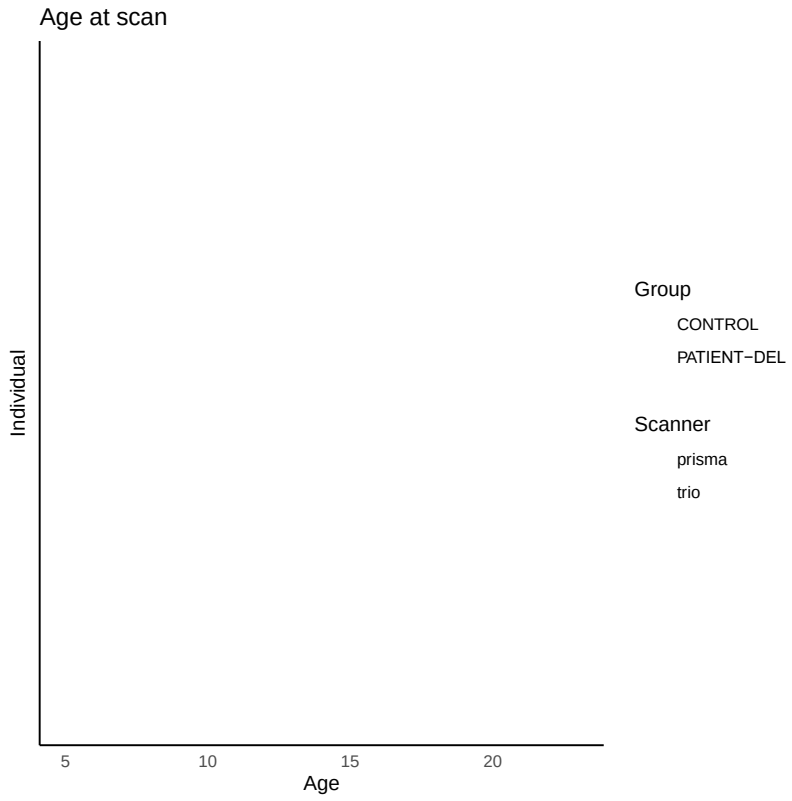

Figure 1-1. Participant age distribution. Typically developing controls in blue, 22qDel in red, with lines connecting follow-up visits from the same individual. Scanner type (Siemens Trio or Prisma) indicated by circle or triangle, respectively.

Neuroimaging acquisition and processing

Rs-fMRI and high-resolution structural images were collected on two scanners (Siemens Trio and Siemens Prisma) at the UCLA Center for Cognitive Neuroscience, and processed with the Quantitative Neuroimaging Environment & Toolbox (QuNex) (33), which adapts the Human Connectome Project (HCP) preprocessing pipelines (34) for broader use. Additional processing of the fMRI time series included bandpass filtering, motion scrubbing for frames exceeding either a framewise displacement or signal change threshold (32), spatial smoothing, and regression of mean signal from ventricles, deep white matter, and mean gray matter (35). Scans with >50% frames flagged for motion were excluded. For a detailed description of preprocessing methods, see Supplemental Methods and previous work in a subset of these data (15).

For each scan, TCC was computed based on the correlation in fMRI signal between the thalamic and cortical components of nine networks (frontoparietal, somatomotor, cingulo-opercular, default mode, dorsal attention, auditory, posterior multimodal, primary visual, and secondary visual) defined by the Cole-Anticevic Brain-wide Network Partition, a recently developed whole-brain functional atlas (36) (see Figure 2). Data from the two scanners were harmonized using the longitudinal ComBat (longComBat) package in R (37), a linear mixed effects adaptation of the ComBat approach which uses empirical Bayes methods to estimate and remove site/batch effects with increased robustness to outliers in small samples compared with general linear model methods (38) (see Supplemental Methods).

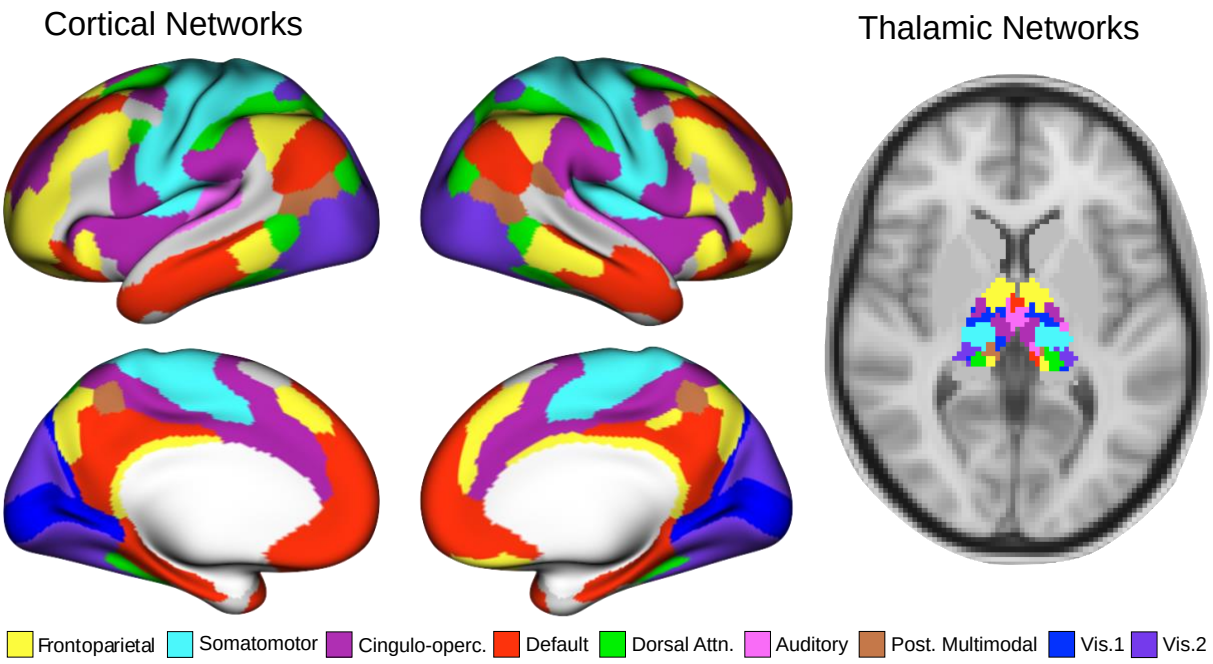

Figure 1-2. Cortical and thalamic regions for functional connectivity analysis. Left: nine cortical functional networks from the Cole-Anticevic Brain-wide Network Partition (CABNP) (36). Right: the same functional networks in the thalamus. Network thalamocortical connectivity (TCC) was computed between the mean fMRI time series in corresponding cortical and thalamic regions.

Modeling age trajectories

Non-linear relationships between age and TCC in 22qDel and TD cohorts were assessed with generalized additive mixed models (GAMMs) as in Jalbrzikowski et al., 2022 (39). Like linear

mixed effects models, GAMMs can account for repeated within-subject measures with random effects. Non-linear curves are estimated with basis functions, with overfitting prevented by penalization of polynomials and restricted estimation of maximum likelihood (40–42). We examined the effects of age on TCC separately in 22qDel and TD cohorts because GAMMs allow the shape of the relationship between the smoothed predictor and dependent variable to differ between groups. For each network, a GAMM was fitted predicting TCC from the smoothed effect of age and group, controlling for sex and scanner type, with a random intercept for subject ID. Test statistics were computed for the effect of age in each group, and p-values were corrected for multiple comparisons with False Discovery Rate (43). Secondary analyses were performed to assess the impact of outliers, scanner type, movement, medication status, cardiac defect diagnosis, and global signal regression (GSR). Additionally, a secondary thalamocortical connectivity analysis was performed using anatomically defined ROIs segmented by FreeSurfer (44,45), as in Huang et al. 2021 (28) (see Supplemental Methods). As an exploratory analysis, IQ (measured with the Wechsler Abbreviated Scale of Intelligence-2; WASI-2) and positive psychosis symptoms (measured with the Structured Interview for Psychosis-Risk Syndromes; SIPS (46)) were tested for associations with frontoparietal and somatomotor TCC (see Supplemental Methods).

RESULTS

Non-linear age trajectories

For all nine networks in TD controls, there were no significant relationships between TCC and age after multiple comparison correction (see Table 2). In contrast, in 22qDel three networks (frontoparietal, somatomotor, and cingulo-opercular) exhibited a significant effect of age on TCC after FDR correction. Analysis of the 95% confidence intervals (CI) of the first derivatives of the TCC age curves identified age ranges in which significant change occurred (see Table 2). Specifically, frontoparietal connectivity in 22qDel increased between ages 7.5 and 12.8, relative to TD controls, while somatomotor and cingulo-opercular TCC decreased between ages 6 and 22.7. Based on the 95% CI for the group difference in age curves (see Table 2), 22qDel frontoparietal connectivity was significantly lower than TD in childhood, from ages 6 to 9.6, but higher in late adolescence, from age 16.8 to 19. In 22qDel, Somatomotor TCC was higher than TD prior to age 14.5, but switched to lower than TD after age 14.8. Cingulo-opercular TCC showed a similar pattern of age-related decrease in both groups, and thus did not significantly differ between groups at any age. See Figure 3 for a visualization of frontoparietal and somatomotor age effects. Visualizations of all nine networks are included in Figure S1.

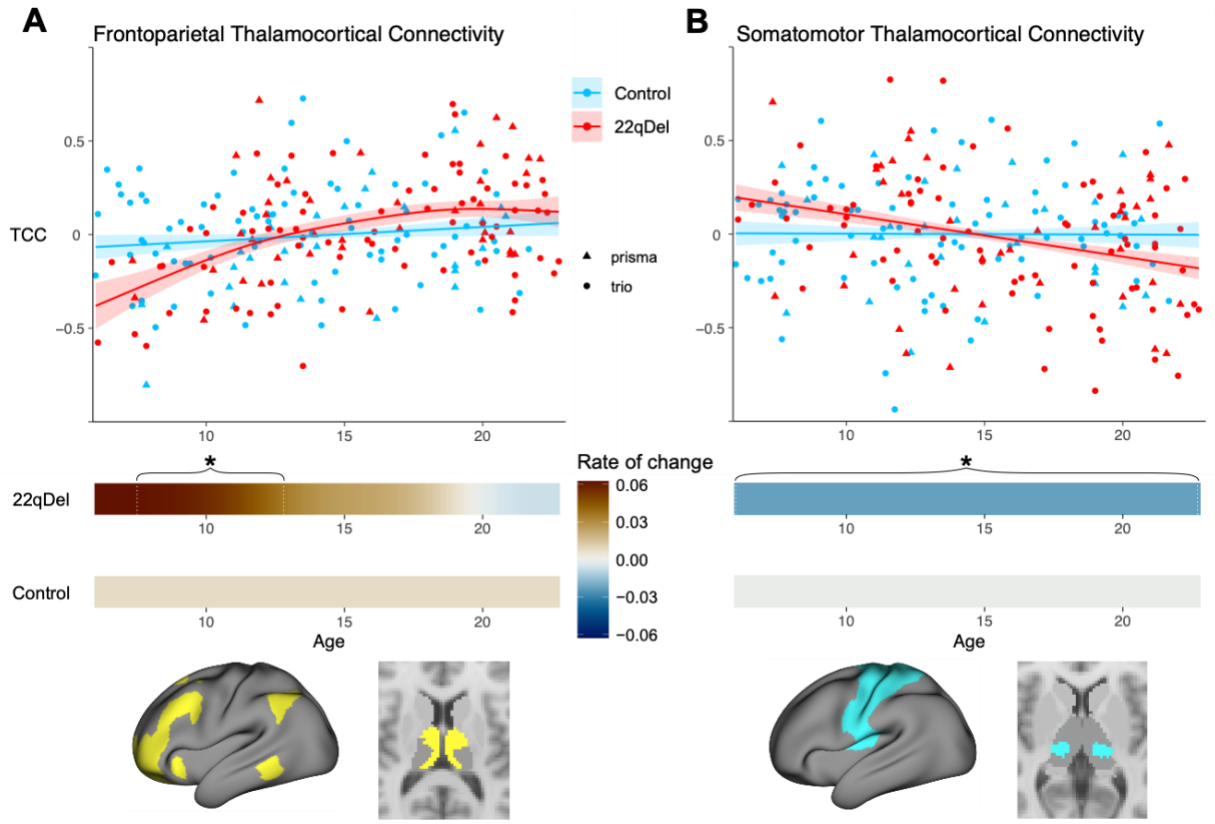

Figure 1-3. Age trajectories of frontoparietal and somatomotor thalamocortical connectivity (TCC). TCC vs age curves in 22qDel and typically developing controls. A) Upper: smoothed age curves and partial residuals for frontoparietal TCC from the GAMM predicting TCC from age, diagnosis, sex, and scanner, with a random intercept for repeated measures within subjects. The partial residual plots reflect the relationship between age and TCC, given the other covariates in the model. Middle: 1st derivatives of the TCC vs age curve in patients and controls, with intervals of significant change determined where the 95% confidence interval for the 1st derivative does not include zero, marked with brackets and asterisk. No change in frontoparietal TCC across the age range for controls, but 22qDel increases across ages 7.5-12.8. Lower: cortical and thalamic regions used for TCC measure. B) Same as A for the GAMM predicting somatomotor thalamocortical connectivity, showing no change across the age range in controls but a negative slope across the full age range for 22qDel.

Group	Network	*F (Df)*	*p*	FDR q	sig_change	sig_difference
22qDel	Frontoparietal	5.89 (2.2)	0.002	0.0177	7.5-12.8	6-9.6|16.8-19
22qDel	Somatomotor	9.84 (1.0)	0.002	0.0177	6-22.7	6-14.5|14.8-22.8
22qDel	Cingulo-Opercular	7.53 (1.0)	0.007	0.0399	6-22.7	
22qDel	Auditory	5.47 (1.0)	0.020	0.0915	6-21.4	
22qDel	Default	2.53 (3.9)	0.031	0.0998	20.7-21.5	12.3-15
22qDel	Dorsal Attention	2.43 (1.6)	0.066	0.1690		
22qDel	Posterior Multimodal	0.01 (1.0)	0.930	0.9520		

22qDel	Visual1	1.79 (1.0)	0.180	0.3290		
22qDel	Visual2	1.39 (1.0)	0.240	0.3910		
TD	Frontoparietal	1.03 (1.0)	0.310	0.4320		6-9.6|16.8-19
TD	Somatomotor	0.00 (1.0)	0.950	0.9520		6-14.5|14.8-22.8
TD	Cingulo-Opercular	4.60 (1.0)	0.033	0.0998	6-22.7	
TD	Auditory	2.57 (1.0)	0.110	0.2200		
TD	Default	0.43 (1.5)	0.680	0.7630		12.3-15
TD	Dorsal Attention	3.04 (1.0)	0.083	0.1870		
TD	Posterior Multimodal	0.28 (1.0)	0.600	0.7160		
TD	Visual1	1.19 (1.8)	0.310	0.4320		
TD	Visual2	0.63 (1.0)	0.430	0.5520		

Table 1-2. Effects of age on thalamocortical connectivity (TCC). Generalized Additive Mixed Model (GAMM) predicting TCC from age, diagnosis, sex, and scanner, with a random intercept for repeated measures within subjects. For each network, a separate TCC age curve was modeled for 22qDel and TD control groups. F-values and p-values are reported for each age effect, as well as FDR-corrected q-values (calculated from the set of n=18 p-values). “sig_change” denotes age ranges with significant change in TCC, determined where zero is not included in the 95% confidence interval (CI) for the 1st derivative of the TCC vs age GAMM. “sig_difference” denotes age ranges with significant group differences in TCC, based on the 95% CI. If multiple discontinuous periods of significant difference are found for a network, they are separated by “|”. sig_change and sig_difference values are reported in grey for age curves where FDR_q>0.05.

Secondary analyses

Various iterations of the final model were tested to confirm robustness to potential confounds (see Supplemental Methods). Test statistics and probabilities are reported in the Supplemental Results. Conclusions from the models were not altered by inclusion of movement, medication status (antipsychotic, yes/no), or history of congenital cardiac diagnosis. Results were also robust to 90% Winsorization (i.e., restricting outliers to the 5th and 95th percentiles) prior to testing GAMMs, and the exclusion of one scanner (i.e., using only Trio data, excluding Prisma). Secondary analysis split by age groups revealed no differences in pre/post pubertal subgroups in terms of which cortical networks are preferentially connected to thalamic networks of interest (see Supplemental Results).

An additional analysis using anatomically defined ROIs broadly corroborated the findings from our primary analysis using a functionally defined atlas. However, the functional atlas analysis was more sensitive to group differences and frontoparietal effects (see Supplemental Results).

Using anatomically defined regions, the only significant age effect was a negative relationship with motor region TCC in 22qDel. Frontal and parietal regions were analyzed separately in this case, and while the effect was not significant in either group, the age curves qualitatively resembled the frontoparietal effect from the functional atlas analysis.

IQ was found to be positively related to frontoparietal network TCC in TD controls (β=0.004, p=0.0174) and trended towards significance in 22qDel (β=0.005, p=0.058) (see Supplemental Results). No relationship was found between IQ and somatomotor connectivity, or between SIPS positive symptoms and somatomotor or frontoparietal connectivity. The observed relationship between frontoparietal TCC and IQ does not survive stringent multiple comparison correction across all behavioral relationships tested.

Effects of Global Signal Regression

Analyses were repeated with fMRI inputs that had not been subjected to GSR as a denoising step. Without inclusion of GSR, the pattern for somatomotor and cingulo-opercular TCC was similar but was reduced to a trend level after multiple comparison correction (see Table S6, Figure S2). The smoothed age effect on TCC no longer met multiple correction adjusted α=0.05 for any network in 22qDel or TD. Despite the inclusion of motion scrubbing and nuisance regression of motion parameters, quality control functional connectivity (QC-FC) analysis showed that inclusion of GSR additionally reduced the relationship between motion and whole-brain FC in this sample, suggesting that GSR improves the data with respect to motion (see Figure S3).

DISCUSSION

Altered FC between the thalamus and brain regions involved in somatomotor and frontoparietal networks has been implicated in cross-sectional studies of individuals with schizophrenia, those at CHR for psychosis, and 22qDel (12,14,15). However, little is known about how thalamic connectivity develops with age in genetic high-risk conditions such as 22qDel. This is the first study to investigate developmental trajectories of thalamic FC in in this population. We used a powerful and flexible GAMM approach to map linear and non-linear age-related changes in network-level thalamocortical connectivity, assessed via rs-fMRI in an accelerated longitudinal cohort of individuals with 22qDel and matched TD controls, ages 6 to 23 years. This novel GAMM approach has only recently been applied for the first time to case-control neuroimaging investigations, and has identified altered developmental trajectories of structural MRI phenotypes associated with 22q11.2 CNVs (39).

We found that 22qDel patients exhibited significant age-related increases in frontoparietal TCC and decreases in somatomotor TCC. Frontoparietal connectivity increased steeply during childhood and the rate of change slowed during adolescence, whereas somatomotor connectivity decreased consistently through the age range. TCC was generally stable across the studied age range in TD controls. TCC in the cingulo-opercular network was also found to significantly decrease across the age range in 22qDel, while the TD group trended towards significance in the same direction.

Development of thalamocortical functional connectivity in 22qDel and TD youth

These results expand on our prior findings from a cross-sectional analysis in a smaller subset of this dataset where, controlling for age, whole-thalamus FC in 22qDel relative to controls was found to be significantly increased to somatomotor regions and decreased to regions involved in the frontoparietal network (15). Our new longitudinal analysis suggests that the younger 22qDel patients were likely driving the previously observed finding of somatomotor hyper-connectivity

and frontoparietal hypo-connectivity, and that this phenotype may normalize or even reverse to an abnormal extent during adolescence. Here, the bi-directional pattern of somatomotor and frontoparietal thalamocortical disruptions in 22qDel can be seen to extend to developmental trajectories. In 22qDel, frontoparietal TCC increases significantly with age, particularly prior to age 13, while somatomotor TCC decreases across the age range, intersecting with the TD curve in early/mid adolescence (see Table 2 and Figure 3). Notably, GAMMs were analyzed across all nine networks represented in the thalamus, in a data driven approach, the results of which support our initial hypothesis of preferential disruptions in somatomotor and frontoparietal TCC.

Only a small number of fMRI studies have investigated typical development of thalamic FC in childhood and adolescence. A recent study in 107 TD participants found a linear decrease in salience network (cingulo-opercular) thalamic connectivity across ages 5-25 (29). Another recent study of thalamocortical FC in a large community sample (Philadelphia Neurodevelopmental Cohort), which included 1100 total scans, comprised of TD youth as well as individuals with psychosis spectrum symptoms and other psychopathology, found a negative linear association between age and somatosensory thalamic connectivity, but no age by psychiatric group interactions (28). Unlike the previous two described studies, an analysis of thalamic connectivity in 52 TD individuals, which treated age as a categorical variable (child, adolescent, adult) found greater thalamic-frontal FC in adults compared to children (47). In the context of this literature, our results can be seen to generally replicate the finding of normative age-related decreases in salience network connectivity (29) in both 22qDel and TD (for whom the effect of age on cingulo-opercular TCC trended towards significance and the 95% CI of the first derivative didn't include zero; see Table 2). It is still not clear how much age-related change is to be expected in typical development of somatomotor and frontoparietal thalamocortical networks (28,47). Our finding of significant age effects in these networks for 22qDel but not TD youth could be explained by either a pathological developmental mechanism in 22qDel or a compensatory "exaggeration" of typical developmental pathways. Future research in 22qDel mouse models can

shed light on genetic and cellular mechanisms underlying age-related FC disruptions, which may in turn suggest potential interventions for such aberrant maturational patterns.

Exploratory analysis of brain behavior relationships revealed that increased frontoparietal TCC was associated with higher Full Scale IQ in TD controls, with a similar relationship trending towards significance in the 22qDel cohort (see Supplemental Results). Future studies in larger cohorts should characterize this relationship in more detail. SIPS positive symptom severity was not found to be associated with frontoparietal or somatomotor TCC in 22qDel. Notably, in our baseline sample, 30.8% of 22qDel participants had subthreshold positive symptoms in the prodromal range, but only 7.7% had overt psychosis (see Table 1).

Strengths, limitations, and future directions

This study has several key strengths that support the reliability of our findings. The sample size of 112 scans from 65 22qDel patients is large for this population or similar rare disorders (48). We took advantage of an accelerated longitudinal recruitment design to map cohort-level FC-age trajectories across a key developmental window, whereas prior studies of thalamocortical FC development have relied on cross-sectional samples (28,29,47). Our GAMM analyses leveraged this longitudinal design, with the additional benefit of being able to capture developmental trajectories whose shapes differ between cohorts (40). Potential confounds were addressed through multiple complementary approaches. To minimize the impact of scanner type, we used the longitudinal ComBat algorithm, which was specifically adapted for longitudinal neuroimaging data and represents the state-of-the-art in batch correction methods (37). Our secondary analyses showed that our primary results were robust to outliers via Winsorization, scanner effects via exclusion of data collected on one of two scanners, and to inclusion of movement parameters, antipsychotic medication status, and congenital cardiac defect diagnosis as covariates of no interest in the final model. Together, these results support a robust finding in a unique clinical

population that allows for genetics-first study of phenotypes relevant to neurodevelopmental disorders.

However, certain limitations of this study must be noted. First, this dataset is not well suited for analyses of within-subject change, which might be more informative for analyses of symptom relationships over time. An additional limitation is that the GAMM results differed if fMRI inputs were used that had not been subject to GSR as a preprocessing step (see Table S6). Without GSR, no age effects remained significant after multiple comparison correction, although 22qDel somatomotor and cingulo-opercular connectivity trended in the same direction. QC-FC analysis, developed by Power et al. to quantify the effect of participant movement on FC (49), indicated that, despite motion scrubbing and regression of motion parameters, GSR additionally reduced the relationship between movement (framewise displacement) and FC. To reduce the impact of motion on FC results in our neurodevelopmental sample, and for consistency with our prior work and other similar studies in the field (15,29), we thus present our primary results with GSR included. Another limitation is that the data were acquired on two different Siemens scanners, and the data from the Prisma scanner (approximately 25% of the full sample) used a HCP-style sequence with a multi-band factor of 8, which can increase subcortical noise compared to single-band acquisitions (50). Band-pass temporal filtering, which we applied during preprocessing, can help mitigate this noise (50). Importantly, scanner type was controlled for through longitudinal ComBat, inclusion of a scanner covariate in the final model, and a secondary analysis using only data from the same Trio scanner, which corroborated our findings of altered development of somatomotor and frontoparietal TCC in 22qDel (see Supplementary Table S1). An additional consideration is diagnostic heterogeneity within the 22qDel sample (46% meet criteria for ADHD, 55% for autism; see Table 1).

Future research directions include mapping thalamocortical FC development in other clinical populations including autistic individuals, youth at CHR for psychosis, and individuals with other neuropsychiatric CNVs, in order to determine unique versus shared maturational patterns of this

circuitry. Characterizing changes across the lifespan, including early through late adulthood, in these populations will also be valuable. While our sample is large in the context of rare genetic disorders, even larger studies of 22qDel will be important for more precise characterization of developmental trajectories and brain behavior relationships. International multi-site studies such as the Enhancing Neuroimaging Genetics through Meta-Analysis (ENIGMA) CNV working group are currently making progress towards this goal (48). Other methods for assessing TCC related phenotypes, such as EEG and sleep spindle detection, will also be highly informative in 22qDel and related conditions (51). Additionally, the high construct validity of 22qDel animal models will allow for testing molecular and cell/circuit level hypotheses about development in 22qDel.

Conclusions

This study is the first to characterize longitudinal age-related changes in thalamocortical functional connectivity in children and adolescents with 22qDel. Using a novel functional atlas approach to investigate network-specific thalamocortical connectivity, we found that children with 22qDel exhibit altered maturation of these functional networks, involving a pattern of increased thalamocortical FC in the somatomotor network, concomitant with decreased connectivity in the frontoparietal network relative to TD controls. This pattern normalizes by early/mid adolescence, and potentially reverses by late adolescence. TD controls do not show the same age-related changes in frontoparietal and somatomotor connectivity. Future research in animal and in vitro models can shed light on biological mechanisms underlying the observed alterations in FC development in 22qDel.

CHAPTER ONE AUTHOR CONTRIBUTIONS

Charles H. Schleifer: Conceptualization, Methodology, Software, Formal Analysis, Data Curation, Writing - Original Draft, Writing - Review & Editing, Visualization

Kathleen P. O'Hora: Data Curation, Validation, Writing - Review & Editing

Maria Jalbrzikowski: Conceptualization, Methodology, Software, Writing - Review & Editing

Elizabeth Bondy: Data Curation

Leila Kushan-Wells: Investigation, Resources, Data Curation, Project Administration

Amy Lin: Data Curation

Lucina Q. Uddin: Conceptualization, Methodology, Writing - Review & Editing

Carrie E. Bearden: Conceptualization, Investigation, Writing - Review & Editing, Supervision, Project Administration, Funding Acquisition.

Disclosures

All authors reported no biomedical financial interests or potential conflicts of interest.

Data availability

Data are publicly available from the National Institute of Mental Health Data Archives: https://nda.nih.gov/edit_collection.html?id=2414

To facilitate reproducibility and rigor, analysis code is publicly available on GitHub: https://github.com/charles-schleifer/22q_tcc_longitudinal

A draft of this manuscript prior to peer review has been shared on the preprint server bioRxiv: https://www.biorxiv.org/content/10.1101/2023.06.22.546178v1.full

Funding

The work in this chapter was supported by the National Institute of Mental Health Grant Nos. R01 MH085953 (to C.E.B), U01MH101779 (to C.E.B); the Simons Foundation (SFARI Explorer Award to C.E.B), and the Joanne and George Miller Family Endowed Term Chair (to C.E.B.), and the UCLA Training Program in Neurobehavioral Genetics T32NS048004 (to C.H.S), R01MH129636 (to MJ)

CHAPTER ONE REFERENCES

1. McDonald-McGinn DM, Sullivan KE, Marino B, Philip N, Swillen A, Vorstman JAS, et al. (2015): 22q11.2 deletion syndrome. Nat Rev Dis Primer 1: 15071.

2. Provenzani U, Damiani S, Bersano I, Singh S, Moschillo A, Accinni T, et al. (2022): Prevalence and incidence of psychotic disorders in 22q11.2 deletion syndrome: a meta-analysis. Int Rev Psychiatry Abingdon Engl 34: 676–688.

3. Óskarsdóttir S, Boot E, Crowley TB, Loo JCY, Arganbright JM, Armando M, et al. (2023): Updated clinical practice recommendations for managing children with 22q11.2 deletion syndrome. Genet Med 25. https://doi.org/10.1016/j.gim.2022.11.006

4. Girirajan S, Brkanac Z, Coe BP, Baker C, Vives L, Vu TH, et al. (2011): Relative Burden of Large CNVs on a Range of Neurodevelopmental Phenotypes. PLoS Genet 7: e1002334.

5. Niklasson L, Rasmussen P, Óskarsdóttir S, Gillberg C (2001): Neuropsychiatric disorders in the 22q11 deletion syndrome. Genet Med 3: 79–84.

6. Niklasson L, Rasmussen P, Óskarsdóttir S, Gillberg C (2009): Autism, ADHD, mental retardation and behavior problems in 100 individuals with 22q11 deletion syndrome. Res Dev Disabil 30: 763–773.

7. Morrow BE, McDonald-McGinn DM, Emanuel BS, Vermeesch JR, Scambler PJ (2018): Molecular genetics of 22q11.2 deletion syndrome. Am J Med Genet A 176: 2070–2081.

8. Chawner SJRA, Doherty JL, Anney RJL, Antshel KM, Bearden CE, Bernier R, et al. (2021): A Genetics-First Approach to Dissecting the Heterogeneity of Autism: Phenotypic Comparison of Autism Risk Copy Number Variants. Am J Psychiatry 178: 77–86.

9. Moreau CA, Ching CR, Kumar K, Jacquemont S, Bearden CE (2021): Structural and functional brain alterations revealed by neuroimaging in CNV carriers. Curr Opin Genet Dev 68: 88–98.

10. Anticevic A, Cole MW, Repovs G, Murray JD, Brumbaugh MS, Winkler AM, et al. (2014): Characterizing Thalamo-Cortical Disturbances in Schizophrenia and Bipolar Illness. Cereb Cortex N Y NY 24: 3116–3130.

11. Welsh RC, Chen AC, Taylor SF (2010): Low-Frequency BOLD Fluctuations Demonstrate Altered Thalamocortical Connectivity in Schizophrenia. Schizophr Bull 36: 713–722.

12. Woodward ND, Karbasforoushan H, Heckers S (2012): Thalamocortical Dysconnectivity in Schizophrenia. Am J Psychiatry 169: 1092–1099.

13. Woodward ND, Heckers S (2016): Mapping thalamocortical functional connectivity in chronic and early stages of psychotic disorders. Biol Psychiatry 79: 1016–1025.

14. Anticevic A, Haut K, Murray JD, Repovs G, Yang GJ, Diehl C, et al. (2015): Association of Thalamic Dysconnectivity and Conversion to Psychosis in Youth and Young Adults at Elevated Clinical Risk. JAMA Psychiatry 72: 882–891.

15. Schleifer C, Lin A, Kushan L, Ji JL, Yang G, Bearden CE, Anticevic A (2019): Dissociable Disruptions in Thalamic and Hippocampal Resting-State Functional Connectivity in Youth with 22q11.2 Deletions. J Neurosci Off J Soc Neurosci 39: 1301–1319.

16. Chun S, Westmoreland JJ, Bayazitov IT, Eddins D, Pani AK, Smeyne RJ, et al. (2014): Specific disruption of thalamic inputs to the auditory cortex in schizophrenia models. Science 344: 1178–1182.

17. Chun S, Du F, Westmoreland JJ, Han SB, Wang Y-D, Eddins D, et al. (2017): Thalamic miR-338-3p mediates auditory thalamocortical disruption and its late onset in models of 22q11.2 microdeletion. Nat Med 23: 39–48.

18. Woodward ND, Giraldo-Chica M, Rogers B, Cascio CJ (2017): Thalamocortical Dysconnectivity in Autism Spectrum Disorder: An Analysis of the Autism Brain Imaging Data Exchange. Biol Psychiatry Cogn Neurosci Neuroimaging 2: 76–84.

19. Cerliani L, Mennes M, Thomas RM, Di Martino A, Thioux M, Keysers C (2015): Increased Functional Connectivity Between Subcortical and Cortical Resting-State Networks in Autism Spectrum Disorder. JAMA Psychiatry 72: 767–777.

20. Nair A, Carper RA, Abbott AE, Chen CP, Solders S, Nakutin S, et al. (2015): Regional specificity of aberrant thalamocortical connectivity in autism. Hum Brain Mapp 36: 4497–4511.

21. Chen H, Uddin LQ, Zhang Y, Duan X, Chen H (2016): Atypical effective connectivity of thalamo-cortical circuits in autism spectrum disorder. Autism Res 9: 1183–1190.

22. Moreau CA, Harvey A, Kumar K, Huguet G, Urchs SGW, Douard EA, et al. (2023): Genetic Heterogeneity Shapes Brain Connectivity in Psychiatry. Biol Psychiatry 93: 45–58.

23. Moreau CA, Kumar K, Harvey A, Huguet G, Urchs SGW, Schultz LM, et al. (2023): Brain functional connectivity mirrors genetic pleiotropy in psychiatric conditions. Brain 146: 1686–1696.

24. Jones EG (2012): The Thalamus. Springer Science & Business Media.

25. Yuan R, Di X, Taylor PA, Gohel S, Tsai Y-H, Biswal BB (2016): Functional topography of the thalamocortical system in human. Brain Struct Funct 221: 1971–1984.

26. Shine JM, Lewis LD, Garrett DD, Hwang K (2023): The impact of the human thalamus on brain-wide information processing. Nat Rev Neurosci 1–15.

27. Alcauter S, Lin W, Smith JK, Short SJ, Goldman BD, Reznick JS, et al. (2014): Development of Thalamocortical Connectivity during Infancy and Its Cognitive Correlations. J Neurosci 34: 9067–9075.

28. Huang AS, Rogers BP, Sheffield JM, Vandekar S, Anticevic A, Woodward ND (2021): Characterizing effects of age, sex and psychosis symptoms on thalamocortical functional connectivity in youth. NeuroImage 243: 118562.

29. Steiner L, Federspiel A, Slavova N, Wiest R, Grunt S, Steinlin M, Everts R (2020): Functional topography of the thalamo-cortical system during development and its relation to cognition. NeuroImage 223: 117361.

30. Benoit LJ, Canetta S, Kellendonk C (2022): Thalamocortical Development: A Neurodevelopmental Framework for Schizophrenia. Biol Psychiatry 92: 491–500.

31. Mancini V, Zöller D, Schneider M, Schaer M, Eliez S (2020): Abnormal Development and Dysconnectivity of Distinct Thalamic Nuclei in Patients With 22q11.2 Deletion Syndrome Experiencing Auditory Hallucinations. Biol Psychiatry Cogn Neurosci Neuroimaging 5: 875–890.

32. Power JD, Barnes KA, Snyder AZ, Schlaggar BL, Petersen SE (2012): Spurious but systematic correlations in functional connectivity MRI networks arise from subject motion. Neuroimage 59: 2142–2154.

33. Ji JL, Demšar J, Fonteneau C, Tamayo Z, Pan L, Kraljič A, et al. (2022, October 2): QuNex – An Integrative Platform for Reproducible Neuroimaging Analytics. bioRxiv, p 2022.06.03.494750.

34. Glasser MF, Sotiropoulos SN, Wilson JA, Coalson TS, Fischl B, Andersson JL, et al. (2013): The Minimal Preprocessing Pipelines for the Human Connectome Project. NeuroImage 80: 105–124.

35. Power JD, Plitt M, Laumann TO, Martin A (2017): Sources and implications of whole-brain fMRI signals in humans. NeuroImage 146: 609–625.

36. Ji JL, Spronk M, Kulkarni K, Repovš G, Anticevic A, Cole MW (2019): Mapping the human brain's cortical-subcortical functional network organization. NeuroImage 185: 35–57.

37. Beer JC, Tustison NJ, Cook PA, Davatzikos C, Sheline YI, Shinohara RT, Linn KA (2020): Longitudinal ComBat: A method for harmonizing longitudinal multi-scanner imaging data. NeuroImage 220: 117129.

38. Johnson WE, Li C, Rabinovic A (2007): Adjusting batch effects in microarray expression data using empirical Bayes methods. Biostatistics 8: 118–127.

39. Jalbrzikowski M, Lin A, Vajdi A, Grigoryan V, Kushan L, Ching CRK, et al. (2022): Longitudinal trajectories of cortical development in 22q11.2 copy number variants and typically developing controls. Mol Psychiatry 27: 4181–4190.

40. Hastie TJ (1992): Generalized Additive Models. Statistical Models in S. Routledge.

41. Wood SN (2004): Stable and Efficient Multiple Smoothing Parameter Estimation for Generalized Additive Models. J Am Stat Assoc 99: 673–686.

42. Wood SN (2011): Fast stable restricted maximum likelihood and marginal likelihood estimation of semiparametric generalized linear models. J R Stat Soc Ser B Stat Methodol 73: 3–36.

43. Benjamini Y, Hochberg Y (1995): Controlling the False Discovery Rate: A Practical and Powerful Approach to Multiple Testing. J R Stat Soc Ser B Methodol 57: 289–300.

44. Desikan RS, Ségonne F, Fischl B, Quinn BT, Dickerson BC, Blacker D, et al. (2006): An automated labeling system for subdividing the human cerebral cortex on MRI scans into gyral based regions of interest. NeuroImage 31: 968–980.

45. Iglesias JE, Insausti R, Lerma-Usabiaga G, Bocchetta M, Van Leemput K, Greve DN, et al. (2018): A probabilistic atlas of the human thalamic nuclei combining ex vivo MRI and histology. Neuroimage 183: 314–326.

46. Miller TJ, McGlashan TH, Rosen JL, Somjee L, Markovich PJ, Stein K, Woods SW (2002): Prospective diagnosis of the initial prodrome for schizophrenia based on the Structured Interview for Prodromal Syndromes: preliminary evidence of interrater reliability and predictive validity. Am J Psychiatry 159: 863–865.

47. Fair DA, Bathula D, Mills KL, Dias TGC, Blythe MS, Zhang D, et al. (2010): Maturing Thalamocortical Functional Connectivity Across Development. Front Syst Neurosci 4: 10.

48. Sønderby IE, Ching CRK, Thomopoulos SI, van der Meer D, Sun D, Villalon-Reina JE, et al. (2022): Effects of copy number variations on brain structure and risk for psychiatric illness: Large-scale studies from the ENIGMA working groups on CNVs. Hum Brain Mapp 43: 300–328.

49. Power JD, Schlaggar BL, Petersen SE (2015): Recent progress and outstanding issues in motion correction in resting state fMRI. NeuroImage 0: 536–551.

50. Risk BB, Murden RJ, Wu J, Nebel MB, Venkataraman A, Zhang Z, Qiu D (2021): Which multiband factor should you choose for your resting-state fMRI study? NeuroImage 234: 117965.

51. Manoach DS, Pan JQ, Purcell SM, Stickgold R (2016): Reduced Sleep Spindles in Schizophrenia: A Treatable Endophenotype That Links Risk Genes to Impaired Cognition? Biol Psychiatry 80: 599–608.

CHAPTER ONE SUPPLEMENTAL MATERIAL

Supplemental Methods

Participants

The total longitudinal sample consisted of 220 scans from 135 participants (6–23 years of age; n= 65 22qDel baseline, 63.1% female; n= 69 TD controls baseline, 49.3% female), recruited from an ongoing longitudinal study at the University of California, Los Angeles (UCLA). A prior cross-sectional study of whole-thalamus FC in 22qDel included a single time point from 79 individuals included in the current longitudinal sample (1). The 22qDel participants all had a molecularly confirmed 22q11.2 deletion. 22qDel and TD participants were statistically matched based on baseline age, sex, handedness, and fMRI motion (percent frames flagged based on displacement/intensity thresholds recommended by Power et al. 2012 (2)), as well as mean number of longitudinal visits and interval between visits, using appropriate tests (ANOVA, or chi-squared). Exclusion criteria for all study participants were as follows: significant neurological or medical conditions (unrelated to 22q11.2 deletion) that might affect brain structure, history of head injury with loss of consciousness, insufficient fluency in English, and/or substance or alcohol use disorder within the past 6 months. As we aimed to include a representative cohort of CNV carriers, patients with cardiac-related issues were not excluded, as this is a hallmark of 22qDel. Healthy controls were free from significant intellectual disability and did not meet criteria for any psychiatric disorder, with the exception of attention deficit-hyperactivity disorder or a past episode of depression, due to their prevalence in childhood and adolescence (3–5). After study procedures had been fully explained, adult participants provided written consent, while participants under the age of 18 years provided written assent with the written consent of their parent or guardian. The UCLA Institutional Review Board approved all study procedures and informed consent documents.

Clinical assessment

At each study time point, demographic information and clinical measures were collected for each participant by trained Master's-level clinicians, supervised by a clinical psychologist. Psychiatric diagnoses were established with the Structured Clinical Interview for DSM-IV (SCID) (6). Verbal IQ was assessed via the Wechsler Abbreviated Scale of Intelligence (WASI) Vocabulary subtest, and nonverbal IQ was assessed via the WASI Matrix Reasoning subtest. Psychiatric and dimensional psychotic-like symptoms were assessed via the Structured Interview for Psychosis-Risk Syndromes (SIPS) (7). For more details on study ascertainment and recruitment procedures, see Jalbrzikowski et al. 2012 and 2013 (8,9)

Neuroimaging acquisition

All subjects were imaged at the UCLA Center for Cognitive Neuroscience on either a Siemens TimTrio or Prisma scanner. The Prisma data were collected with Human Connectome Project (HCP)-style sequences. 420 volumes (5.6 min) of resting BOLD data were acquired in 72 interleaved slices with multiband-8 acceleration (voxel size = 2 × 2 × 2 mm, TR = 800 ms, TE = 37 ms, flip angle = 52°, FOV = 208 × 208 mm), along with single-band reference images and a pair of spin-echo field maps with phase encoding in the anterior-posterior (AP) and posterior-anterior (PA) directions. T1w MP-RAGE and T2w SPC images were collected in 208 sagittal slices (voxel size = 0.8 × 0.8 × 0.8 mm, FOV = 256 × 256 mm) with (T1w TR = 2400 ms, TE = 2.22 ms) and (T2w TR = 3200 ms, TE = 563 ms). The TimTrio resting BOLD data were acquired in 34 interleaved axial slices using a fast gradient-echo, echo-planar sequence (voxel size = 3 × 3 × 4 mm, TR = 2000 ms, TE = 30 ms, flip angle = 90°, FOV = 192 × 192 mm). Acquisition lasted 5.1 min and produced 152 volumes. High-resolution T1w MP-RAGE images were collected in 160 sagittal slices (voxel size = 1 × 1 × 1 mm, TR = 2300 ms, TE = 2.91 ms, flip angle = 90°, FOV = 240 × 256 mm).

Neuroimaging preprocessing

Structural and functional MRI data were processed using the Quantitative Neuroimaging Environment & Toolbox (10) which includes an extension of the Human Connectome Project (HCP) minimal preprocessing pipeline (11) compatible with multi-band and single-band fMRI. Additional processing of the fMRI time series included bandpass filtering, motion scrubbing for frames exceeding either a framewise displacement threshold of 0.5 mm or signal change threshold of 3 (normalized root mean square difference) proposed by Power et al. (2), and spatial smoothing (4mm Gaussian full width half maximum). Scans with >50% frames flagged for motion were excluded. To correct for spatially pervasive sources of noise including latent physiological factors and unaddressed movement, final analyses were performed on the residuals of the time series after regression of movement, mean signal from the ventricles and deep white matter, and the mean global gray matter signal (12). For a detailed description of preprocessing methods, see previous work in a subset of these data (1).

Functional connectivity

rs-fMRI analyses were performed using the ciftiTools package in R version 4.2.2 (13). Network thalamocortical functional connectivity (TCC) was calculated based on the Cole-Anticevic Brain-Wide Network Partition (CAB-NP) (14) which provides a whole brain cortical-subcortical extension of the HCP multimodal surface parcellation (15) derived from healthy adult resting-state fMRI. For each network, TCC was computed as the Fisher z-transformed Pearson correlation between the mean BOLD time series in the cortical portion of the network and the thalamic portion of the same network. Nine networks were investigated (frontoparietal, somatomotor, cingulo-opercular, default mode, dorsal attention, auditory, posterior multimodal, primary visual, and secondary visual), and three were excluded for lack of representation in the thalamus (orbito-affective, ventral multimodal, and language).

Data harmonization

To harmonize data acquired on two different scanner platforms, we applied a longitudinal implementation of the ComBat algorithm using the longComBat package in R (16,17). ComBat uses empirical Bayes methods to estimate and remove site/batch effects with increased robustness to outliers in small samples compared to general linear model approaches. ComBat was initially developed for genomics data (17), and has been subsequently adapted for neuroimaging and shown to preserve biological associations while effectively removing unwanted non-biological variation associated with site/scanner (18). The longitudinal adaptation, which uses random effects to account for within-subject repeated measures, has been shown to further increase statistical power in longitudinal neuroimaging analyses (16). LongComBat has been used to harmonize structural MRI features in a longitudinal analysis of cortical thickness and volume in a largely overlapping cohort of individuals 22qDel and controls (19).

Modeling age trajectories

Nonlinear relationships between age and thalamocortical connectivity in 22qDel and TD youth were assessed with generalized additive mixed models (GAMMs) as in Jalbrzikowski et al., 2022 (19) using the mgcv package in R. Like linear mixed effects models, GAMMs can account for repeated within-subject measures with random effects. Non-linear curves are estimated with basis functions, with overfitting prevented by penalization of polynomials and restricted estimation of maximum likelihood (20–22). We examined the smoothed effects of age on TCC separately in 22qDel and TD cohorts because GAMMs allow the shape of the relationship between the smoothed predictor and dependent variable to differ between groups. For each network, a GAMM was fitted predicting TCC from the smoothed effect of age and group, controlling for sex, scanner, and with a random intercept for subject ID. Test statistics were collected for the smoothed effect of age in each group, and p-values were corrected for multiple comparisons with False Discovery

Rate (23). To identify age ranges of significant TCC change in each group, the first derivative of the age curve was taken, and ages in which the 95% confidence interval (CI) did not include zero for the first derivative were considered to represent significant age-associated change. Similarly, age ranges with significant group differences in TCC were determined where the 95% CI for the group difference in age smooths did not include zero.

IQ and symptom analyses

To investigate the relationship between TCC and cognition, we tested linear mixed models in each cohort (TD and 22qDel) predicting frontoparietal or somatomotor TCC from WASI Full Scale IQ, controlling for sex, with a random intercept for subject. To characterize the relationship between TCC and psychosis symptoms, we tested linear mixed models in the 22qDel cohort predicting TCC from SIPS positive symptom scores with the same covariates. We also tested a model with log transformed SIPS positive scores because the distribution of SIPS positive severity was right skewed in the 22qDel cohort. We did not test for psychosis symptom relationships in the TD control cohort because there were not enough individuals with scores above zero to fit a reliable model.

Secondary analyses

To test the robustness of our models to various assumptions we performed a range of additional analyses. In our primary analyses, movement was corrected by scrubbing and by regression of motion traces from the BOLD time series, but as a supplementary analysis we repeated the main GAMMs with motion (percent frames flagged) as an additional covariate. Similarly, additional separate models were tested with antipsychotic medication status or congenital cardiac diagnosis. To test robustness to outliers, 90% Winsorization was performed, restricting extreme values to the 5th and 95th percentiles, and the main GAMM analysis was repeated on this modified input. Additionally, we repeated the main analyses with inputs that had

not been subjected to global signal regression (GSR) as a preprocessing step. To quantify the relationship between movement and FC with and without GSR, we performed QC-FC analysis, an approach developed by Power et al. (24). To test the impact of using data from two scanners, the main GAMM analysis was repeated with only the Trio data (Prisma scans excluded). The Prisma cohort alone did not have sufficient scans to test an equivalent model. To test if the overall cortical connectivity patterns of the thalamic frontoparietal and somatomotor regions were generally stable across development, we computed the functional connectivity of these regions to all nine cortical networks, then for each individual, tested if thalamic somatomotor or frontoparietal connectivity was highest to the corresponding cortical network (e.g., thalamic somatomotor to cortical somatomotor, compared to other cortical networks). We then split our full baseline cohort into two groups, over and under 13 years old (roughly pre/post puberty) and tested if the proportion of individuals differed for whom thalamic somatomotor or frontoparietal regions had preferential FC to the corresponding cortical network. There was no significant difference for the frontoparietal network (chi-squared=2.3, p=0.13) or the somatomotor network (chi-squared=1.07, p=0.30), suggesting that the functional atlas similarly indexes frontoparietal and somatomotor TCC in both younger and older participants.

Additionally, we conducted a thalamocortical connectivity analysis using anatomically defined ROIs, as in Huang et al 2021 (27). FreeSurfer 7.3 was used to generate individual subject cortical parcellations based on the Desikan-Killiany atlas (25), and thalamic parcellations based on a high resolution ex vivo atlas derived from MRI and histology (26). Regions were grouped into six thalamic and cortical ROIs per hemisphere, functional connectivity was computed for each pairing of thalamic and cortical regions, and then averaged between hemispheres.

Supplemental Results

Group	Network	F	p	FDR_q	sig_change	sig_difference
22qDel	Frontoparietal	4.31	0.007	0.0375	9.4-12.5	6-10.4|15.8-20.4
22qDel	Somatomotor	11.97	0.001	0.0127	6-22.7	6-14.3|14.6-22.8
22qDel	Cingulo Opercular	8.7	0.004	0.0342	6-22.7	
22qDel	Auditory	7.15	0.008	0.0375	6-22.7	
22qDel	Default	1.72	0.13	0.282		7.2-7.9|13.3-14.1
22qDel	Dorsal Attention	3.03	0.1	0.262		
22qDel	Posterior Multimodal	1.16	0.28	0.371		
22qDel	Visual1	1.32	0.25	0.371		
22qDel	Visual2	1.06	0.43	0.486		
TD	Frontoparietal	0.02	0.98	0.98		6-10.4|15.8-20.4
TD	Somatomotor	0	0.98	0.98		6-14.3|14.6-22.8
TD	Cingulo Opercular	3.31	0.031	0.093	7.3-10.1	
TD	Auditory	1.13	0.29	0.371		
TD	Default	0.63	0.43	0.486		7.2-7.9|13.3-14.1
TD	Dorsal Attention	5.17	0.025	0.0891	6-22.7	
TD	Posterior Multimodal	1.99	0.16	0.32		
TD	Visual1	1.66	0.22	0.371		
TD	Visual2	1.14	0.29	0.371		

Table 1-S1. Excluding Prisma data. GAMM age coefficients, *p*-values, FDR corrected *q*-values, and periods of significant change, tested using only data from the Siemens TimTrio scanner.

Group	Network	F	p	FDR_q	sig_change	sig_difference
22qDel	Frontoparietal	5.96	0.002	0.0174	7.6-13.4	6-10.1|16.3-19.5
22qDel	Somatomotor	9.09	0.003	0.0174	6-22.7	
22qDel	Cingulo Opercular	9.48	0.002	0.0174	6-22.7	
22qDel	Auditory	4.52	0.035	0.104	6-22.7	
22qDel	Default	2.8	0.019	0.0858	10.4-11.5|20.6-21.6	12.1-15
22qDel	Dorsal Attention	2.38	0.067	0.151		
22qDel	Posterior Multimodal	0.04	0.85	0.846		
22qDel	Visual1	2.59	0.11	0.197		
22qDel	Visual2	1.22	0.27	0.442		
TD	Frontoparietal	0.54	0.46	0.596		6-10.1|16.3-19.5
TD	Somatomotor	0.04	0.84	0.846		
TD	Cingulo Opercular	4.46	0.024	0.0864	7.8-16.4	
TD	Auditory	3.68	0.057	0.145		
TD	Default	0.56	0.66	0.744		12.1-15
TD	Dorsal Attention	2.95	0.088	0.175		
TD	Posterior Multimodal	0.24	0.63	0.744		
TD	Visual1	1.04	0.35	0.488		
TD	Visual2	1.01	0.32	0.473		

Table 1-S2. Winsorization for outliers. Repeat of main analyses (with full TimTrio + Prisma dataset) with the additional step of 90% Winsorization, which transforms all outliers above the 95th percentile to the 95th percentile, and all below the 5th percentile to the 5th percentile.

Group	Network	F	p	FDR_q	sig_change	sig_difference
22qDel	Frontoparietal	4.82	0.005	0.0331	7.9-12.4	6-9.4|17.5-18.7
22qDel	Somatomotor	11.11	0.001	0.0184	6-22.7	6-14.5|14.8-22.8
22qDel	Cingulo Opercular	9.72	0.002	0.019	6-22.7	
22qDel	Auditory	3.4	0.067	0.133		
22qDel	Default	2.38	0.049	0.111	20.7-21.4	12.3-14.8
22qDel	Dorsal Attention	4.76	0.034	0.102	16.2-19.9	
22qDel	Posterior Multimodal	0.02	0.88	0.876		
22qDel	Visual1	0.44	0.51	0.61		
22qDel	Visual2	4.87	0.028	0.102	6-22.7	
TD	Frontoparietal	0.65	0.42	0.585		
TD	Somatomotor	0.09	0.76	0.805		6-9.4|17.5-18.7
TD	Cingulo Opercular	6.1	0.014	0.065	6-22.7	6-14.5|14.8-22.8
TD	Auditory	1.42	0.23	0.384		
TD	Default	0.45	0.62	0.701		12.3-14.8
TD	Dorsal Attention	3.96	0.048	0.111	6-22.7	
TD	Posterior Multimodal	0.49	0.49	0.61		
TD	Visual1	0.96	0.41	0.585		
TD	Visual2	2.57	0.11	0.198		

Table 1-S3. Controlling for movement. Repeat of main analyses with movement (percent of frames scrubbed) as an additional fixed effect in the GAMM.

Group	Network	F	p	FDR_q	sig_change	sig_difference
22qDel	Frontoparietal	5.8500	0.002	0.0144	7.5-12.8	6-9.6|17-19
22qDel	Somatomotor	10.7300	0.001	0.0144	6-22.7	6-14.5|14.8-22.8
22qDel	Cingulo Opercular	8.3100	0.004	0.0264	6-22.7	
22qDel	Auditory	5.2900	0.023	0.1010	6-22.7	
22qDel	Default	2.4500	0.046	0.1370	20.9-21.4	12.3-14.8
22qDel	Dorsal Attention	3.1200	0.081	0.1950		
22qDel	Posterior Multimodal	0.0200	0.890	0.9100		
22qDel	Visual1	2.3000	0.130	0.2360		
22qDel	Visual2	1.3600	0.250	0.4020		
TD	Frontoparietal	1.0300	0.310	0.4480		6-9.6|17-19
TD	Somatomotor	0.0100	0.910	0.9100		6-14.5|14.8-22.8
TD	Cingulo Opercular	4.7000	0.031	0.1130	6-22.7	
TD	Auditory	2.4500	0.120	0.2360		
TD	Default	0.3000	0.770	0.8620		12.3-14.8
TD	Dorsal Attention	2.9700	0.086	0.1950		
TD	Posterior Multimodal	0.2600	0.610	0.7350		
TD	Visual1	1.1400	0.320	0.4480		
TD	Visual2	0.6100	0.430	0.5590		

Table 1-S4. Controlling for antipsychotic medication. Repeat of main analyses with current antipsychotic medication status (yes/no) as an additional fixed effect in the GAMM.

Group	Network	F	p	FDR_q	sig_change	sig_difference
22qDel	Frontoparietal	5.7400	0.002	0.0250	7.6-12.9	6-9.6|17-18.7
22qDel	Somatomotor	9.1700	0.003	0.0250	6-22.7	6-14.5|14.8-22.8
22qDel	Cingulo Opercular	7.1200	0.008	0.0498	6-22.7	
22qDel	Auditory	4.9400	0.028	0.1040	8.9-19	
22qDel	Default	2.5000	0.033	0.1040	20.8-21.4	12.3-15
22qDel	Dorsal Attention	2.4800	0.062	0.1600		
22qDel	Posterior Multimodal	0.0200	0.900	0.9550		
22qDel	Visual1	2.1000	0.150	0.2680		
22qDel	Visual2	1.1900	0.280	0.4310		
TD	Frontoparietal	1.0000	0.320	0.4420		6-9.6|17-18.7
TD	Somatomotor	0.0000	0.960	0.9600		6-14.5|14.8-22.8
TD	Cingulo Opercular	4.5200	0.035	0.1040	6-22.7	
TD	Auditory	2.5000	0.120	0.2310		
TD	Default	0.4300	0.680	0.7650		12.3-15
TD	Dorsal Attention	3.0300	0.083	0.1870		
TD	Posterior Multimodal	0.2800	0.600	0.7190		
TD	Visual1	1.2700	0.290	0.4310		
TD	Visual2	0.6000	0.440	0.5630		

Table 1-S5. Controlling for cardiac defect diagnosis. Repeat of main analyses with an additional covariate for lifetime congenital cardiac defect diagnosis including ventral/atrial septal defect, valvular anomalies, and conotruncal anomalies.

Group	Network	F	p	FDR_q	sig_change	sig_difference
22qDel	Frontoparietal	0.63	0.49	0.617		
22qDel	Somatomotor	4.27	0.04	0.18	6-22.7	6-22.8
22qDel	Cingulo Opercular	8.48	0.004	0.0737	6-22.7	
22qDel	Auditory	3.38	0.022	0.131	8.8-12.5	6-11.1|16.2-22.6
22qDel	Default	0.01	0.91	0.912		
22qDel	Dorsal Attention	3.13	0.018	0.131	19.3-21.5	20.7-22.8
22qDel	Posterior Multimodal	0.77	0.38	0.571		
22qDel	Visual1	1.15	0.28	0.527		
22qDel	Visual2	2.78	0.097	0.291		
TD	Frontoparietal	0.36	0.55	0.62		
TD	Somatomotor	3.41	0.066	0.239		6-22.8
TD	Cingulo Opercular	1.11	0.29	0.527		
TD	Auditory	1.43	0.23	0.526		6-11.1|16.2-22.6
TD	Default	0.43	0.51	0.617		
TD	Dorsal Attention	0.14	0.71	0.749		20.7-22.8
TD	Posterior Multimodal	1.56	0.21	0.526		
TD	Visual1	0.62	0.43	0.598		
TD	Visual2	0.94	0.33	0.544		

Table 1-S6. Omission of global signal regression (GSR). Repeat of main analyses without GSR as a preprocessing step. Age effects in 22qDel were significant at $p<0.05$ uncorrected for somatomotor, cingulo-opercular, auditory, and dorsal attention networks, but reduced to trend level after FDR correction.

Group	Network	F	p	FDR_q	sig_change	sig_difference
22qDel	motor	9.1800	0.003	0.0339	6-22.7	
22qDel	somatosensory	4.6400	0.032	0.1310	6-22.7	
22qDel	parietal	2.3000	0.091	0.1550	9.5-9.9	6-8|14.1-15.5
22qDel	prefrontal	2.6800	0.100	0.1550		
22qDel	temporal	4.4700	0.036	0.1310	6-22.7	19.7-22.8
22qDel	visual	3.3400	0.069	0.1550		6-22.8
TD	motor	3.1100	0.080	0.1550		
TD	somatosensory	4.1300	0.044	0.1310	6-22.7	
TD	parietal	1.3900	0.240	0.3190		6-8|14.1-15.5
TD	prefrontal	0.7300	0.390	0.4290		
TD	temporal	0.6200	0.490	0.4940		19.7-22.8
TD	visual	1.2500	0.270	0.3190		6-22.8

Table 1-S7. Thalamocortical functional connectivity between anatomical ROIs. Six pairs of thalamic and cortical regions were derived from subject-specific anatomical atlases generated by FreeSurfer (25,26) (see Tables S8 and S9 and Figure S4 for region groupings, and Figure S5 for GAMM visualizations). A significant negative relationship was observed between age and TCC for motor regions in 22qDel.

Region of Interest	FreeSurfer Parcellation	FreeSurfer Label
Prefrontal Cortex	Superior Frontal	1028, 2028
	Caudal Anterior Cingulate	1003, 2003
	Rostral Anterior Cingulate	1026, 2026
	Medial Orbitofrontal	1014, 2014
	Lateral Orbitofrontal	1012, 2012
	Rostral Middle Frontal	1027, 2027
	IFG Par Opercularis	1018, 2018
	IFG Pars Orbitalis	1019, 2019
	IFG Pars Triangularis	1020, 2020
Parietal Cortex	Inferior Parietal	1008, 2008
	Superior Parietal	1029, 2029
	Precuneus	1025, 2025
	Isthmus Cingulate	1010, 2010
	Posterior Cingulate	1023, 2023
	Supramarginal	1031, 2031
Temporal Cortex	Superior Temporal	1030, 2030
	Transverse Temporal	1034, 2034
	Middle Temporal	1015, 2015
	Fusiform	1007, 2007
	Inferior Temporal	1009, 2009
	Parahippocampal	1016, 2016
	Entorhinal	1006, 2006
Motor	Caudal Middle Frontal	1003, 2003
	Paracentral	1017, 2017
	Precentral	1024, 2024
Somatosensory	Postcentral	1022, 2022
Visual	Pericalcarine	1021, 2021
	Lateral Occipital	1011, 2011
	Lingual	1013, 2013
	Cuneus	1005, 2005

Table 1-S8. Cortical regions for secondary anatomical analysis. Regions from the Desikan-Killiany Atlas (25) were grouped as in Huang et al. 2021 (27).

Region of Interest	FreeSurfer Parcellation	FreeSurfer Label
Prefrontal	Mediodorsal Lateral	8112, 8212
	Mediodorsal Medial	8113, 8213
Parietal	Pulvinar Anterior	8120, 8220
	Pulvinar Inferior	8121, 8221
	Pulvinar Lateral	8122, 8222
	Pulvinar Medial	8123, 8223
Motor	Ventral Anterior	8126, 8226
	Ventral Anterior magnocellular	8127, 8227
	Ventral Lateral anterior	8128, 8228
	Ventral Lateral posterior	8129, 8229
	Ventromedial	8130, 8230
Somatosensory	Ventral Posterolateral	8133, 8233
Temporal	Medial Geniculate	8109, 8209
Visual	Lateral Geniculate	8115, 8215

Table 1-S9. Thalamic regions for secondary anatomical analysis. Regions from the FreeSurfer automated thalamic segmentation (26) were grouped as in Huang et al. 2021 (27).

		Control	22qDel	p-value
Scanner, n (%)	prisma	28 (25.9)	39 (34.8)	0.198
	trio	80 (74.1)	73 (65.2)	
fMRI % movement, mean (SD)		6.47 (9.67)	9.10 (11.73)	0.071
Visit, n (%)	1	69 (63.9)	65 (58.0)	0.467
	2	30 (27.8)	30 (26.8)	
	3	5 (4.6)	12 (10.7)	
	4	2 (1.9)	4 (3.6)	
	5	1 (0.9)	1 (0.9)	
	6	1 (0.9)	0 (0.0)	

Table 1-S10. Composition of TD and 22qDel cohorts in the full longitudinal sample with regards to scanner type (Siemens Trio or Siemens Prisma), fMRI % movement (percentage of frames removed for exceeding displacement and/or signal change thresholds per subject), and longitudinal visit number. *p*-values from chi-squared test or ANOVA between 22qDel and TD.

	Percent of Sample from Trio Scanner		
Visit	**Control**	**22qDel**	**p-value (chi-squared)**
1	72.5	73.8	1.000
2	83.3	66.7	0.233
3	100	41.7	0.092
4	0	0	
5	0	0	
6	0		

Table 1-S11. Percentage of scans acquired on the Trio scanner (versus Prisma) at each study visit. The balance of Trio vs. Prisma scans is compared between groups with chi-squared tests for the study time points with ≥ 5 individuals per group.

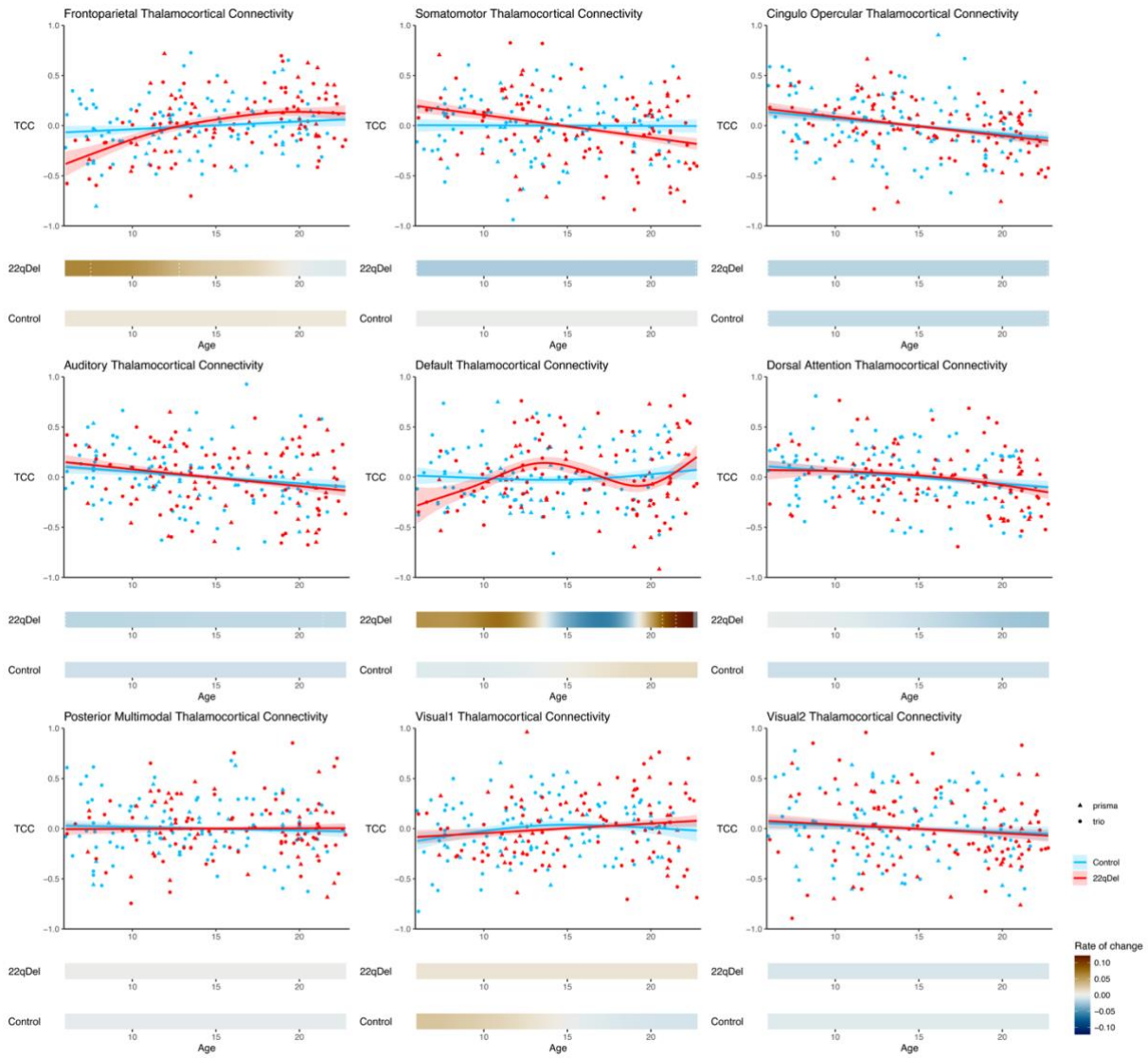

Figure 1-S1. Age trajectories for all networks. Visualization of GAMM curves and partial residuals *(above)* and first derivatives *(below*) for all nine networks from the primary analysis.

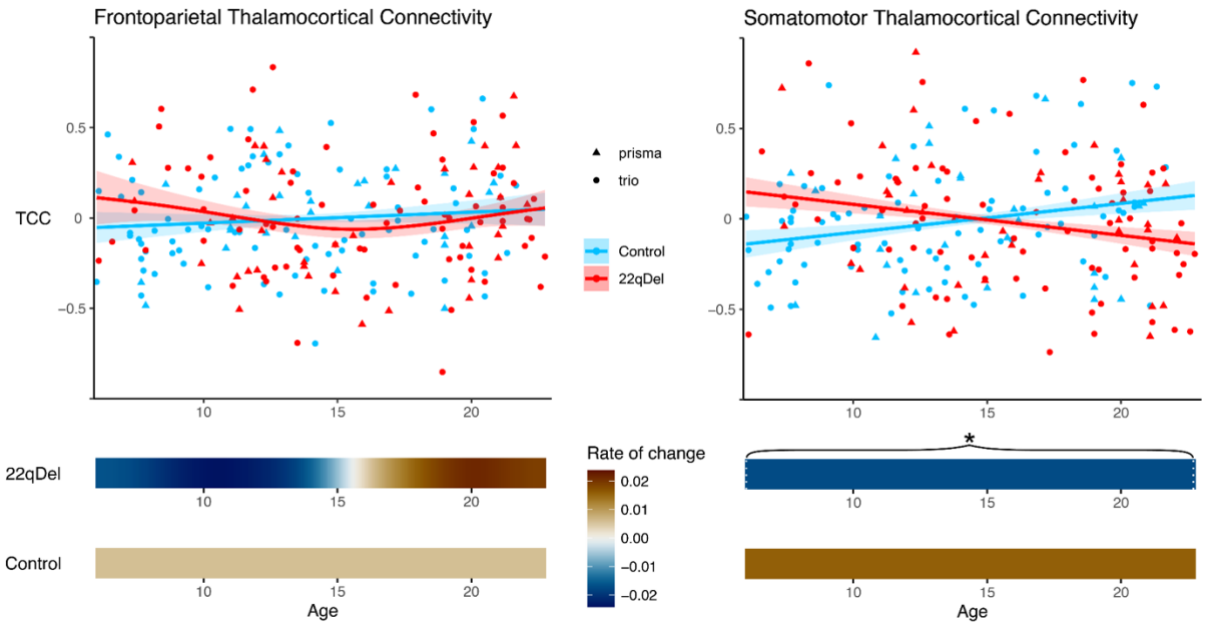

Figure 1-S2. Age trajectories of frontoparietal and somatomotor thalamocortical connectivity without GSR. Visualization of GAMM curves and partial residuals *(above)* and first derivatives *(below*) for frontoparietal *(left)* and somatomotor *(right)* networks.

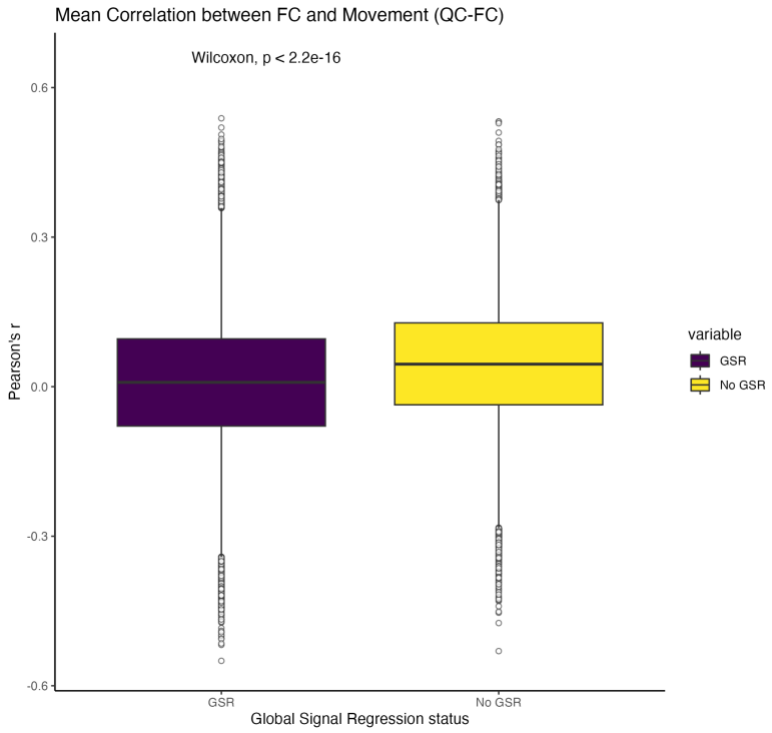

Figure 1-S3. QC-FC relationships with and without GSR. For each pair of regions in the n=718 region CAB-NP parcellation, QC-FC was calculated as the Pearson correlation between functional connectivity and movement across all baseline 22qDel and TD scans (24). QC-FC values were compared for data with and without GSR using a Wilcoxon signed rank test indicating a significantly decreased relationship between movement and functional connectivity in the global signal regressed data (purple) compared to the data without GSR (yellow).

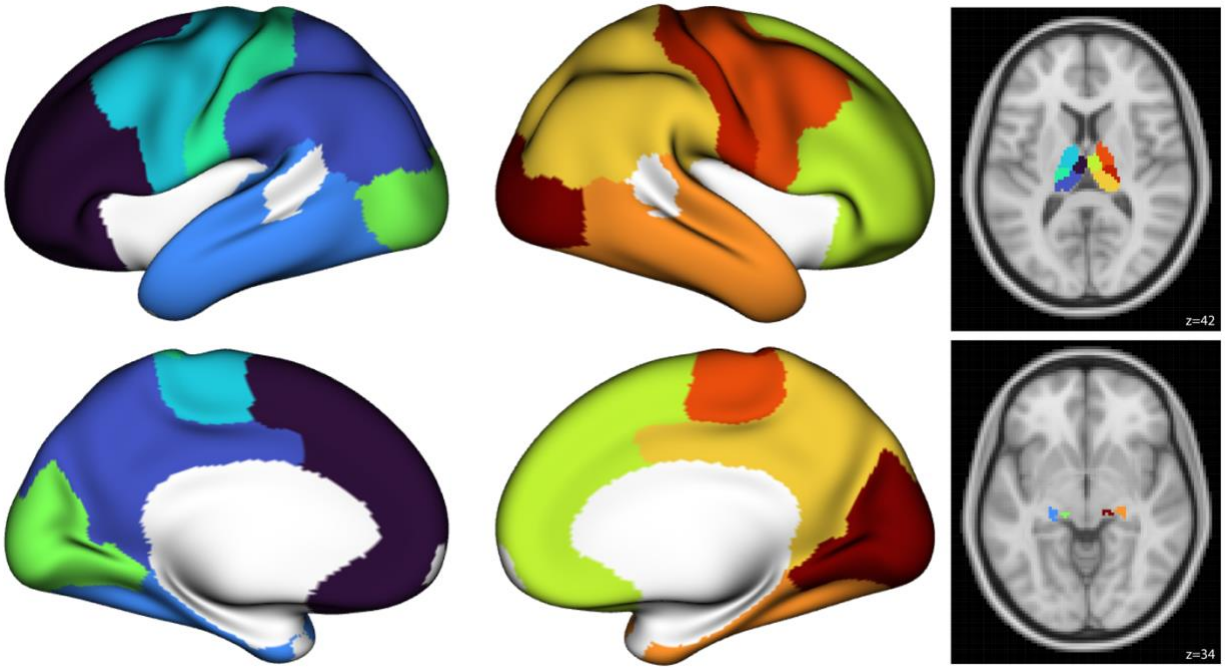

Figure 1-S4. Anatomical regions derived from FreeSurfer. Segmentation visualized for one example individual. Cortical regions were grouped into six ROIs per hemisphere (prefrontal, parietal, motor, somatosensory, temporal, visual), and thalamic subregions were grouped to correspond with these cortical ROIs.

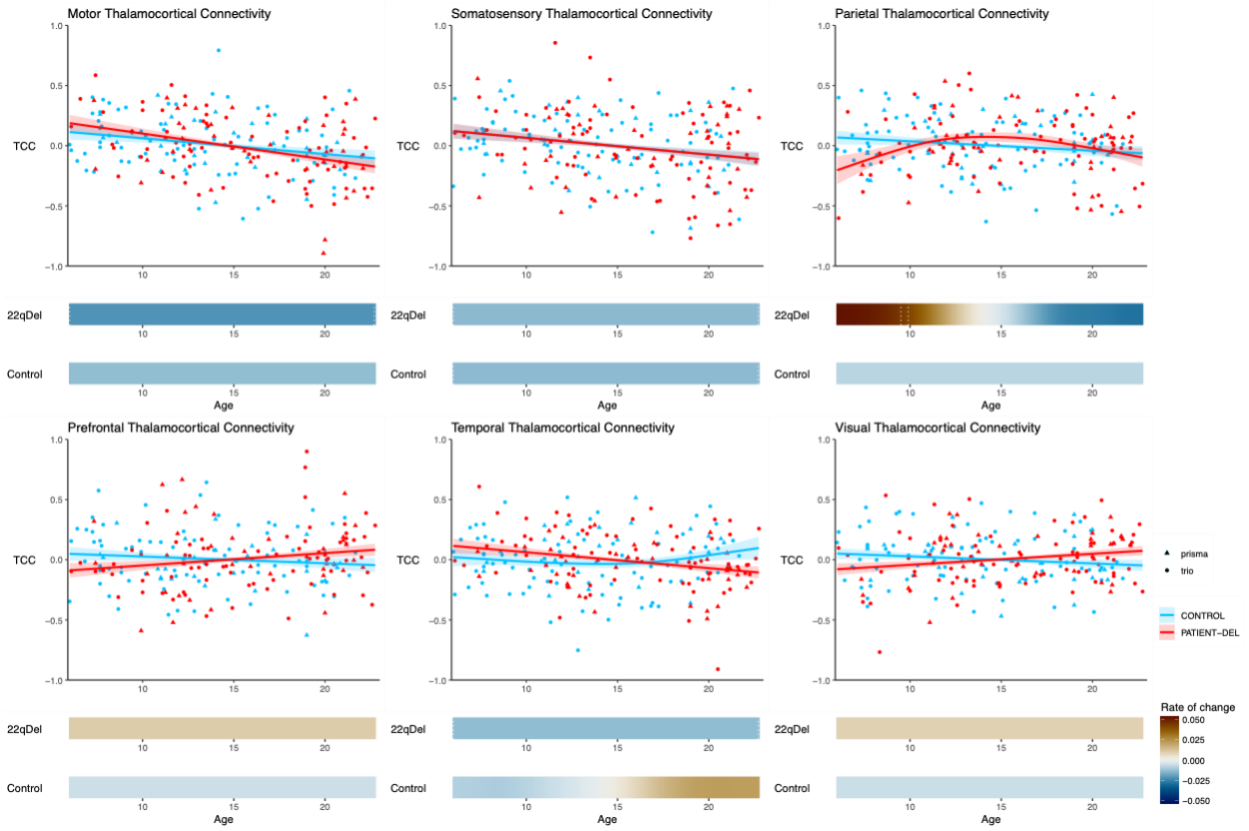

Figure 1-S5. Age trajectories for anatomically defined regions. Visualization of GAMM curves and partial residuals *(above)* and first derivatives *(below)* for the supplementary analysis of anatomical ROI-to-ROI thalamocortical functional connectivity using FreeSurfer derived regions. The motor and somatosensory effects in 22qDel qualitatively resemble the somatomotor effects from the primary analysis which used a functionally defined atlas. The frontoparietal effects from the primary analysis resemble a combination of the prefrontal and parietal effects observed here.

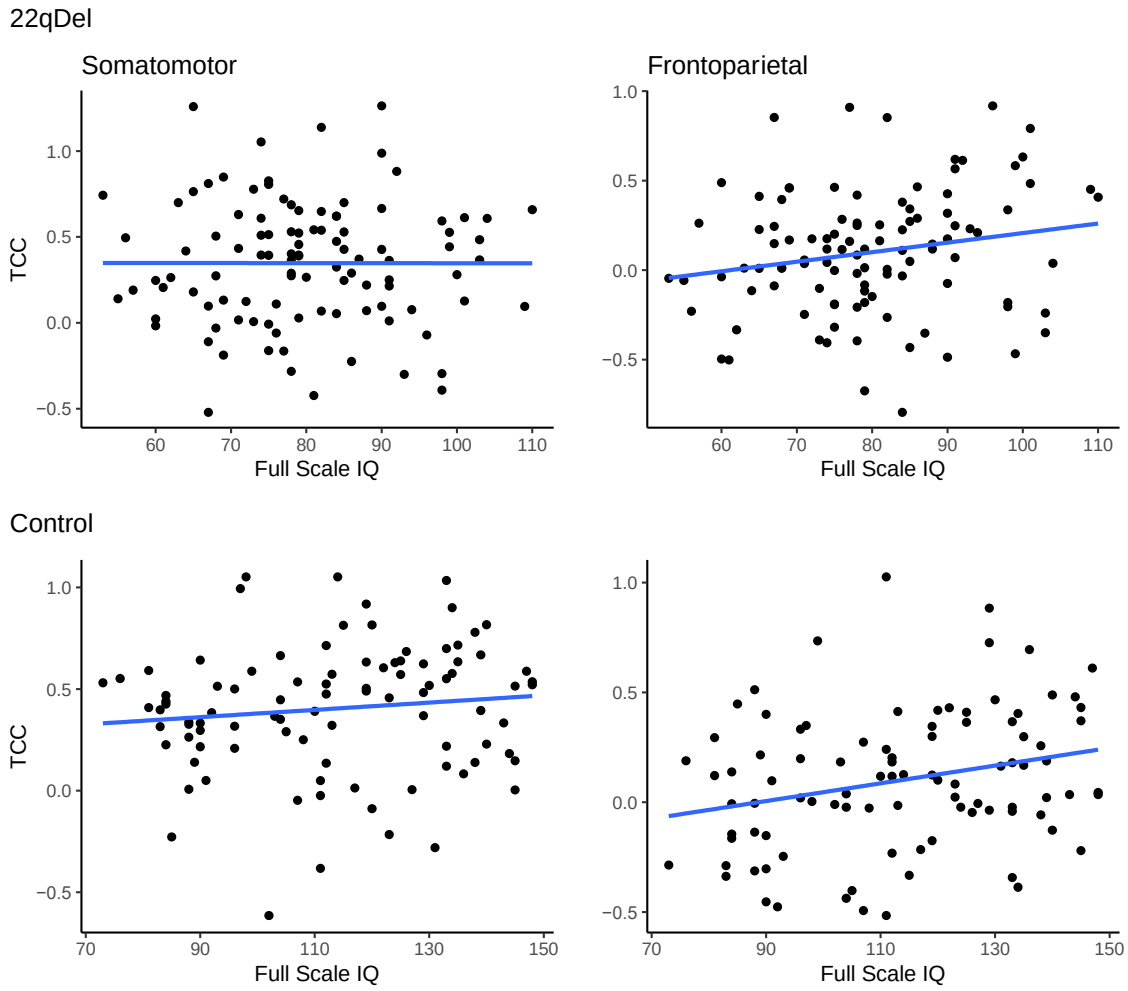

Figure 1-S6. Relationship between IQ and TCC. Linear mixed models in both cohorts predicting frontoparietal or sensorimotor TCC from WASI Full Scale IQ, controlling for sex, with a random intercept for subject. IQ was significantly related to frontoparietal TCC in TD controls (β=0.004, p=0.0174) and trended towards significance in 22qDel (β=0.005, p=0.058). IQ was not related to somatomotor connectivity in either group (β=0.002, p=0.239; β=-0.0001, p=0.970).

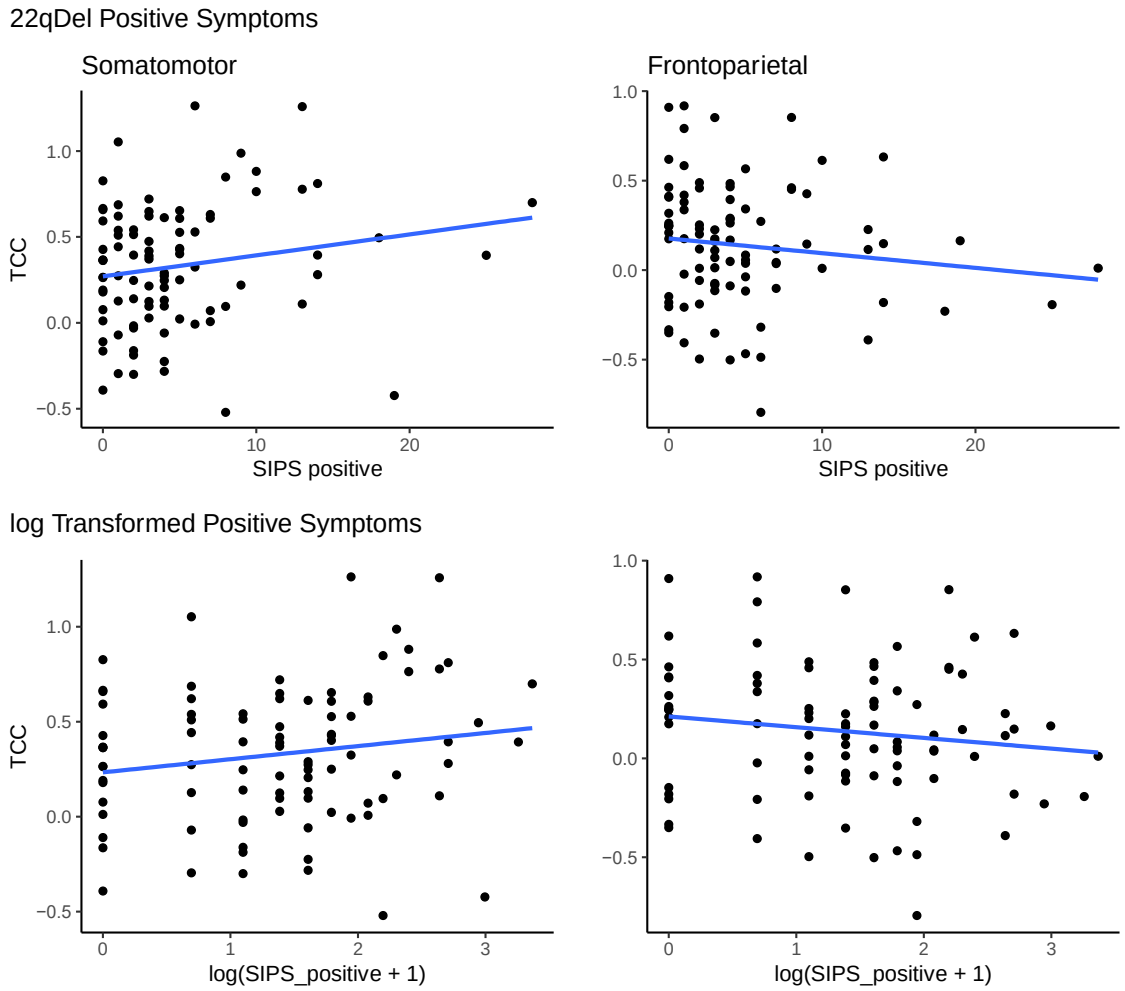

Figure 1-S7. Linear mixed models in 22qDel predicting frontoparietal or sensorimotor TCC from SIPS positive symptom total or log transformed positive symptom total, controlling for sex, with a random intercept for subject. The p-value for the effect of SIPS positive score on TCC was >0.05 in all models.

CHAPTER ONE SUPPLEMENTAL REFERENCES

1. Schleifer C, Lin A, Kushan L, Ji JL, Yang G, Bearden CE, Anticevic A (2019): Dissociable Disruptions in Thalamic and Hippocampal Resting-State Functional Connectivity in Youth with 22q11.2 Deletions. J Neurosci Off J Soc Neurosci 39: 1301–1319.

2. Power JD, Barnes KA, Snyder AZ, Schlaggar BL, Petersen SE (2012): Spurious but systematic correlations in functional connectivity MRI networks arise from subject motion. Neuroimage 59: 2142–2154.

3. Ghandour RM, Sherman LJ, Vladutiu CJ, Ali MM, Lynch SE, Bitsko RH, Blumberg SJ (2019): Prevalence and Treatment of Depression, Anxiety, and Conduct Problems in US Children. J Pediatr 206: 256-267.e3.

4. Sayal K, Prasad V, Daley D, Ford T, Coghill D (2018): ADHD in children and young people: prevalence, care pathways, and service provision. Lancet Psychiatry 5: 175–186.

5. Thapar A, Collishaw S, Pine DS, Thapar AK (2012): Depression in adolescence. The Lancet 379: 1056–1067.

6. First MB, Gibbon M (2004): The Structured Clinical Interview for DSM-IV Axis I Disorders (SCID-I) and the Structured Clinical Interview for DSM-IV Axis II Disorders (SCID-II). Comprehensive Handbook of Psychological Assessment, Vol. 2: Personality Assessment. Hoboken, NJ, US: John Wiley & Sons, Inc., pp 134–143.

7. Miller TJ, McGlashan TH, Rosen JL, Somjee L, Markovich PJ, Stein K, Woods SW (2002): Prospective diagnosis of the initial prodrome for schizophrenia based on the Structured Interview for Prodromal Syndromes: preliminary evidence of interrater reliability and predictive validity. Am J Psychiatry 159: 863–865.

8. Jalbrzikowski M, Carter C, Senturk D, Chow C, Hopkins JM, Green MF, et al. (2012): Social Cognition in 22q11.2 Microdeletion Syndrome: Relevance to Psychosis. Schizophr Res 142: 99–107.

9. Jalbrzikowski M, Jonas R, Senturk D, Patel A, Chow C, Green MF, Bearden CE (2013): Structural abnormalities in cortical volume, thickness, and surface area in 22q11.2 microdeletion syndrome: Relationship with psychotic symptoms. NeuroImage Clin 3: 405–415.

10. Ji JL, Demšar J, Fonteneau C, Tamayo Z, Pan L, Kraljič A, et al. (2022, October 2): QuNex – An Integrative Platform for Reproducible Neuroimaging Analytics. bioRxiv, p 2022.06.03.494750.

11. Glasser MF, Sotiropoulos SN, Wilson JA, Coalson TS, Fischl B, Andersson JL, et al. (2013): The Minimal Preprocessing Pipelines for the Human Connectome Project. NeuroImage 80: 105–124.

12. Power JD, Plitt M, Laumann TO, Martin A (2017): Sources and implications of whole-brain fMRI signals in humans. NeuroImage 146: 609–625.

13. Pham DD, Muschelli J, Mejia AF (2022): ciftiTools: A package for reading, writing, visualizing, and manipulating CIFTI files in R. NeuroImage 250: 118877.

14. Ji JL, Spronk M, Kulkarni K, Repovš G, Anticevic A, Cole MW (2019): Mapping the human brain's cortical-subcortical functional network organization. NeuroImage 185: 35–57.

15. Glasser MF, Coalson TS, Robinson EC, Hacker CD, Harwell J, Yacoub E, et al. (2016): A multi-modal parcellation of human cerebral cortex. Nature 536: 171–178.

16. Beer JC, Tustison NJ, Cook PA, Davatzikos C, Sheline YI, Shinohara RT, Linn KA (2020): Longitudinal ComBat: A method for harmonizing longitudinal multi-scanner imaging data. NeuroImage 220: 117129.

17. Johnson WE, Li C, Rabinovic A (2007): Adjusting batch effects in microarray expression data using empirical Bayes methods. Biostatistics 8: 118–127.

18. Fortin J-P, Cullen N, Sheline YI, Taylor WD, Aselcioglu I, Cook PA, et al. (2018): Harmonization of cortical thickness measurements across scanners and sites. NeuroImage 167: 104–120.

19. Jalbrzikowski M, Lin A, Vajdi A, Grigoryan V, Kushan L, Ching CRK, et al. (2022): Longitudinal trajectories of cortical development in 22q11.2 copy number variants and typically developing controls. Mol Psychiatry 27: 4181–4190.

20. Hastie TJ (1992): Generalized Additive Models. Statistical Models in S. Routledge.

21. Wood SN (2004): Stable and Efficient Multiple Smoothing Parameter Estimation for Generalized Additive Models. J Am Stat Assoc 99: 673–686.

22. Wood SN (2011): Fast stable restricted maximum likelihood and marginal likelihood estimation of semiparametric generalized linear models. J R Stat Soc Ser B Stat Methodol 73: 3–36.

23. Benjamini Y, Hochberg Y (1995): Controlling the False Discovery Rate: A Practical and Powerful Approach to Multiple Testing. J R Stat Soc Ser B Methodol 57: 289–300.

24. Power JD, Schlaggar BL, Petersen SE (2015): Recent progress and outstanding issues in motion correction in resting state fMRI. NeuroImage 0: 536–551.

25. Desikan RS, Ségonne F, Fischl B, Quinn BT, Dickerson BC, Blacker D, et al. (2006): An automated labeling system for subdividing the human cerebral cortex on MRI scans into gyral based regions of interest. NeuroImage 31: 968–980.

26. Iglesias JE, Insausti R, Lerma-Usabiaga G, Bocchetta M, Van Leemput K, Greve DN, et al. (2018): A probabilistic atlas of the human thalamic nuclei combining ex vivo MRI and histology. Neuroimage 183: 314–326.

27. Huang AS, Rogers BP, Sheffield JM, Vandekar S, Anticevic A, Woodward ND (2021): Characterizing effects of age, sex and psychosis symptoms on thalamocortical functional connectivity in youth. NeuroImage 243: 118562.

CHAPTER TWO

Effects of Gene Dosage and Development on Subcortical Nuclei Volumes in Individuals with 22q11.2 Copy Number Variations

Charles H. Schleifer[1,2], Kathleen P. O'Hora[1], Hoki Fung[1], Jennifer Xu[1], Taylor-Ann Robinson[1], Angela S. Wu[1], Leila Kushan-Wells[1], Amy Lin[1], Christopher R. K. Ching[3], Carrie E. Bearden[1,4]

1. Department of Psychiatry and Biobehavioral Sciences, Semel Institute for Neuroscience and Human Behavior, University of California, Los Angeles, CA, USA.
2. David Geffen School of Medicine, University of California, Los Angeles, CA, USA.
3. Imaging Genetics Center, Mark and Mary Stevens Institute for Neuroimaging and Informatics, Keck School of Medicine, University of Southern California, Marina del Rey, CA, USA
4. Department of Psychology, University of California, Los Angeles, CA, USA.

ABSTRACT

The 22q11.2 locus contains genes critical for brain development. Reciprocal Copy Number Variations (CNVs) at this locus impact risk for neurodevelopmental and psychiatric disorders. Both 22q11.2 deletions (22qDel) and duplications (22qDup) are associated with autism, but 22qDel uniquely elevates schizophrenia risk. Understanding brain phenotypes associated with these highly penetrant CNVs can provide insights into genetic pathways underlying neuropsychiatric disorders. Human neuroimaging and animal models indicate subcortical brain alterations in 22qDel, yet little is known about developmental differences across specific nuclei between reciprocal 22q11.2 CNV carriers and typically developing (TD) controls. We conducted a longitudinal MRI study in a total of 385 scans from 22qDel (n=96, scans=191, 53.1% female), 22qDup (n=37, scans=64, 45.9% female), and TD controls (n=80, scans=130, 51.2% female), across a wide age range (5.5-49.5 years). Volumes of the thalamus, hippocampus, amygdala, and anatomical subregions were estimated using FreeSurfer, and the linear effects of 22q11.2 gene dosage and non-linear effects of age were characterized with generalized additive mixed models (GAMMs). Positive gene dosage effects (volume increasing with copy number) were observed for total intracranial and whole hippocampus volumes, but not whole thalamus or amygdala volumes. Several amygdala subregions exhibited similar positive effects, with bi-directional effects found across thalamic nuclei. Distinct age-related trajectories were observed across the three groups. Notably, both 22qDel and 22qDup carriers exhibited flattened development of hippocampal CA2/3 subfields relative to TD controls. This study provides novel insights into the impact of 22q11.2 CNVs on subcortical brain structures and their developmental trajectories.

INTRODUCTION

Genomic copy number variations (CNVs) at the 22q11.2 locus strongly increase risk for neurodevelopmental and psychiatric disorders including autism and schizophrenia [1]. 22q11.2 Deletion Syndrome (22qDel) and 22q11.2 Duplication Syndrome (22qDup) result from reciprocal CNVs that involve hemizygous deletion or duplication of approximately 2.6 Megabases (Mb) of genomic material from the long arm of chromosome 22. The brain and behavioral phenotypes resulting from these related CNVs provide a valuable genetics-first framework for investigating biological pathways relevant to brain development and neuropsychiatric disorders [2,3].

22qDel (OMIM #188400, #192430) is one of the strongest known genetic risk factors for schizophrenia, with over 1 in 10 individuals with 22qDel having a comorbid psychotic disorder and over one-third experiencing subthreshold psychosis symptoms [4,5]. 22qDel also increases risk for autism, attention-deficit hyperactivity disorder (ADHD), intellectual disability, and anxiety disorders [6–8]. This microdeletion occurs in approximately 1 in 4000 people [9].

A duplication of this same region causes 22qDup (OMIM #608363) and is often inherited, unlike 22qDel which typically arises de novo [10]. 22qDup was discovered more recently than 22qDel and has not yet been as deeply characterized [11,12]. Individuals with 22qDup experience higher rates of neurodevelopmental disorders, including intellectual disability and autism, compared to the general population; however, the duplication generally has a milder impact on neurodevelopment compared to 22qDel [1,13]. In contrast to 22qDel, 22qDup is less common in individuals with schizophrenia compared to the general population, suggesting a potential protective effect against schizophrenia in 22qDup [14–16].

In addition to widespread cortical anomalies, including reductions in surface area, concomitant with relatively increased cortical thickness [17,18], studies of 22qDel have consistently identified structural and functional alterations in subcortical structures. A large multi-site, cross-sectional study from the ENIGMA 22q11.2 Working Group found decreased subcortical volumes in 22qDel compared to TD controls, with larger effects in those with psychosis [19]. These

subcortical brain structures play key roles in cognitive, sensory, and affective processes [20]. Individual differences in subcortical anatomy have been related to both common and rare genetic variation [21,22], and to psychiatric and neurodevelopmental disorders including schizophrenia, autism, and ADHD [23,24].

While most of the literature to date has investigated whole subcortical structures and/or voxel-wise shape differences, these structures are composed of many small distinct nuclei [20,25]. More recent studies have begun to investigate volumes of specific anatomical subregions of structures such as the thalamus and hippocampus. Bi-directional effects on FreeSurfer-derived thalamic nuclei volumes have been observed in 22qDel, wherein volumes of subregions involved in sensory processes (e.g., medial geniculate) were found to be smaller than controls, while subregions involved in cognitive processes (e.g., anteroventral) were larger [26]. Longitudinally, there were steeper thalamic volume decreases over time in individuals with 22qDel who experienced auditory hallucinations. In 22qDel, lower hippocampal tail volume has been related to verbal learning impairments [27], and hippocampal volume loss over time in 22qDel has been linked to altered local balance of excitatory and inhibitory neurotransmitter metabolites [28].

Few studies have directly compared brain phenotypes in 22qDel and 22qDup. In the first study comparing regional brain volumes of reciprocal 22q11.2 CNV carriers to typically developing (TD) controls, in a cross-sectional sample our group found that gene dosage (i.e., the number of copies of the 22q11.2 locus) was positively related to cortical surface area (22qDel < TD < 22qDup) and negatively related to cortical thickness (22qDel > TD > 22qDup) [18]. This study also found larger hippocampal volumes in 22qDup relative to 22qDel, and radial thickness differences in subcortical structures, including the thalamus and amygdala. Recently, a large study of subcortical volumes in 11 different CNVs found convergent evidence for hippocampal volume differences in 22qDel versus 22qDup [21].

No study has assessed subcortical subregional volumes or longitudinal subcortical development in 22qDup, nor directly compared subregion-level volumes between 22qDup and

22qDel. Studies of subcortical shape show complex alterations in 22q11.2 CNV carriers compared to controls, with localized volume increases and decreases suggesting differential vulnerabilities across subregions [19,21]. Mapping gene dosage effects to functionally and histologically defined nuclei can facilitate causal links between macro-scale MRI brain signatures and cellular and molecular mechanisms inferred from other data sources including post-mortem brain tissue [29,30], and animal models [31]. Examples of genes in the 22q11.2 locus that have been related to cortical structural phenotypes and which may have broad or region-specific effects on subcortical development include DGCR8, a gene involved in microRNA regulation, and AIFM3, a gene involved in apoptosis pathways [32].

In this longitudinal structural MRI study of reciprocal 22q11.2 CNV carriers and TD controls, across a wide age range (ages 5.5-49.5), we present the first investigation of the effects of gene dosage at the 22q11.2 locus on anatomical subregion volumes in the thalamus, hippocampus, and amygdala. We also characterize, for the first time, developmental trajectories of these subcortical volumes in individuals with 22q11.2 CNVs.

METHODS

Participants

The total longitudinal sample consisted of 385 scans from 213 participants (5.5–49.5 years of age; n=96 22qDel baseline; n=37 22qDup baseline; n=80 TD controls baseline; see Table 1, and Figure S1). Participants had data from 1-6 timepoints separated by an average of approximately 1.75 years. The groups were matched on baseline age and sex, mean number of longitudinal visits, and interval between visits. See Supplemental Methods for details on inclusion/exclusion criteria and clinical assessment. After study procedures had been fully explained, adult participants provided written consent, while participants under the age of 18 years provided written assent with the written consent of their parent/guardian. The UCLA Institutional Review Board approved all study procedures and informed consent documents.

Neuroimaging acquisition/preprocessing

All participants were imaged at the UCLA Center for Cognitive Neuroscience on either a Siemens TimTrio or Siemens Prisma scanner with the same T1-weighted (T1w) sequence [33]. Scan sessions at all timepoints were first processed cross-sectionally using the recon-all anatomical segmentation pipeline in FreeSurfer 7.3.2 [34–36]. The FreeSurfer longitudinal stream was subsequently applied, which has been shown to significantly improve reliability and statistical power in repeated measure analyses [37].

	TD	22qDel	22qDup	p-value
n	80	96	37	
Age, mean (SD)	14.89 (7.34)	15.52 (7.62)	17.83 (13.50)	0.24
Sex, n (%) Female	41 (51.3)	51 (53.1)	17 (45.9)	0.759
Full Scale IQ, mean (SD)	111.27 (19.28)	78.65 (12.74)	95.44 (17.84)	<0.001
SIPS Positive total, mean (SD)	1.23 (1.88)	5.86 (6.52)	2.96 (3.25)	<0.001
Psychosis Risk Symptoms, n (%)	4 (5.0)	24 (25.0)	5 (13.5)	0.002
Psychotic Disorder, n (%)	0 (0.0)	8 (8.3)	0 (0.0)	0.022
ADHD, n (%)	5 (6.2)	41 (42.7)	14 (37.8)	<0.001
Autism, n (%)	0 (0.0)	45 (46.9)	15 (40.5)	<0.001
Antipsychotic Med, n (%)	0 (0.0)	11 (11.5)	2 (5.4)	<0.001
Visit count, mean (SD)	1.62 (0.89)	1.99 (1.16)	1.73 (0.93)	0.058
Days between visits, mean (SD)	667.68 (546.90)	676.78 (383.58)	483.15 (111.84)	0.26
Visit 1 Prisma scanner, n (%)	25 (31.2)	23 (24.0)	16 (43.2)	0.090
Visit 2 Prisma scanner, n (%)	8 (22.9)	16 (29.6)	16 (100.0)	<0.001
Visit 3 Prisma scanner, n (%)	4 (36.4)	13 (46.4)	10 (100.0)	0.005
Visit 4-6 Prisma scanner, n (%)	4 (100.0)	15 (100.0)	1 (100.0)	NA

Table 2-1. Baseline Demographics. TD controls, 22qDel, and 22qDup with p-values for between group comparisons (ANOVA for continuous variables and chi-squared for categorical). Baseline cohorts are statistically matched based on age and sex as well as mean number of longitudinal visits and interval between visits. Cognition was measured with the Wechsler Abbreviated Scale of Intelligence-2 (WASI-2). Prodromal (psychosis-risk) symptoms were assessed with the Structured Interview for Psychosis-Risk Syndromes (SIPS). Psychosis Risk Symptoms are operationalized here as having any score of 3 or greater (i.e., prodromal range) on any SIPS positive symptom item. Psychotic disorder diagnosis is based on structured clinical interview (SCID) for DSM-IV/V and includes schizophrenia, schizoaffective disorder, brief psychotic disorder, and psychotic disorder not otherwise specified. The number and percentage of each group scanned on the Siemens Prisma scanner (versus Siemens Tim Trio) is reported at each time point.

Subcortical nuclei

For each scan, volume was estimated for the whole thalamus, amygdala, and hippocampus, and their subregions using Bayesian methods to automatically segment T1w images using template atlases based on histological data and ultra-high-resolution ex vivo MRI

[38–41]. These segmentations are well-validated and have been applied by multiple consortia to large scale neuroimaging analyses [42–46]. See Supplemental Figure S2 for visualization of the FreeSurfer segmentation and Supplemental Methods for a list of all regions analyzed as well as details on segmentation, qualitative and statistical quality control (QC) procedures, and between-scanner harmonization using longitudinal ComBat [47].

Gene dosage and maturational effects

To investigate the linear effect of CNV status on subcortical volumes, and to capture the non-linear relationship between age and volume, we used a generalized additive mixed model (GAMM) with a linear fixed effect for gene dosage, which was numerically coded by CNV status: 22qDel=1, TD=2, and 22qDup=3 copies of the 22q11.2 locus. Age was modeled with separate thin plate regression splines in each group [48], restricted to exactly 2 degrees of freedom to facilitate comparison [49]. GAMMs are a nonlinear extension of mixed effects regression, allowing for repeat visits to be modeled with a random intercept [50]. Biological sex and site were also included as fixed effects. Total intracranial volume (ICV) was included as a fixed effect in all models except where ICV was the dependent variable. ComBat-adjusted volumes for each region were normalized based on the TD mean and standard deviation.

Gene dosage effects were tested for total ICV, whole thalamus, hippocampus, and amygdala volumes, and 38 subregions. All tests were corrected for multiple comparisons using the standard False Discovery Rate (FDR) at a threshold of $q<0.05$ across the 42 volumes [51]. To characterize maturational trajectories, p-values for the non-linear effect of age in each group were computed and evaluated at $q<0.05$ across all 126 models. Age ranges of significant difference between CNV groups and controls were computed from the 95% confidence interval for the difference in curves.

Secondary analyses

Regional volume differences compared to the TD group were tested separately for 22qDel and 22qDup groups. Gene dosage analyses were also repeated without averaging structures bilaterally, to detect any asymmetric hemispheric effects. Secondary analyses of the interaction between sex and gene dosage on brain volumes were also tested. The effect of antipsychotic medication was also investigated.

Cognition and symptom analyses

Motivated by literature relating low hippocampal tail volume to verbal learning impairment in 22qDel [27], we assessed verbal and non-verbal IQ [Wechsler Abbreviated Scale of Intelligence (WASI-2) Vocabulary and Matrix subtest scaled scores] for associations with hippocampal tail volume in each group. Given the relationship between 22qDel and psychosis risk [9,26,52], we additionally tested relationships between psychosis risk symptoms and all subcortical volumes in the 22qDel group.

RESULTS

Gene dosage effects

Total ICV was positively related to gene dosage (Table 2, Figure 1). All other models controlled for ICV. Positive gene dosage effects on volume were observed for the whole hippocampus, but not the whole thalamus or amygdala.

Within the thalamus and amygdala, individual subregions showed significant gene dosage effects (Table 2, Figure 1). There were bi-directional gene dosage effects on thalamic volumes; negative gene dosage effects were observed for the mediodorsal and ventral lateral nuclei, while positive gene dosage effects were observed in the lateral posterior, lateral geniculate, and reuniens nuclei. Within the amygdala, positive gene dosage effects were observed for the accessory basal, paralaminar, and basal nuclei. Multiple hippocampal subregions exhibited positive gene dosage effects in line with the whole structure findings, with the strongest effect in the hippocampal tail.

Structure	Region	beta	p	FDR q	sig
whole brain	total ICV	0.28	1.3e-03	0.0038	*
whole volumes	whole thalamus	-0.03	7.0e-01	0.8	
	whole amygdala	0.14	8.7e-02	0.17	
	whole hippocampus	0.47	7.3e-07	7.7e-06	**
thalamus subregions	mediodorsal	-0.36	3.3e-05	0.00015	**
	ventral lateral	-0.30	1.3e-04	0.00046	**
	lateral posterior	0.22	1.8e-02	0.047	*
	lateral geniculate	0.37	9.1e-05	0.00038	**
	medial ventral (reuniens)	0.39	1.1e-04	0.00042	**
hippocampus subregions	GC ML DG	0.41	1.4e-05	7.3e-05	**
	CA4	0.42	9.8e-06	5.9e-05	**
	subiculum	0.47	1.3e-07	1.9e-06	**
	CA1	0.48	3.9e-06	2.8e-05	**
	molecular layer	0.49	1.2e-06	1e-05	**
	hippocampal fissure	0.54	2.2e-08	4.7e-07	**
	hippocampal tail	0.61	1.4e-09	5.9e-08	**
amygdala subregions	accessory basal nucleus	0.21	1.9e-02	0.048	*
	paralaminar nucleus	0.28	1.8e-03	0.005	*
	basal nucleus	0.31	4.5e-04	0.0014	**

Table 2-2. Gene dosage effects on subcortical volumes. Generalized additive mixed models (GAMMs) linearly predicting normalized brain volumes from gene dosage (22qDel=1, TD=2, 22qDup=3), controlling for sex, site, participant, and non-linear age effects. Gene dosage was positively related to total intracranial volume (ICV; all other models control for ICV), and whole hippocampus volume, but not to the whole thalamus or amygdala. Bi-directional effects within the thalamus and localized amygdala effects were observable at the subregion level. Gene dosage was negatively related to volume for thalamic mediodorsal and ventral lateral regions. All other subregions of the thalamus, hippocampus, or amygdala with significant effects exhibited positive relationships between gene dosage and volume. Results are presented for all whole structure volumes (whole thalamus, amygdala, hippocampus, and total intracranial volume), and for subregions with significant type I error corrected gene dosage effects. In the “sig” column, one star “*” indicates False Discovery Rate (FDR) q<0.05, and two stars “**” indicate both FDR significance and significance at Bonferroni adjusted □<0.05. Abbreviations; GC ML DG, granule cell and molecular layer of the dentate gyrus; CA, cornu ammonis.

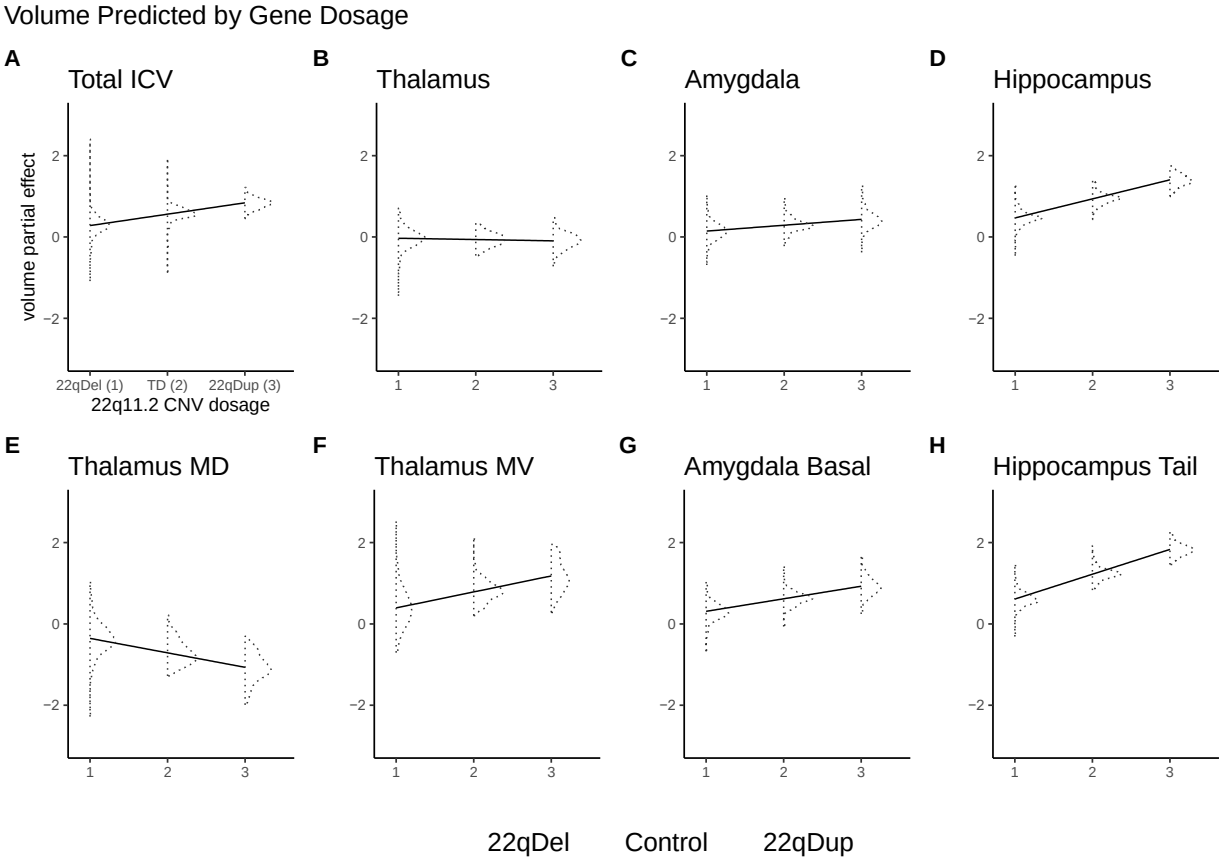

Figure 2-1. Visualization of gene dosage effects on selected volumes. Estimated linear partial effects of gene dosage on volume with 95% confidence intervals (CI) for the estimate. Red CI indicates significant positive gene dosage relationship (False Discovery Rate $q<0.05$), blue indicates significant negative relationship, and gray indicates no relationship. Partial residual scatterplots are shown for 22qDel (purple) control (green) and 22qDup (yellow), with kernel density estimates for each group in gray. A) Total intracranial volume (ICV). All other models control for ICV. B-D) There was a significant positive relationship between gene dosage and whole hippocampus volume, which was not observed for the thalamus or amygdala. E-F) Within the thalamus, some subregions (e.g., MD; mediodorsal) showed negative gene dosage-volume relationships, while others (e.g., MV; medial ventral) exhibited positive effects. G) Several amygdala subregions (e.g., basal nucleus) exhibited positive gene dosage effects, despite the whole amygdala having no relationship between gene dosage and volume. H) Significant hippocampal subregions (e.g., hippocampal tail) had the same direction of effect as the whole hippocampus.

Maturational effects

GAMM analysis revealed multiple subcortical regions with significant age-related changes in each cohort (Figures 2&3, and Table S5). Overall, 22qDel and TD cohorts exhibited age-related changes across various subregions in the thalamus, hippocampus, and amygdala, while in 22qDup, age-related changes were only detected in thalamic regions and the hippocampal tail. All three groups exhibited significant age-related decreases in thalamic medial geniculate volumes, but medial geniculate volumes in 22qDup increased slightly after approximately age 30, whereas in the other groups they continued to decrease. Developmental trajectories after age 30 should be interpreted with caution, though, due to the lower number of participants in this age range. For this reason, we repeated the maturational analyses in a subset of participants under 35 years of age (Figures S4-7), finding broadly similar patterns to those observed in the analyses including the full age range.

Several regions exhibited significant age-related changes in only CNV carriers, but not TD controls (Figure 2). The anteroventral thalamus showed age effects in only 22qDel, involving steeper decreases in childhood and adolescence compared to the other groups (Figure 3). Ventral anterior thalamus results were similar. Medial ventral and laterodorsal thalamus showed significant age effects in only 22qDup, but the curves overlapped TD at all ages. Several hippocampus and amygdala subregions exhibited significant age effects in TD controls but neither CNV group. In the hippocampal CA2/3 and CA4 regions, TD controls exhibited an inverted-U-shaped developmental curve, which was mostly flattened in 22qDel and 22qDup (Figure 3). CA2/3 volumes in 22qDel were greater than TD between ages 5.5-8.8 and lower than TD between ages 14.7-26.1, with similar periods of difference for 22qDup versus TD (Table S5).

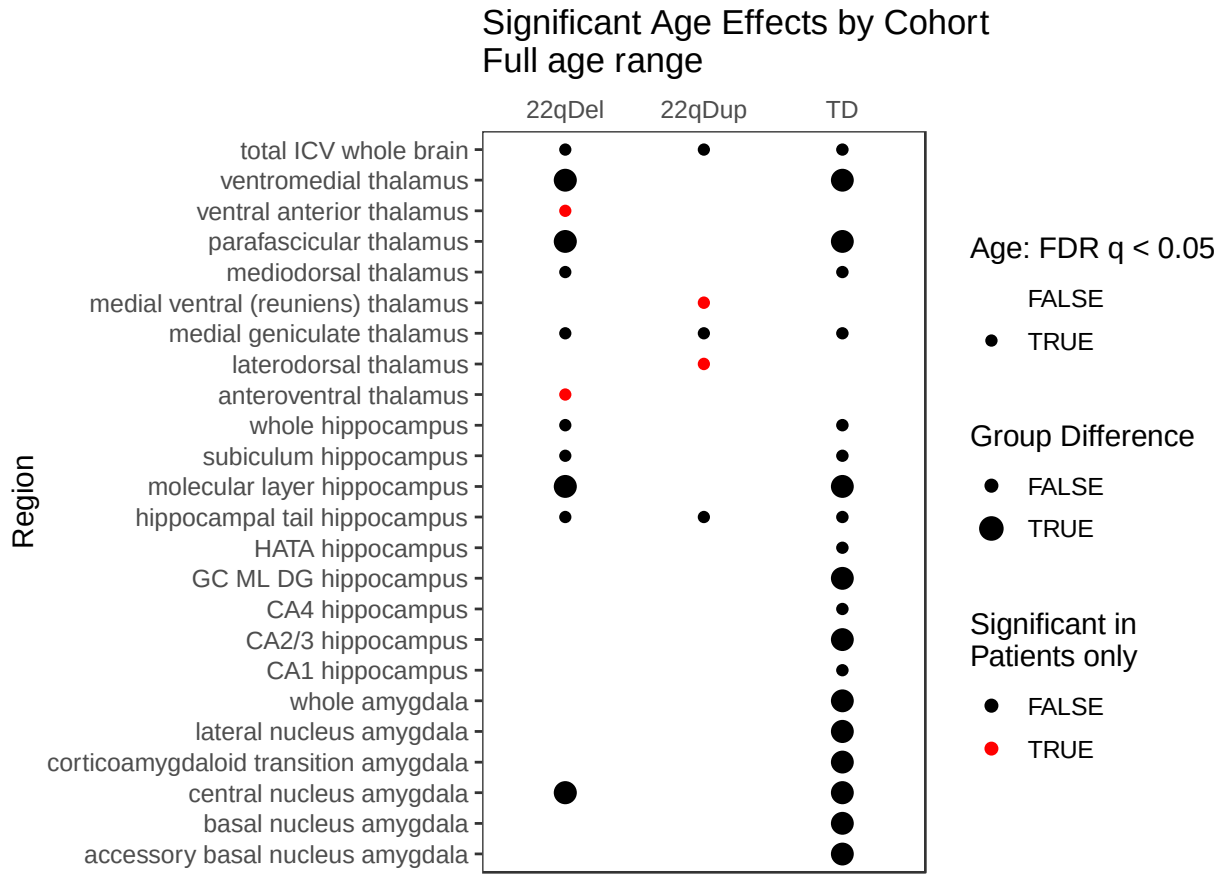

Figure 2-2. Summary of age effects on subcortical volumes. For each group, regions with FDR-corrected significant age effects on volume (q<0.05) are marked with a dark circle. Large circles indicate at least one age range with a significant difference between CNV patients (22qDel or 22qDup) and TD control age curves based on the 95% confidence interval (CI), whereas small circles indicate overlapping patient and control curves. Red circles indicate regions where the smoothed effect of age is significant in either patient group but not controls. Lines connect regions with significant age effects in all three groups. See Supplemental Figure S5 for results of the same GAMMs restricted to participants under 35 years of age.

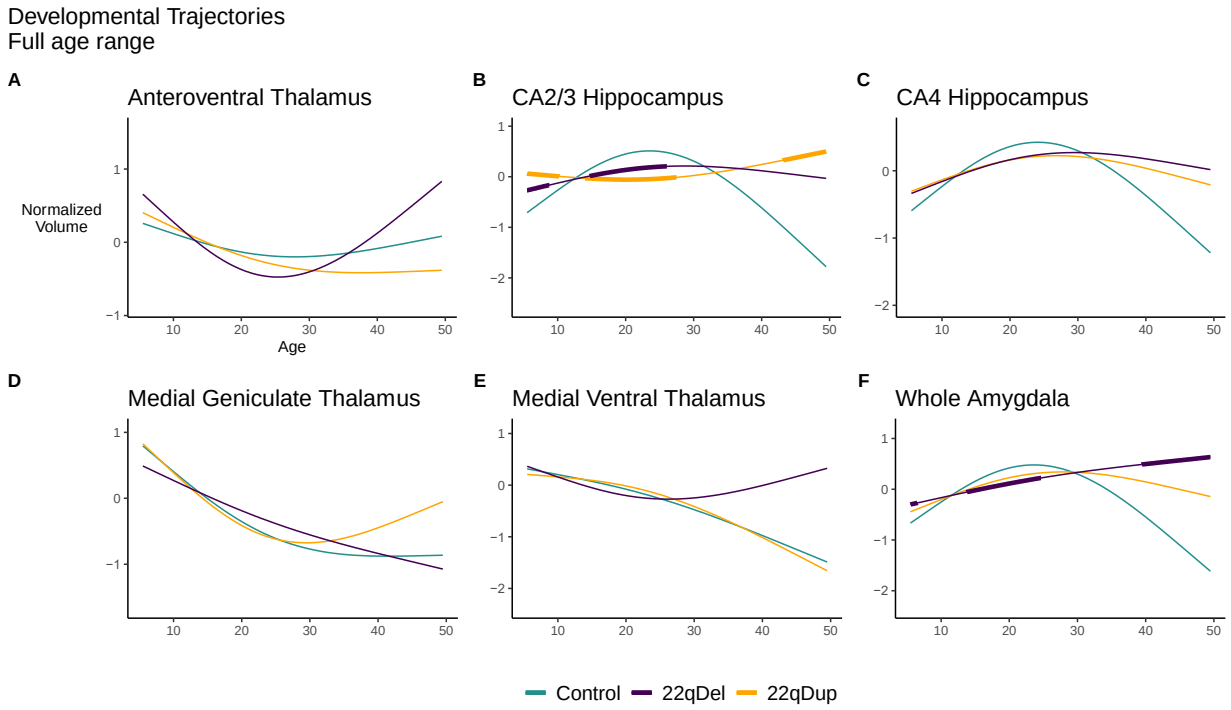

Figure 2-3. Selected age curves. GAMMs in 22qDel (purple), 22qDup (yellow/orange), and TD controls (green), showing the relationship between age and selected subregion volumes, controlling for covariates. Thick lines in the 22qDel and 22qDup curves indicate age ranges of significant difference from controls based on the 95% confidence interval. A) 22qDel experience steeper early life declines in anteroventral thalamus volume. B-C) In the hippocampal CA2/3 and CA4 regions, TD controls exhibit an inverted-U-shaped developmental curve, which is mostly flattened in both 22qDel and 22qDup. CA2/3 volumes in 22qDel and 22qDup were greater than TD in childhood, lower in early to middle adulthood, and potentially higher in later adulthood. D) All groups show significant age-related decreases in medial geniculate thalamus volumes. E) Medial ventral (reuniens) thalamus development is similar between groups, especially in childhood through early adulthood, but only 22qDup show a significant age effect. F) 22qDel whole amygdala development is flattened compared to controls. See Supplemental Figure S4 for the same curves with scatterplots of partial residuals for each participant, and Supplemental Figures S6-7 for GAMMs restricted to participants under age 35.

Secondary analyses

When tested in separate case-control analyses, 14 regions showed significant effects of 22qDel versus TD (Table S2), and one region (mediodorsal thalamus) showed a significant effect of 22qDup versus TD (Table S3), at a threshold of $q<0.05$ across the 86 tests across both groups.

Secondary analyses of separate left and right hemispheres showed strong concordance in gene dosage effects on regional volumes across both hemispheres (Table S4). Significant main effects of sex on subcortical volumes were found for 27 regions (see Table S6). However, no

significant interactions were found with gene dosage. Additionally, when the gene dosage analysis was repeated with the addition of a covariate for antipsychotic medication status, the results were highly comparable to the primary analysis (Table S7).

Cognition and symptom analyses

Hippocampal tail volume in 22qDel was significantly associated with Verbal IQ (□=1.86, p=0.011) but not Nonverbal IQ; however, no relationships were observed in the 22qDup or TD groups. See Figure S3 for scatter plots and p-values in all groups.

No subcortical regions were found to exhibit significant relationships between volume and either continuous or categorical measures of positive psychosis-risk symptoms in the 22qDel group. In the 22qDel group, no subcortical regions exhibited a significant relationship between antipsychotic medication status and volume.

DISCUSSION

This is the first study to systematically characterize the relationship between the dosage of genomic material at the 22q11.2 locus and the volumes of specific subcortical nuclei. It is also the first study to investigate longitudinal subcortical development in 22qDup. We used an accelerated longitudinal design to recruit an unprecedented sample of 22qDel and 22qDup carriers and TD controls, spanning from childhood to middle adulthood. Using linear and nonlinear mixed effects regression approaches to map gene dosage and age effects on regional volumes, we identified several novel findings, specifically: 1) gene dosage at the 22q11.2 locus is positively related to total intracranial and hippocampal volume, but not whole thalamus or amygdala volume; 2) 22q11.2 gene dosage has positive relationships to specific amygdala subregions, and bi-directional relationships to specific thalamic nuclei; and, 3) longitudinal development of subcortical structures is differentially altered in 22qDel and 22qDup across subcortical regions.

Gene dosage effects

Standardized beta effect sizes for gene dosage effects on volume were of similar magnitude to effect sizes from previous large studies of cortical and subcortical brain structure in neurodevelopmental CNVs including 22qDel [3,19] and idiopathic neurodevelopmental and psychiatric disorders [23,24]. For example, hippocampal volume was found to be -0.46 standard deviations in patients with schizophrenia compared to controls [24], compared to our whole hippocampus effect size of -0.85 standard deviations between 22qDel and TD (Table S2). Case-control effect sizes were somewhat smaller in 22qDup versus TD, with the single significant region (mediodorsal thalamus; Table S3), exhibiting an effect size of -0.44.

These findings extend prior work from Lin et al., who provided the first evidence for a gene dosage relationship to cortical thickness, surface area, ICV, and hippocampal volume in individuals with reciprocal 22q11.2 CNVs [18]. Anatomical subregions were not investigated in that study, but a shape analysis suggested that these structures may be non-uniformly impacted.

In that analysis, hippocampal thickness was found to be greater in 22qDup relative to 22qDel in regions roughly corresponding to the subiculum and CA1, which is corroborated by our current study. However, our approach did not find any regions of decreased hippocampal volume in 22qDup relative to 22qDel, whereas Lin et al. found support for some localized thickness decreases in 22qDup in regions approximately corresponding to CA2-4. Here, we expand on and broadly replicate the previous hippocampal findings in this larger longitudinal sample and have increased sensitivity to detect effects localized to specific nuclei.

Notably, within the thalamus we found bi-directional gene dosage effects across subregions. Volumes of the mediodorsal and ventral lateral nuclei decreased with increasing 22q11.2 copy number, whereas the opposite was observed for the lateral posterior, lateral geniculate and reuniens nuclei. Contrary to our hypothesis, the bi-directional effects did not follow a sensory/executive pattern; both the mediodorsal and reuniens nuclei have strong connections to the prefrontal cortex, whereas the ventral lateral, lateral posterior and lateral geniculate nuclei are more strongly connected to motor and visual cortex [53–55]. Interestingly, the reuniens nucleus, which exhibited the strongest thalamic effects, is a key hub in a network connecting the thalamus, hippocampus, and prefrontal cortex [56–58]. In 22qDel, bi-directional disruptions have been observed in functional connectivity of the thalamus and hippocampus to regions including the prefrontal cortex [59].

Analysis of hippocampal tail volume relationships to IQ suggests that this region may be particularly related to verbal cognition in 22qDel, but not 22qDup or TD. This broadly supports the recent finding of hippocampal tail volume relationships with verbal learning scores in 22qDel [27]. Our analysis was specifically motivated by this prior literature; however, this effect would not have remained significant after correction for multiple comparisons in an exploratory analysis of cognition relationships to all subregional volumes.

Exploratory analyses did not find significant psychosis-risk symptom/volume relationships. However, a large multi-site study of subcortical volumes in 22qDel did find evidence for lower

thalamus, hippocampus, and amygdala volumes in 22qDel individuals with psychotic disorder, compared to those without [19]. This suggests that, within the 22qDel population decreased subcortical volumes may only be detectable in those meeting full criteria for psychotic disorder, rather than subthreshold symptomatology. The current 22qDel sample was only powered to test psychosis-risk associations (Table 1).

Maturational effects

Studies of normative subcortical development often show volume increases in childhood followed by decreases later in life, and this pattern is particularly prominent in the hippocampus and amygdala [60–62]. We find that in hippocampal CA2/3, and to a lesser extent CA4, both 22qDel and 22qDup failed to exhibit the expected early life increases and adult decreases observed in TD. This was not observable in the whole hippocampus, where curves overlapped across the age range. Amygdala volumes in the three groups followed more similar developmental trajectories, except that in 22qDel volumes continued to increase in adulthood, while plateauing or decreasing in the other groups. All groups exhibited similar age-related decreases across many thalamic subregions. These trajectories were more linear compared to the hippocampus and amygdala. 22qDel had abnormally steep decreases in anteroventral thalamic volumes, a thalamic subregion implicated in spatial learning and memory [63]. The steep declines in 22qDel anteroventral thalamus volumes may reflect either an abnormal developmental mechanism, or compensatory changes related to the abnormally high volume in early childhood. A prior independent longitudinal study of 22qDel and TD using a similar thalamic parcellation found an overall pattern of age-related volume decreases resembling many of the thalamic age effects in our current study [26]. However, that study used linear models rather than nonlinear splines, and as such was not sensitive to differential rates of change across different age periods, which we observe for certain regions.

Our analyses of maturational trajectories build on recent longitudinal cortical findings of altered developmental trajectories of cortical thickness and surface area in 22q11.2 CNVs [48]. Jalbrzikowski et al. found that 22qDel, 22qDup, and TD controls all showed broad decreases in cortical thickness from childhood to adulthood, but the 22qDel group showed a protracted pattern of cortical thinning. 22qDup did not exhibit the same age-related cortical surface area decreases observed in TD and 22qDel.

Relationship to post-mortem human and animal model findings

The approach of mapping gene dosage effects on MRI-derived volumes to histologically-defined subcortical nuclei allows for more effective comparison between our neuroimaging results and findings from post-mortem brain tissue.

The strongest negative gene dosage effects were in the mediodorsal thalamus, a major source of thalamic input to the prefrontal cortex. This region has been highly studied in post-mortem brain tissue from individuals with schizophrenia, but findings are mixed, with several reporting decreased volumes and cell counts, and others reporting no differences to controls [29]. The strong effect we observe on this structure in 22q11.2 CNVs suggests a particular disruption of thalamic-prefrontal development that may be distinct from the changes underlying most idiopathic schizophrenia cases. Studies of the hippocampus in schizophrenia have demonstrated reductions in the volume and/or neuron number in subfields including the subiculum, CA1, CA2/3, and CA4 [64], which are consistent with our findings of decreased hippocampal volumes in 22qDel patients who are at increased risk for schizophrenia, compared to 22qDup who are at lower risk [14–16].

Subregion-specific analysis also helps connect results to animal model findings, which are often reported relative to these histological regions. Mouse models of 22qDel have repeatedly shown disruption to structure, function, and development of hippocampal regions CA1, CA2 and CA3 [65–67]. GABAergic inhibitory cells are particularly implicated in these disruptions.

Alterations in thalamic-cortical functional connectivity in 22qDel mice have been related to changes in the auditory thalamus mediated by microRNA processes downstream of the 22q11.2 gene Dgcr8, which have been corroborated in human post-mortem tissue from individuals with schizophrenia [68]. Dgcr8 haploinsufficiency has also been linked to decreased dendritic spine density in regions including hippocampal CA1 in a 22qDel mouse model [69].

Strengths, limitations, and future directions

Several strengths of this study should be considered in support of its reliability. The sample size of 191 scans from 96 participants with 22qDel, and 64 scans from 37 individuals with 22qDup is large for rare genetic disorders [70]. The 22qDup neuroimaging sample is unprecedented in size for that syndrome. Our large sample of 22q11.2 CNV carriers and TD controls spans a wide age range, allowing us to test important developmental hypotheses. However, the age distributions are right-skewed, and the data spanning middle adulthood were limited.

Our unique sample with identically acquired structural images from individuals with 22qDel, 22qDup, and TD controls allows for a powerful regression analysis approach in which approximate 22q11.2 gene dosage is operationalized as an integer value. This allows us to go beyond case-control differences to test specifically for brain phenotypes that are related to the content of genomic material in these reciprocal CNVs. While each carrier had a molecularly confirmed CNV at the 22q11.2 locus, breakpoints can vary in some cases [7]. However, breakpoints at this locus are largely consistent due to the pattern of low copy repeats flanking the region [9]. Breakpoint variation is thus not expected to strongly influence results. Gene dosage also likely does not fully reflect differences in gene transcription and translation in brain tissue, which are likely more closely linked to phenotypes, but cannot be measured in vivo or inferred from less invasively collected tissue such as blood [71,72]. Rather than solely focusing on case-control differences, the gene dosage effects detected by our model specifically represent instances where linear variations in the approximate gene dosage are predictive of significant

variation in regional volume. When tested in separate case-control analyses, 22qDel carriers show somewhat stronger effects on subcortical structures relative to TD than do 22qDup, which is consistent with the more severe neurobehavioral/cognitive phenotype in 22qDel [70,73,74]. The smaller 22qDup sample size may partially explain the finding of fewer statistically significant differences between 22qDup and TD compared to 22qDel and TD (Tables S2 and S3). While the differences between 22qDel and the other two groups may be driving some of the gene dosage findings, the results of the primary gene dosage models along with the supplemental case-control analyses are highly informative, highlighting that the overall trend for subcortical regions is towards linear gene dosage relationships to volume, rather than convergent effects in 22qDel and 22qDup. In other words, there are no regions for which 22qDel and 22qDup significantly differ from TD in the same direction.

Future directions of research include characterization of gene dosage effects in other reciprocal CNVs such as the 16p11.2 and 15q11-q13 loci and mapping subcortical development in individuals with idiopathic autism and those at clinical high risk (CHR) for psychosis to determine convergent (and/or divergent) patterns. Larger multi-site studies of 22q11.2 CNVs will be better-powered to elucidate possible roles of breakpoint variation, and brain-behavior relationships. Analysis of cytoarchitecture and gene expression in post-mortem tissue from individuals with 22q11.2 CNVs will also be highly informative. Research in animal and in vitro models will continue to bridge the gap to understanding circuit-level dysfunction, and the roles of individual genes and potential targeted pharmacological interventions.

Conclusions

This study is the first to characterize gene dosage effects on subregional subcortical volumes in individuals with reciprocal 22q11.2 CNVs, and the first study of longitudinal development of

subcortical structures in 22qDup. Using a linear mixed effects approach, we found positive gene dosage effects on total brain volume, hippocampal volumes, and several amygdala subregions, and bi-directional effects across multiple thalamic nuclei. GAMM analyses revealed both distinct and convergent disruptions in developmental trajectories in 22q11.2 CNVs across the thalamus, hippocampus, and amygdala. These results highlight the impact of genes in the 22q11.2 locus on subcortical brain development and motivate future research linking gene expression to brain phenotypes at the levels of cells, circuits, and macro-scale structures.

CHAPTER TWO AUTHOR CONTRIBUTIONS

Charles H. Schleifer: Conceptualization, Methodology, Software, Validation, Formal Analysis, Data Curation, Writing - Original Draft, Writing - Review & Editing, Visualization

Kathleen P. O'Hora: Data Curation, Methodology, Writing - Review & Editing

Hoki Fung: Data Curation, Methodology, Writing - Review & Editing

Jenny Xu: Data Curation, Writing - Review & Editing

Taylor-Ann Robinson: Data Curation

Angela S. Wu: Data Curation, Writing - Review & Editing

Leila Kushan-Wells: Investigation, Resources, Data Curation, Project Administration

Amy Lin: Data Curation

Christopher R. K. Ching: Conceptualization, Writing - Review & Editing

Carrie E. Bearden: Conceptualization, Investigation, Writing - Review & Editing, Supervision, Project Administration, Funding Acquisition.

Disclosures

All authors reported no biomedical financial interests or potential conflicts of interest.

Data availability

Data are publicly available from the National Institute of Mental Health Data Archives: https://nda.nih.gov/edit_collection.html?id=2414

To facilitate reproducibility and rigor, all analysis code is publicly available on GitHub: https://github.com/charles-schleifer/22q_subcort_volumes

A pre-print of this manuscript prior to peer review is hosted on bioRxiv: https://doi.org/10.1101/2023.10.31.564553

Funding

The work in this chapter was supported by the National Institute of Mental Health Grant Nos. R01 MH085953 (to C.E.B), U01MH101779 (to C.E.B); the Simons Foundation (SFARI Explorer Award to C.E.B), and the Joanne and George Miller Family Endowed Term Chair (to C.E.B.), the UCLA Training Program in Neurobehavioral Genetics T32NS048004 (to C.H.S), and the National Institute of Mental Health Grant F31MH133326-01 to (C.H.S.)

CHAPTER TWO REFERENCES

1. Hoeffding LK, Trabjerg BB, Olsen L, Mazin W, Sparsø T, Vangkilde A, et al. Risk of Psychiatric Disorders Among Individuals With the 22q11.2 Deletion or Duplication: A Danish Nationwide, Register-Based Study. JAMA Psychiatry. 2017;74:282–290.

2. Chawner SJRA, Doherty JL, Anney RJL, Antshel KM, Bearden CE, Bernier R, et al. A Genetics-First Approach to Dissecting the Heterogeneity of Autism: Phenotypic Comparison of Autism Risk Copy Number Variants. Am J Psychiatry. 2021;178:77–86.

3. Moreau CA, Ching CR, Kumar K, Jacquemont S, Bearden CE. Structural and functional brain alterations revealed by neuroimaging in CNV carriers. Curr Opin Genet Dev. 2021;68:88–98.

4. Provenzani U, Damiani S, Bersano I, Singh S, Moschillo A, Accinni T, et al. Prevalence and incidence of psychotic disorders in 22q11.2 deletion syndrome: a meta-analysis. Int Rev Psychiatry Abingdon Engl. 2022;34:676–688.

5. Weisman O, Guri Y, Gur RE, McDonald-McGinn DM, Calkins ME, Tang SX, et al. Subthreshold Psychosis in 22q11.2 Deletion Syndrome: Multisite Naturalistic Study. Schizophr Bull. 2017;43:1079–1089.

6. Girirajan S, Brkanac Z, Coe BP, Baker C, Vives L, Vu TH, et al. Relative burden of large CNVs on a range of neurodevelopmental phenotypes. PLoS Genet. 2011;7:e1002334.

7. Morrow BE, McDonald-McGinn DM, Emanuel BS, Vermeesch JR, Scambler PJ. Molecular genetics of 22q11.2 deletion syndrome. Am J Med Genet A. 2018;176:2070–2081.

8. Sayal K, Prasad V, Daley D, Ford T, Coghill D. ADHD in children and young people: prevalence, care pathways, and service provision. Lancet Psychiatry. 2018;5:175–186.

9. McDonald-McGinn DM, Sullivan KE, Marino B, Philip N, Swillen A, Vorstman JAS, et al. 22q11.2 deletion syndrome. Nat Rev Dis Primer. 2015;1:15071.

10. Ou Z, Berg JS, Yonath H, Enciso VB, Miller DT, Picker J, et al. Microduplications of 22q11.2 are frequently inherited and are associated with variable phenotypes. Genet Med Off J Am Coll Med Genet. 2008;10:267–277.

11. Ensenauer RE, Adeyinka A, Flynn HC, Michels VV, Lindor NM, Dawson DB, et al. Microduplication 22q11.2, an emerging syndrome: clinical, cytogenetic, and molecular analysis of thirteen patients. Am J Hum Genet. 2003;73:1027–1040.

12. Portnoï M-F. Microduplication 22q11.2: a new chromosomal syndrome. Eur J Med Genet. 2009;52:88–93.

13. Lin A, Vajdi A, Kushan-Wells L, Helleman G, Hansen LP, Jonas RK, et al. Reciprocal Copy Number Variations at 22q11.2 Produce Distinct and Convergent Neurobehavioral Impairments Relevant for Schizophrenia and Autism Spectrum Disorder. Biol Psychiatry. 2020;88:260–272.

14. Marshall CR, Howrigan DP, Merico D, Thiruvahindrapuram B, Wu W, Greer DS, et al. Contribution of copy number variants to schizophrenia from a genome-wide study of 41,321 subjects. Nat Genet. 2017;49:27–35.

15. Rees E, Kirov G, Sanders A, Walters JTR, Chambert KD, Shi J, et al. Evidence that duplications of 22q11.2 protect against schizophrenia. Mol Psychiatry. 2014;19:37–40.

16. Rees E, Walters JTR, Georgieva L, Isles AR, Chambert KD, Richards AL, et al. Analysis of copy number variations at 15 schizophrenia-associated loci. Br J Psychiatry J Ment Sci. 2014;204:108–114.

17. Sun D, Ching CRK, Lin A, Forsyth JK, Kushan L, Vajdi A, et al. Large-scale mapping of cortical alterations in 22q11.2 deletion syndrome: Convergence with idiopathic psychosis and effects of deletion size. Mol Psychiatry. 2020;25:1822–1834.

18. Lin A, Ching CRK, Vajdi A, Sun D, Jonas RK, Jalbrzikowski M, et al. Mapping 22q11.2 Gene Dosage Effects on Brain Morphometry. J Neurosci. 2017;37:6183–6199.

19. Ching CRK, Gutman BA, Sun D, Villalon Reina J, Ragothaman A, Isaev D, et al. Mapping Subcortical Brain Alterations in 22q11.2 Deletion Syndrome: Effects of Deletion Size and Convergence With Idiopathic Neuropsychiatric Illness. Am J Psychiatry. 2020;177:589–600.

20. Forstmann BU, de Hollander G, van Maanen L, Alkemade A, Keuken MC. Towards a mechanistic understanding of the human subcortex. Nat Rev Neurosci. 2017;18:57–65.

21. Kumar K, Modenato C, Moreau C, Ching CRK, Harvey A, Martin-Brevet S, et al. Subcortical Brain Alterations in Carriers of Genomic Copy Number Variants. Am J Psychiatry. 2023:appi.ajp.20220304.

22. Hibar DP, Stein JL, Renteria ME, Arias-Vasquez A, Desrivières S, Jahanshad N, et al. Common genetic variants influence human subcortical brain structures. Nature. 2015;520:224–229.

23. Boedhoe PSW, van Rooij D, Hoogman M, Twisk JWR, Schmaal L, Abe Y, et al. Subcortical brain volume, regional cortical thickness and cortical surface area across attention-deficit/hyperactivity disorder (ADHD), autism spectrum disorder (ASD), and obsessive-compulsive disorder (OCD). Am J Psychiatry. 2020;177:834–843.

24. van Erp TGM, Hibar DP, Rasmussen JM, Glahn DC, Pearlson GD, Andreassen OA, et al. Subcortical brain volume abnormalities in 2028 individuals with schizophrenia and 2540 healthy controls via the ENIGMA consortium. Mol Psychiatry. 2016;21:547–553.

25. Sherman SM. THE THALAMUS IS MORE THAN JUST A RELAY. Curr Opin Neurobiol. 2007;17:417–422.

26. Mancini V, Zöller D, Schneider M, Schaer M, Eliez S. Abnormal Development and Dysconnectivity of Distinct Thalamic Nuclei in Patients With 22q11.2 Deletion Syndrome Experiencing Auditory Hallucinations. Biol Psychiatry Cogn Neurosci Neuroimaging. 2020;5:875–890.

27. Latrèche C, Maeder J, Mancini V, Bortolin K, Schneider M, Eliez S. Altered developmental trajectories of verbal learning skills in 22q11.2DS: associations with hippocampal development and psychosis. Psychol Med. 2022:1–10.

28. Mancini V, Saleh MG, Delavari F, Bagautdinova J, Eliez S. Excitatory/Inhibitory Imbalance Underlies Hippocampal Atrophy in Individuals With 22q11.2 Deletion Syndrome With Psychotic Symptoms. Biol Psychiatry. 2023. 1 April 2023. https://doi.org/10.1016/j.biopsych.2023.03.021.

29. Dorph-Petersen K-A, Lewis DA. Postmortem structural studies of the thalamus in schizophrenia. Schizophr Res. 2017;180:28–35.

30. Steiner J, Brisch R, Schiltz K, Dobrowolny H, Mawrin C, Krzyżanowska M, et al. GABAergic system impairment in the hippocampus and superior temporal gyrus of patients with paranoid schizophrenia: A post-mortem study. Schizophr Res. 2016;177:10–17.

31. Fiksinski AM, Hoftman GD, Vorstman JAS, Bearden CE. A genetics-first approach to understanding autism and schizophrenia spectrum disorders: the 22q11.2 deletion syndrome. Mol Psychiatry. 2023;28:341–353.

32. Forsyth JK, Mennigen E, Lin A, Sun D, Vajdi A, Kushan-Wells L, et al. Prioritizing Genetic Contributors to Cortical Alterations in 22q11.2 Deletion Syndrome Using Imaging Transcriptomics. Cereb Cortex. 2021;31:3285–3298.

33. Jack Jr. CR, Bernstein MA, Fox NC, Thompson P, Alexander G, Harvey D, et al. The Alzheimer's disease neuroimaging initiative (ADNI): MRI methods. J Magn Reson Imaging. 2008;27:685–691.

34. FreeSurferMethodsCitation. https://surfer.nmr.mgh.harvard.edu/fswiki/FreeSurferMethodsCitation. Accessed 27 February 2023.

35. Fischl B, Salat DH, Busa E, Albert M, Dieterich M, Haselgrove C, et al. Whole brain segmentation: automated labeling of neuroanatomical structures in the human brain. Neuron. 2002;33:341–355.

36. Fischl B, van der Kouwe A, Destrieux C, Halgren E, Ségonne F, Salat DH, et al. Automatically parcellating the human cerebral cortex. Cereb Cortex N Y N 1991. 2004;14:11–22.

37. Reuter M, Schmansky NJ, Rosas HD, Fischl B. Within-subject template estimation for unbiased longitudinal image analysis. Neuroimage. 2012;61:1402–1418.

38. Iglesias JE, Augustinack JC, Nguyen K, Player CM, Player A, Wright M, et al. A computational atlas of the hippocampal formation using ex vivo, ultra-high resolution MRI: Application to adaptive segmentation of in vivo MRI. NeuroImage. 2015;115:117–137.

39. Iglesias JE, Van Leemput K, Augustinack J, Insausti R, Fischl B, Reuter M, et al. Bayesian longitudinal segmentation of hippocampal substructures in brain MRI using subject-specific atlases. NeuroImage. 2016;141:542–555.

40. Iglesias JE, Insausti R, Lerma-Usabiaga G, Bocchetta M, Van Leemput K, Greve DN, et al. A probabilistic atlas of the human thalamic nuclei combining ex vivo MRI and histology. Neuroimage. 2018;183:314–326.

41. Saygin ZM, Kliemann D, Iglesias JE, van der Kouwe AJW, Boyd E, Reuter M, et al. High-resolution magnetic resonance imaging reveals nuclei of the human amygdala: manual segmentation to automatic atlas. NeuroImage. 2017;155:370–382.

42. Sämann PG, Iglesias JE, Gutman B, Grotegerd D, Leenings R, Flint C, et al. FreeSurfer-based segmentation of hippocampal subfields: A review of methods and applications, with a novel quality control procedure for ENIGMA studies and other collaborative efforts. Hum Brain Mapp. 2022;43:207–233.

43. Grace S, Rossetti MG, Allen N, Batalla A, Bellani M, Brambilla P, et al. Sex differences in the neuroanatomy of alcohol dependence: hippocampus and amygdala subregions in a sample of 966 people from the ENIGMA Addiction Working Group. Transl Psychiatry. 2021;11:156.

44. Weeland CJ, Kasprzak S, de Joode NT, Abe Y, Alonso P, Ameis SH, et al. The thalamus and its subnuclei—a gateway to obsessive-compulsive disorder. Transl Psychiatry. 2022;12:70.

45. Huang AS, Rogers BP, Sheffield JM, Jalbrzikowski ME, Anticevic A, Blackford JU, et al. Thalamic Nuclei Volumes in Psychotic Disorders and in Youths With Psychosis Spectrum Symptoms. Am J Psychiatry. 2020;177:1159–1167.

46. Hoang D, Lizano P, Lutz O, Zeng V, Raymond N, Miewald J, et al. Thalamic, Amygdalar, and Hippocampal Nuclei Morphology and their Trajectories in First Episode Psychosis: A Preliminary Longitudinal Study. Psychiatry Res Neuroimaging. 2021;309:111249.

47. Beer JC, Tustison NJ, Cook PA, Davatzikos C, Sheline YI, Shinohara RT, et al. Longitudinal ComBat: A method for harmonizing longitudinal multi-scanner imaging data. NeuroImage. 2020;220:117129.

48. Jalbrzikowski M, Lin A, Vajdi A, Grigoryan V, Kushan L, Ching CRK, et al. Longitudinal trajectories of cortical development in 22q11.2 copy number variants and typically developing controls. Mol Psychiatry. 2022:1–10.

49. Larsen B, Bourque J, Moore TM, Adebimpe A, Calkins ME, Elliott MA, et al. Longitudinal Development of Brain Iron Is Linked to Cognition in Youth. J Neurosci. 2020;40:1810–1818.

50. Hastie TJ. Generalized Additive Models. Stat. Models S, Routledge; 1992.

51. Benjamini Y, Hochberg Y. Controlling the False Discovery Rate: A Practical and Powerful Approach to Multiple Testing. J R Stat Soc Ser B Methodol. 1995;57:289–300.

52. Jalbrzikowski M, Lin A, Vajdi A, Grigoryan V, Kushan L, Ching CRK, et al. Longitudinal trajectories of cortical development in 22q11.2 copy number variants and typically developing controls. Mol Psychiatry. 2022;27:4181–4190.

53. Georgescu IA, Popa D, Zagrean L. The Anatomical and Functional Heterogeneity of the Mediodorsal Thalamus. Brain Sci. 2020;10:624.

54. Kosif R. ‘The Thalamus: A Review of its Functional Anatomy’. Med Res Arch. 2016;4.

55. McFarland NR, Haber SN. Thalamic Relay Nuclei of the Basal Ganglia Form Both Reciprocal and Nonreciprocal Cortical Connections, Linking Multiple Frontal Cortical Areas. J Neurosci. 2002;22:8117–8132.

56. Dolleman-van der Weel MJ, Griffin AL, Ito HT, Shapiro ML, Witter MP, Vertes RP, et al. The nucleus reuniens of the thalamus sits at the nexus of a hippocampus and medial prefrontal cortex circuit enabling memory and behavior. Learn Mem. 2019;26:191–205.

57. Ferraris M, Cassel J-C, Pereira de Vasconcelos A, Stephan A, Quilichini PP. The nucleus reuniens, a thalamic relay for cortico-hippocampal interaction in recent and remote memory consolidation. Neurosci Biobehav Rev. 2021;125:339–354.

58. Herkenham M. The connections of the nucleus reuniens thalami: Evidence for a direct thalamo-hippocampal pathway in the rat. J Comp Neurol. 1978;177:589–609.

59. Schleifer C, Lin A, Kushan L, Ji JL, Yang G, Bearden CE, et al. Dissociable Disruptions in Thalamic and Hippocampal Resting-State Functional Connectivity in Youth with 22q11.2 Deletions. J Neurosci Off J Soc Neurosci. 2019;39:1301–1319.

60. Coupé P, Catheline G, Lanuza E, Manjón JV, Alzheimer's Disease Neuroimaging Initiative. Towards a unified analysis of brain maturation and aging across the entire lifespan: A MRI analysis. Hum Brain Mapp. 2017;38:5501–5518.

61. Bethlehem R a. I, Seidlitz J, White SR, Vogel JW, Anderson KM, Adamson C, et al. Brain charts for the human lifespan. Nature. 2022;604:525–533.

62. Dima D, Modabbernia A, Papachristou E, Doucet GE, Agartz I, Aghajani M, et al. Subcortical volumes across the lifespan: Data from 18,605 healthy individuals aged 3–90 years. Hum Brain Mapp. 2021;43:452–469.

63. Nelson AJD. The anterior thalamic nuclei and cognition: A role beyond space? Neurosci Biobehav Rev. 2021;126:1–11.

64. Roeske MJ, Konradi C, Heckers S, Lewis AS. Hippocampal volume and hippocampal neuron density, number and size in schizophrenia: a systematic review and meta-analysis of postmortem studies. Mol Psychiatry. 2021;26:3524–3535.

65. Al-Absi A-R, Thambiappa SK, Khan AR, Glerup S, Sanchez C, Landau AM, et al. Df(h22q11)/+ mouse model exhibits reduced binding levels of GABAA receptors and structural

and functional dysregulation in the inhibitory and excitatory networks of hippocampus. Mol Cell Neurosci. 2022;122:103769.

66. Piskorowski RA, Nasrallah K, Diamantopoulou A, Mukai J, Hassan SI, Siegelbaum SA, et al. Age-Dependent Specific Changes in Area CA2 of the Hippocampus and Social Memory Deficit in a Mouse Model of the 22q11.2 Deletion Syndrome. Neuron. 2016;89:163–176.

67. Drew LJ, Stark KL, Fénelon K, Karayiorgou M, MacDermott AB, Gogos JA. Evidence for altered hippocampal function in a mouse model of the human 22q11.2 microdeletion. Mol Cell Neurosci. 2011;47:293–305.

68. Chun S, Du F, Westmoreland JJ, Han SB, Wang Y-D, Eddins D, et al. Thalamic miR-338-3p mediates auditory thalamocortical disruption and its late onset in models of 22q11.2 microdeletion. Nat Med. 2017;23:39–48.

69. Stark KL, Xu B, Bagchi A, Lai W-S, Liu H, Hsu R, et al. Altered brain microRNA biogenesis contributes to phenotypic deficits in a 22q11-deletion mouse model. Nat Genet. 2008;40:751–760.

70. Sønderby IE, Ching CRK, Thomopoulos SI, van der Meer D, Sun D, Villalon-Reina JE, et al. Effects of copy number variations on brain structure and risk for psychiatric illness: Large-scale studies from the ENIGMA working groups on CNVs. Hum Brain Mapp. 2022;43:300–328.

71. Lin A, Forsyth JK, Hoftman GD, Kushan-Wells L, Jalbrzikowski M, Dokuru D, et al. Transcriptomic profiling of whole blood in 22q11.2 reciprocal copy number variants reveals that cell proportion highly impacts gene expression. Brain Behav Immun - Health. 2021;18:100386.

72. Aguet F, Brown AA, Castel SE, Davis JR, He Y, Jo B, et al. Genetic effects on gene expression across human tissues. Nature. 2017;550:204–213.

73. Lin A, Vajdi A, Kushan-Wells L, Helleman G, Hansen LP, Jonas RK, et al. Reciprocal Copy Number Variations at 22q11.2 Produce Distinct and Convergent Neurobehavioral Impairments Relevant for Schizophrenia and Autism Spectrum Disorder. Biol Psychiatry. 2020;88:260–272.

74. O'Hora KP, Kushan-Wells L, Hoftman GD, Jalbrzikowski M, Gur RC, Gur R, et al. Distinct Neurocognitive Profiles and Clinical Phenotypes Associated with Copy Number Variation at the 22q11.2 Locus. MedRxiv Prepr Serv Health Sci. 2023:2023.05.12.23289905.

CHAPTER TWO SUPPLEMENTAL MATERIAL

Supplemental Methods

Participants

The total longitudinal sample consisted of 385 scans from 213 participants (5.5–49.5 years of age; n=96 22qDel baseline, 53.1% female; n=37 22qDup baseline, 45.9% female; n=80 TD controls baseline, 51.3% female), recruited from an ongoing longitudinal study at the University of California, Los Angeles (UCLA). The 22qDel and 22qDup participants all had a molecularly confirmed 22q11.2 CNV. Participants had data from between 1 and 6 time points (mean=1.81 visits, SD=1.04), separated by an average of approximately one- and three-quarter years (mean=1.76 years, SD=1.16). The three groups were statistically matched based on baseline age and sex, as well as mean number of longitudinal visits and interval between visits, using appropriate tests (ANOVA, or chi-squared). Exclusion criteria for all study participants were as follows: significant neurological or medical conditions (unrelated to 22q11.2 deletion or duplication) that might affect brain structure, history of head injury with loss of consciousness, insufficient fluency in English, and/or substance or alcohol use disorder within the past 6 months. As we aimed to include a representative cohort of CNV carriers, patients with cardiac-related and/or immune issues were not excluded, as these are common medical comorbidities in 22qDel. Healthy controls were free from significant intellectual disability and/or family history of psychotic disorder, and did not meet criteria for any psychiatric disorder, with the exception of attention deficit-hyperactivity disorder, anxiety disorders, or a past episode of depression, due to their prevalence in childhood and adolescence [1–3]. After study procedures had been fully explained, adult participants provided written consent, while participants under the age of 18 years provided written assent with the written consent of their parent or guardian. The UCLA Institutional Review Board approved all study procedures and informed consent documents.

Clinical assessment

At each study time point, demographic information and clinical measures were collected for each participant by trained Master's-level clinicians, supervised by a licensed clinical psychologist. Psychiatric diagnoses were established with the Structured Clinical Interview for DSM-IV (SCID), with an additional developmental disorders module [4]. Verbal IQ was assessed via the Wechsler Abbreviated Scale of Intelligence (WASI-2) Vocabulary subtest, and nonverbal IQ was assessed via the WASI-2 Matrix Reasoning subtest. Dimensional psychosis-risk and general psychiatric symptoms were assessed via the Structured Interview for Psychosis-Risk Syndromes (SIPS) [5]. For more details on study ascertainment and recruitment procedures, see Jalbrzikowski et al. 2012 and 2013 [6,7].

Neuroimaging acquisition

All subjects were imaged at the UCLA Center for Cognitive Neuroscience on either a Siemens TimTrio scanner (with a 12-channel head coil) or Siemens Prisma (with a 32-channel head coil). T1w scans were acquired in sagittal slices with 1mm3 voxels, as described in Jalbrzikowski et al. 2022 [8], using MPRAGE sequences adapted from the Alzheimer's Disease Neuroimaging Initiative (ADNI) protocol [9]. Trio and Prisma MPRAGE scans used nearly identical parameters: TR = 2.3 s, FOV = 256 mm, matrix = 240 × 256, flip angle = 9°, slice thickness = 1.20 mm, 160 slices. TE was 2.91 ms for Trio scans, and 2.94 ms for Prisma.

Neuroimaging preprocessing

T1w MRI scans were processed with the FreeSurfer analysis package, version 7.3.2 [10]. Scan sessions at all timepoints were first processed cross-sectionally using the recon-all anatomical segmentation pipeline [11,12]. The FreeSurfer longitudinal stream was subsequently applied, which has been shown to significantly improve reliability and statistical power in repeated-measure analyses [13]. This method generates unbiased within-subject templates using robust,

inverse consistent registration, and uses these templates to improve initialization of several processing steps, such as skull-stripping, Talairach transforms, atlas registration, spherical surface maps, and parcellations [13].

Subcortical nuclei volumes

For each MRI scan, the FreeSurfer longitudinal segment subregions pipeline was used to estimate volumes for 25 thalamic subregions, 19 hippocampal subregions, and 9 amygdala subregions, as well as whole-structure volumes [14–17]. These methods use Bayesian inference to automatically segment T1w MRI images using probabilistic template atlases based on histological data and ultra-high-resolution ex vivo MRI. These segmentations have been highly validated and have been applied by multiple groups and consortia to large scale neuroimaging analyses of development and group differences in various psychiatric conditions [18–22]. For analysis, several hippocampal subregions were combined as follows: the head and tail of hippocampal CA1 were added to give a single CA1 volume, similarly for CA2/3, CA4, molecular layer, GC-ML-DG, presubiculum, and subiculum, as in Mancini et al. 2010, and Latrèche et al. 2023) [23,24]. Hippocampal regions CA2 and CA3 are combined into a single CA2/3 region in the FreeSurfer segment subregions atlas due to difficulty reliably determining the boundary between regions [14]. In the thalamus several regions were combined, as in Huang et al. 2020 [21]: the mediodorsal medial and lateral regions were combined to give one mediodorsal region; the ventral lateral anterior and posterior subregions were combined into one ventral lateral region; the ventral anterior and ventral anterior magnocellular regions were combined into one ventral anterior region; the anterior, lateral, and inferior pulvinar were combined into one pulvinar region.

The full list of analyzed regions is as follows. Amygdala: accessory basal, anterior amygdaloid, basal, central, cortical, corticoamygdaloid transition, lateral, medial, and paralaminar. Hippocampus (body + head volume summed for all relevant regions): CA1, CA2/3, CA4, granule cell and molecular layer of the dentate gyrus (GC ML DG), fimbria, hippocampal amygdala

transition area, hippocampal fissure, hippocampal tail, molecular layer, parasubiculum, presubiculum, and subiculum. Thalamus: anteroventral, central lateral, central medial, centromedian, lateral geniculate, lateral posterior, laterodorsal, limitans suprageniculate, medial geniculate, medial ventral reuniens, mediodorsal (medial+lateral), parafascicular, pulvinar (anterior + lateral + inferior, excluding unreliable medial subregion), ventral anterior (ventral anterior + magnocellular), ventral lateral (posterior + anterior), ventral posterolateral, and ventromedial.

For the primary analyses, regional volumes were averaged within subjects between left and right hemispheres to reduce multiple comparisons and facilitate interpretation. See Supplemental Results Table S4 for bilateral gene dosage analyses without this averaging step. An example image was generated for visualization purposes (see Figure S2) using the FreeSurfer recon-all and segment subregions pipelines with the MNI152 template brain as the input [25].

Quality control

Several qualitative and quantitative approaches were taken to prevent inclusion of inaccurately estimated volumes in the analysis. First, each raw T1w image was visually assessed for quality prior to preprocessing, and excluded if quality was low (e.g., significant motion artifact, signal loss, or incomplete brain coverage). After subcortical segmentation, each image was visually checked to ensure alignment of thalamus, hippocampus, and amygdala masks with their associated structures. In four scans, bilateral thalamic volumes were excluded from further analysis because the thalamic segmentation was found to include parts of the striatum. We also excluded the medial pulvinar from further analysis in all subjects because the boundaries of the medial pulvinar mask were observed to extend beyond the thalamus in many cases. Finally, we calculated the mean and standard deviation of each subregion volume in the full cohort, and for each individual, excluded a given subregion from further analysis if the volume was greater than 3 standard deviations absolute difference from the overall group mean. Out of the total set of

33,196 regions from 386 subjects, 139 total regions across 67 subjects were flagged for exclusion by this metric. Two additional thalamic regions, the paracentral and paratenial nuclei, were excluded because the average volume was found to be less than 10 mm3 in each group. For the main analyses, volumes were averaged bilaterally except in the cases where a region had been excluded as an outlier in one hemisphere, in which case the non-outlier volume was used.

Data harmonization

To harmonize data acquired on two different scanners, we applied a longitudinal implementation of the ComBat algorithm using the longComBat package in R version 4.2.2 [26,27]. ComBat uses empirical Bayes methods to estimate and remove scanner/batch effects with increased robustness to outliers in small samples compared to general linear model approaches. ComBat was initially developed for genomics data [27], and has been subsequently adapted for neuroimaging and shown to preserve biological associations while effectively removing unwanted non-biological variation associated with site/scanner [28]. The longitudinal adaptation, which uses random effects to account for within-subject repeated measures, has been shown to further increase statistical power in longitudinal neuroimaging analyses [26]. LongComBat has been used to harmonize structural and functional MRI features in largely overlapping cohorts of individuals with 22qDel and controls [8,29]. LongComBat requires that the input data matrix not contain missing values, so for regions that were to be excluded from the final analysis, we imputed values based on the mean of that region's volume in individuals collected on the same scanner (Trio or Prisma) with the same CNV status (22qDel, 22qDup, or TD). Excluded volumes were then set to "NA" after longComBat harmonization, prior to regression analysis.

Gene dosage and maturational effects

To investigate the linear effect of CNV status on subcortical volumes, and to capture the non-linear relationship between age and volume, we used a generalized additive mixed model

(GAMM) approach with a linear fixed effect for gene dosage, which was numerically coded based on CNV status: 22qDel=1, TD=2, and 22qDup=3 copies of the 22q11.2 locus. Age was modeled with separate flexible thin plate regression splines in each group [8], restricted to exactly 2 degrees of freedom (DoF) per group to facilitate comparison [30]. GAMMs are a nonlinear extension of mixed effects regression, allowing for repeat visits from the same participant to be modeled with a random intercept [31]. Biological sex and site were also included as fixed effects in each model. Total intracranial volume (ICV) was included as a fixed effect in all models except where ICV was the dependent variable. Models were fit with restricted estimation of maximum likelihood, using mgcv in R [32]. Prior to testing, the ComBat-adjusted volume for each region was normalized based on the TD group mean and standard deviation.

An example R mgcv::gam formula for a GAMM to model the volume in a given region is:

volume ~ s(age, by = group, bs = "tp", k = 3, fx = TRUE) + gene_dosage + sex + icv + site + s(subject_id, bs = "re", k = 3)

In which regional volume is predicted by an age smooth in each group using thin plate regression splines with exactly k-1=2 DoF per smooth, with linear fixed effects for gene dosage, sex, total ICV, site, and a random effect for subject ID accounting for repeat visits.

Gene dosage effects were tested using this model for total ICV and whole thalamus, hippocampus, and amygdala volumes, followed by each of the 38 subregions. All tests were corrected for multiple comparisons using the standard False Discovery Rate (FDR) at a threshold of $q<0.05$ across the 42 volumes [33].

To characterize maturational trajectories, p-values for the non-linear effect of age in each group were computed and evaluated at $q<0.05$ across all 126 models. Age ranges of significant difference between CNV groups and controls were computed from the 95% confidence interval for the difference in curves.

Secondary analyses

Several secondary analyses were performed to complement the primary gene dosage analyses. Regional volume differences compared to the TD group were tested separately for 22qDel and 22qDup groups. Gene dosage analyses were repeated with antipsychotic medication status as an additional covariate. Additional models of antipsychotic status effects on volume were tested in only 22qDel, which was the only group with multiple more than 10% of participants taking antipsychotic medication. Gene dosage analyses were also repeated without averaging structures bilaterally to detect any asymmetric hemispheric effects. Secondary analyses of the interaction between sex and gene dosage on brain volumes were also tested.

Cognition and symptom analyses

Motivated by existing literature relating low hippocampal tail volume to verbal learning impairment in 22qDel [23], we assessed verbal and non-verbal IQ (Wechsler Abbreviated Scale of Intelligence (WASI-2) Vocabulary and Matrix subtest scaled scores) for associations with hippocampal tail volume in each group. A recent study of hippocampal volumes in 22qDel from another research group found that decreased hippocampal tail volume was associated with impaired development of verbal learning [23]. Here we sought to replicate that finding and extend to 22qDup. In each group (22qDel, 22qDup, and TD) we tested a linear mixed model predicting verbal and non-verbal IQ (WASI-2 Vocabulary Verbal and Matrix Reasoning subtest scaled scores) from hippocampal tail volume, controlling for sex and scanner, with a random intercept for subject ID. See Supplemental Figure S3 for results.

Because 22qDel is associated with psychosis risk, we tested relationships between psychosis risk symptoms and subcortical volumes in the 22qDel group. Specifically, we tested models relating positive symptom scores from the Structured Interview for Psychosis-Risk Syndromes (SIPS) [5] to volume across each region, controlling for age, age2, sex, and scanner, with a random intercept for each individual participant. We also similarly tested models relating volume to categorical diagnosis of Psychosis Risk Symptoms, operationalized here as having any score of 3 or greater (i.e., prodromal range) on any SIPS positive symptom item.

Supplemental Results

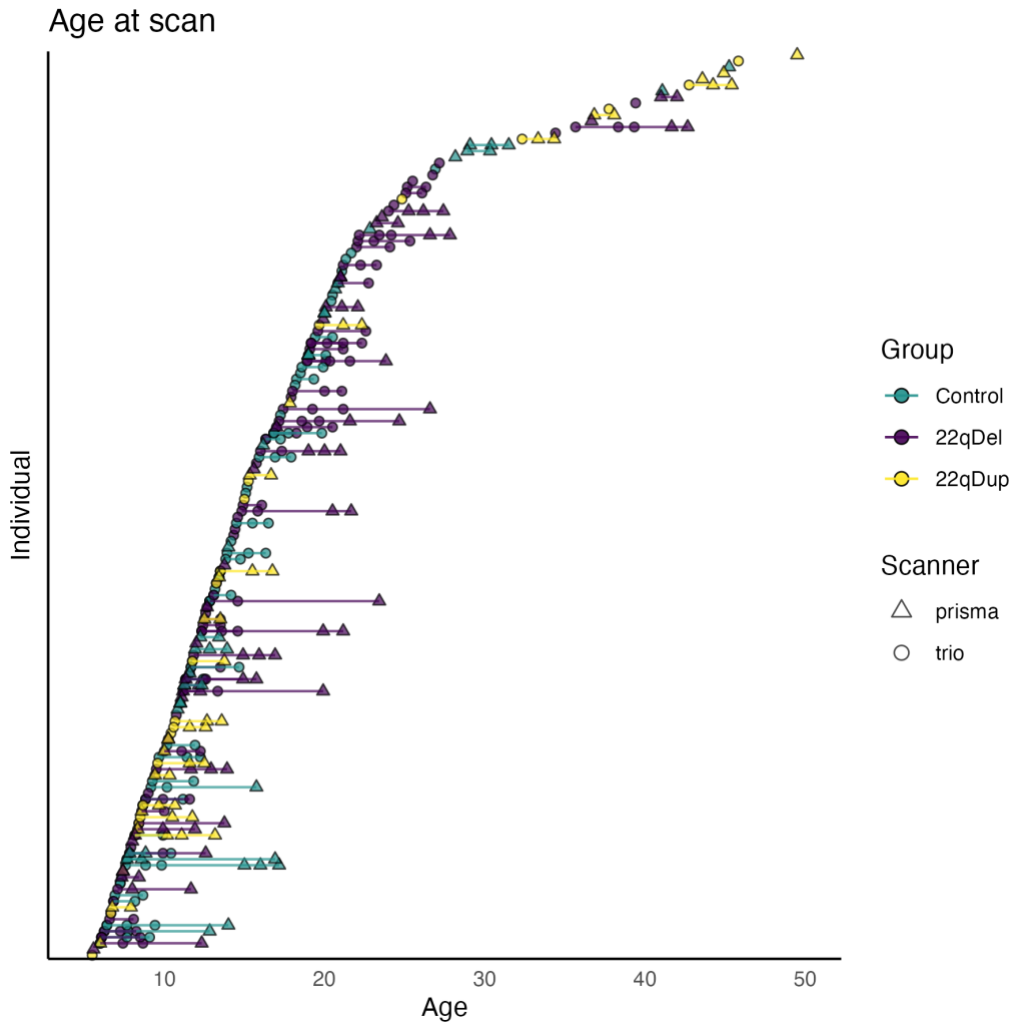

Figure 2-S1. Participant age distribution. Typically developing controls in green, 22qDel in purple, and 22qDup in yellow, with lines connecting follow-up visits from the same individual. Scanner type (Siemens Trio or Prisma) indicated by circle or triangle, respectively.

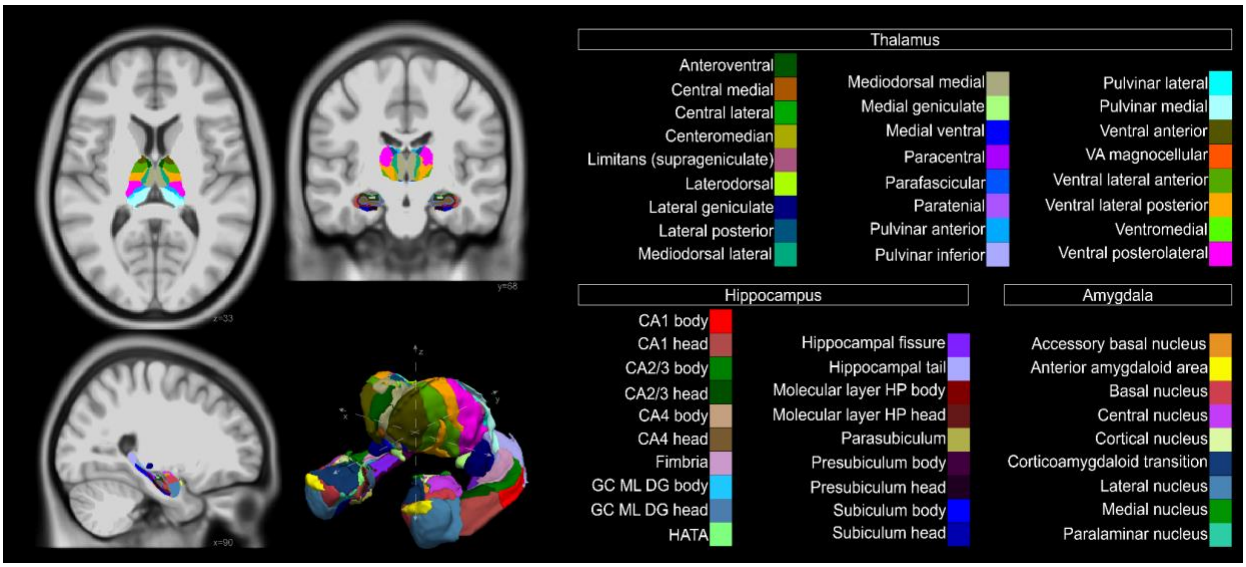

Figure 2-S2. Anatomical parcellation of thalamus, hippocampus, and amygdala nuclei. *Left:* axial, coronal, and sagittal slices, and 3D reconstruction of structures. Generated for visualization purposes using the FreeSurfer recon-all and segment subregions pipelines with the MNI152 template brain as the input. *Right:* structure names and color key. Abbreviations: VA = Ventral Anterior, CA = Cornu Ammonis (areas 1, 3 and 4), GC ML DG = Granule Cell and Molecular Layer of the Dentate Gyrus, HATA = Hippocampus Amygdala Transition Area, HP = Hippocampus.

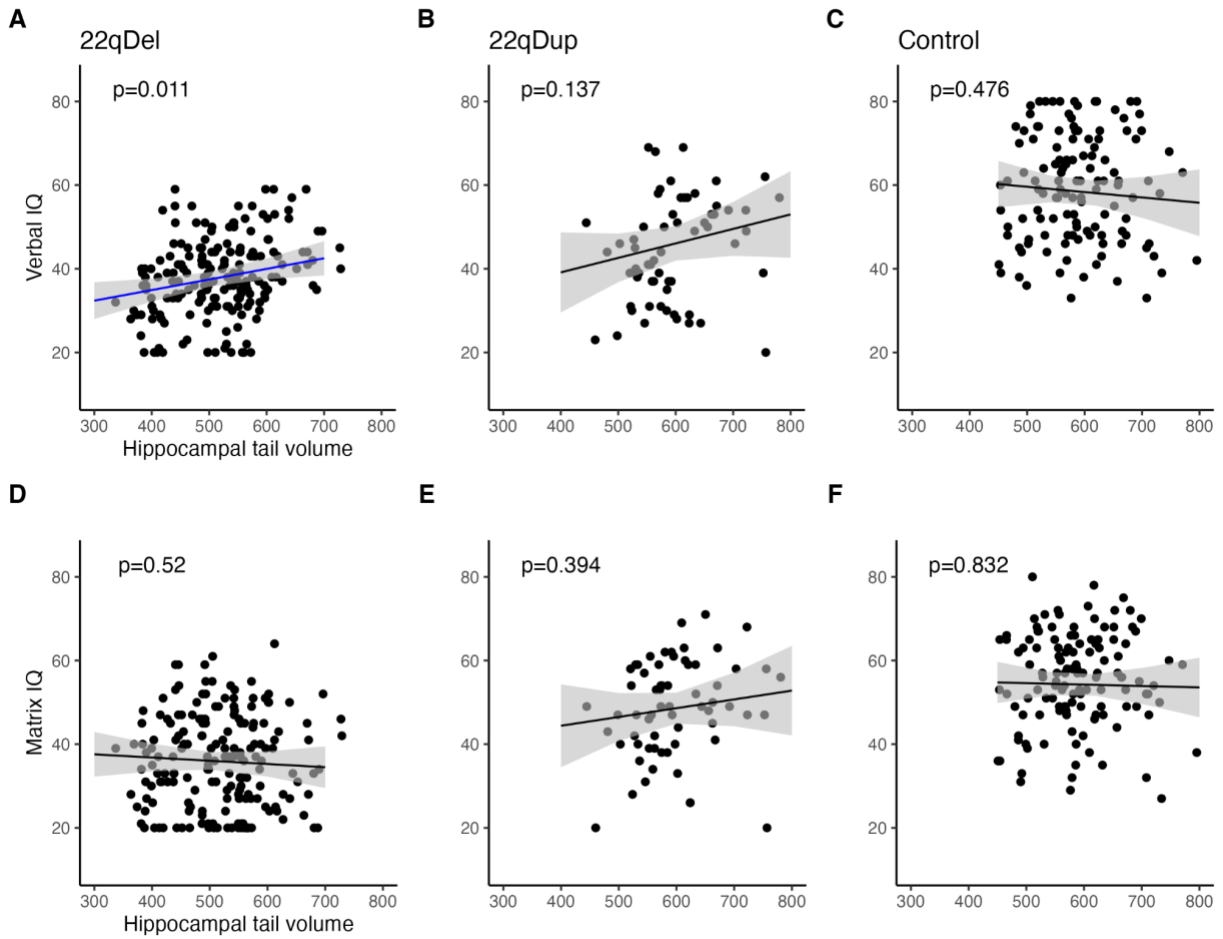

Figure 2-S3. Relationships between IQ subtests and hippocampal tail volume. A-C) WASI-2 Verbal IQ scaled scores were significantly predicted by hippocampal tail volume controlling for sex, site, and participant in 22qDel (*beta*=1.86, *p*=0.011) but not 22qDup or TD controls. D-F) Matrix Reasoning (Nonverbal IQ) subscale scores were not related to hippocampal tail volume in any group. Adding Nonverbal IQ as a covariate in the model predicting Verbal IQ from hippocampal tail volumes increased the strength of the verbal IQ relationship in 22qDel (*beta*=2.07, *p*=0.0018).

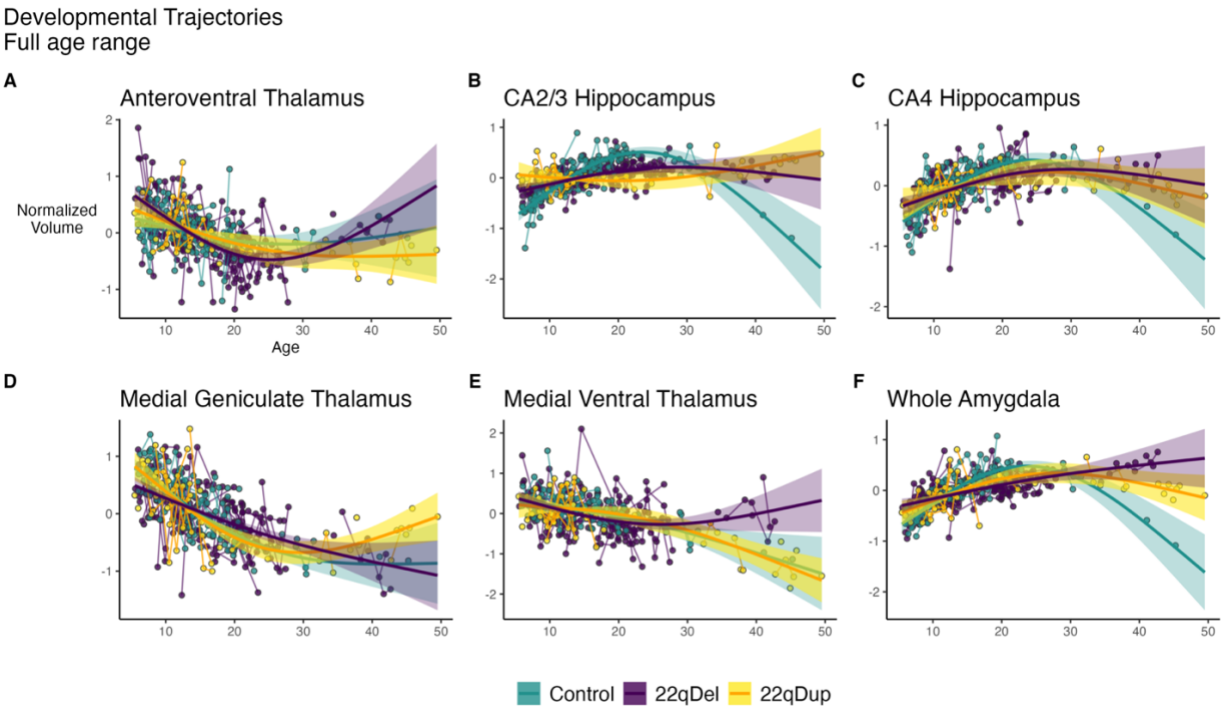

Figure 2-S4. Age curves with partial residuals. The same curves as main text Figure 3, with the addition of scatter plots for partial residuals for each scan, with repeat scans from the same individual connected with lines.

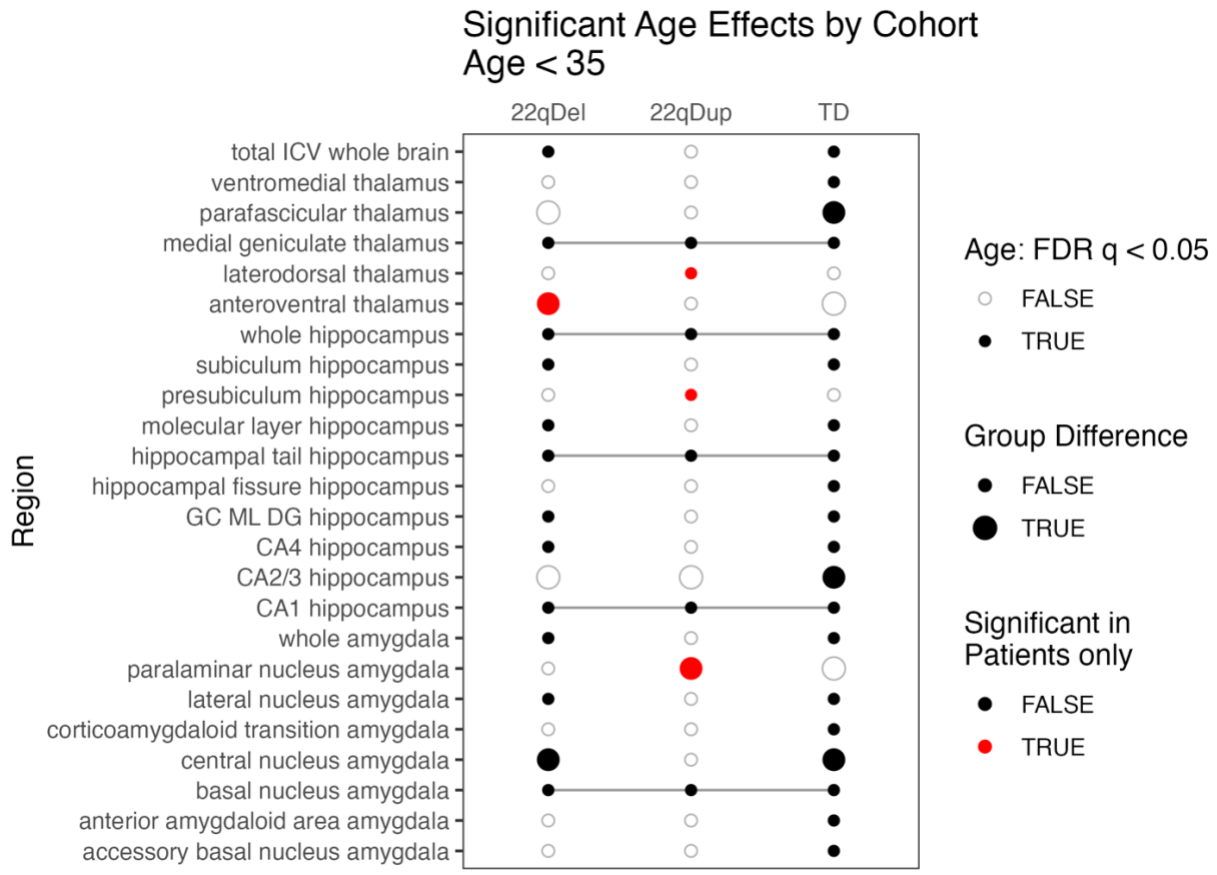

Figure 2-S5. Summary of age effects on subcortical volumes for participants under 35 years of age. Same as main text Figure 2, for models with the maximum age restricted to 35 years to exclude the relatively small set of subjects between ages 35 and 49.5 (n=13 excluded across all groups). Key results are similar: all three groups show significant age effects in the medial geniculate thalamus, 22qDel show steeper declines in anteroventral thalamus, and both 22qDel and 22qDup show flattened hippocampal CA2/3 development.

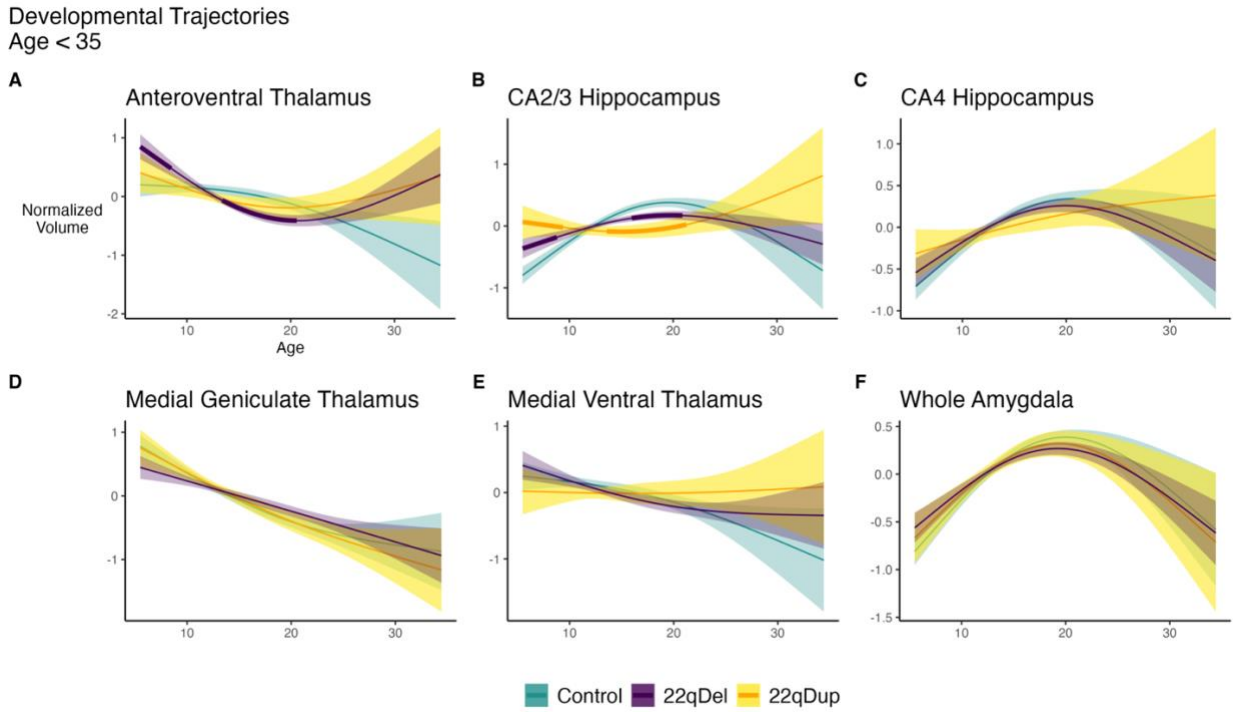

Figure 2-S6. Age curves with group differences, under 35 years old. The same plots as main text Figure 3, restricted to participants under 35 years of age. Key results are similar: all three groups show significant age effects in the medial geniculate thalamus, 22qDel show steeper declines in anteroventral thalamus, and both 22qDel and 22qDup show flattened hippocampal CA2/3 development.

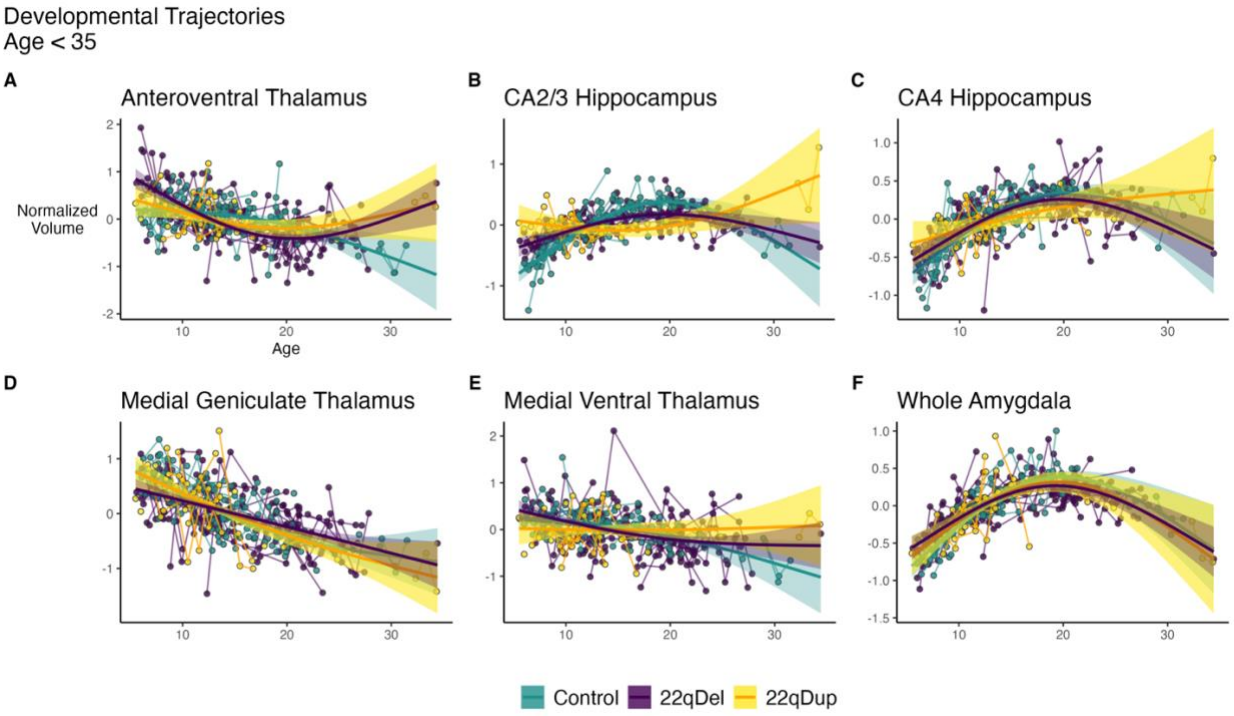

Figure 2-S7. Age curves with partial residuals, under 35 years old. The same plots as supplemental Figure S4, restricted to participants under 35 years of age.

Average volumes (mm^3) by group				
Structure	Region	22qDel	TD	22qDup
thalamus	medial ventral (reuniens)	14	16	16
thalamus	ventromedial	22	22	21
amygdala	cortical nucleus	24	26	24
amygdala	medial nucleus	24	27	25
thalamus	laterodorsal	30	31	33
thalamus	limitans (suprageniculate)	31	31	33
thalamus	central lateral	38	39	40
amygdala	central nucleus	46	50	50
amygdala	paralaminar nucleus	51	55	55
thalamus	parafascicular	54	58	57
hippocampus	hippocampal amygdala transition area	55	54	58
amygdala	anterior amygdaloid area	62	64	62
thalamus	central medial	76	81	81
hippocampus	parasubiculum	76	75	76
hippocampus	fimbria	82	86	90
thalamus	lateral posterior	113	121	125
thalamus	medial geniculate	124	141	137
hippocampus	hippocampal fissure	127	140	151
thalamus	anteroventral	133	144	150
amygdala	corticoamygdaloid transition	180	181	185
hippocampus	CA2/3	206	214	221
hippocampus	CA4	248	273	280
thalamus	centromedian	248	258	256
thalamus	lateral geniculate	258	289	284
amygdala	accessory basal nucleus	259	277	283
hippocampus	GC ML DG	283	312	316
hippocampus	presubiculum	303	315	310
hippocampus	subiculum	391	439	438
amygdala	basal nucleus	454	489	494
thalamus	ventral anterior	482	510	508
hippocampus	hippocampal tail	517	588	596
hippocampus	molecular layer	535	589	593
hippocampus	CA1	616	669	688
amygdala	lateral nucleus	640	659	659
thalamus	pulvinar	696	716	730
thalamus	ventral posterolateral	860	893	870
thalamus	mediodorsal	1202	1219	1159
thalamus	ventral lateral	1536	1543	1507
amygdala	whole amygdala	1740	1828	1838
hippocampus	whole hippocampus	3316	3616	3667
thalamus	whole thalamus	7091	7363	7294

Table 2-S1. Average volumes by group. Reported for whole thalamus, hippocampus, and amygdala and all analyzed subregions. Sorted by ascending volume in the 22qDel group.

Structure	Region	beta	p	FDR_q
thalamus	lateral geniculate	-0.73	5.2e-07	1.4e-05
	medial ventral (reuniens)	-0.60	6.7e-05	0.00092
	medial geniculate	-0.31	0.008	0.044
	parafascicular	-0.34	0.01	0.051
	mediodorsal	0.30	0.022	0.095
	lateral posterior	-0.25	0.11	0.33
	anteroventral	-0.30	0.12	0.35
	central medial	-0.24	0.15	0.42
	limitans (suprageniculate)	0.19	0.19	0.48
	ventral lateral	0.21	0.26	0.54
	laterodorsal	0.15	0.29	0.57
	ventral anterior	-0.14	0.41	0.67
	whole thalamus	-0.15	0.5	0.76
	pulvinar	-0.12	0.51	0.76
	centromedian	-0.05	0.75	0.91
	ventral posterolateral	-0.04	0.78	0.91
	ventromedial	-0.03	0.84	0.93
	central lateral	-0.02	0.87	0.93
hippocampus	hippocampal tail	-1.01	1.6e-07	1.3e-05
	subiculum	-0.94	3.5e-07	1.4e-05
	molecular layer	-0.91	1.6e-05	0.00032
	whole hippocampus	-0.85	4.2e-05	0.00069
	hippocampal fissure	-0.61	8.7e-05	0.00093
	GC ML DG	-0.78	9.1e-05	0.00093
	CA4	-0.75	0.00012	0.0011
	CA1	-0.77	0.00023	0.0019
	presubiculum	-0.25	0.14	0.41
	CA2/3	-0.22	0.18	0.48
	parasubiculum	0.21	0.2	0.49
	fimbria	-0.14	0.32	0.59
	hippocampal amygdala transition area	0.17	0.33	0.59
amygdala	basal nucleus	-0.54	0.0011	0.008
	medial nucleus	-0.46	0.0012	0.008
	paralaminar nucleus	-0.48	0.0014	0.0086
	accessory basal nucleus	-0.39	0.013	0.061
	cortical nucleus	-0.33	0.022	0.095
	whole amygdala	-0.36	0.027	0.11
	central nucleus	-0.30	0.043	0.16
	lateral nucleus	-0.17	0.23	0.51
	anterior amygdaloid area	-0.12	0.36	0.62
	corticoamygdaloid transition	0.11	0.51	0.76

Table 2-S2. 22qDel versus TD comparisons. Generalized additive mixed models (GAMMs) linearly predicting normalized brain volumes from group (22qDel or TD), controlling for sex, site, participant, total brain volume, and non-linear age in the full longitudinal sample.

Structure	Region	beta	p	FDR_q
thalamus	mediodorsal	-0.44	0.0077	0.044
	ventral posterolateral	-0.32	0.087	0.28
	limitans (suprageniculate)	0.31	0.11	0.33
	ventromedial	-0.24	0.2	0.49
	laterodorsal	0.24	0.22	0.51
	lateral posterior	0.23	0.24	0.53
	pulvinar	0.26	0.27	0.56
	central lateral	0.22	0.33	0.59
	ventral lateral	-0.17	0.38	0.65
	lateral geniculate	-0.16	0.41	0.67
	medial geniculate	-0.11	0.52	0.76
	medial ventral (reuniens)	0.07	0.71	0.91
	anteroventral	0.05	0.79	0.91
	ventral anterior	-0.04	0.81	0.92
	central medial	0.04	0.83	0.93
	whole thalamus	-0.04	0.86	0.93
	centromedian	0.03	0.9	0.94
	parafascicular	-0.02	0.92	0.94
hippocampus	hippocampal fissure	0.48	0.024	0.1
	hippocampal amygdala transition area	0.23	0.22	0.51
	fimbria	0.20	0.35	0.62
	CA1	0.17	0.44	0.71
	CA4	0.13	0.5	0.76
	CA2/3	0.10	0.62	0.9
	parasubiculum	0.10	0.67	0.91
	presubiculum	-0.19	0.67	0.91
	subiculum	-0.13	0.68	0.91
	GC ML DG	0.06	0.77	0.91
	whole hippocampus	0.08	0.79	0.91
	molecular layer	0.01	0.97	0.98
	hippocampal tail	0.00	0.99	0.99
amygdala	cortical nucleus	-0.37	0.048	0.17
	medial nucleus	-0.37	0.08	0.27
	anterior amygdaloid area	-0.17	0.31	0.59
	corticoamygdaloid transition	0.07	0.7	0.91
	basal nucleus	0.10	0.71	0.91
	paralaminar nucleus	0.79	0.75	0.91
	central nucleus	-0.07	0.75	0.91
	accessory basal nucleus	0.06	0.77	0.91
	whole amygdala	0.04	0.88	0.94
	lateral nucleus	-0.02	0.9	0.94

Table 2-S3. 22qDup versus TD comparisons. Generalized additive mixed models (GAMMs) linearly predicting normalized brain volumes from group (22qDup or TD), controlling for sex, site, participant, total brain volume, and non-linear age in the full longitudinal sample.

Structure	Region	Hemi	beta	p	FDR q
whole volumes	whole thalamus	L	-0.10	0.22	0.23
	whole thalamus	R	-0.00	0.97	0.97
	whole amygdala	R	0.11	0.18	0.19
	whole amygdala	L	0.13	0.15	0.17
	whole hippocampus	L	0.42	2.1e-05	6.9e-05
	whole hippocampus	R	0.46	1.5e-06	1.1e-05
thalamus subregions	mediodorsal	R	-0.35	8.7e-05	0.00017
	mediodorsal	L	-0.35	5.9e-05	0.00015
	ventral lateral	R	-0.31	7.9e-05	0.00017
	ventral lateral	L	-0.29	0.00024	0.00044
	ventral posterolateral	L	-0.21	0.013	0.016
	ventromedial	L	-0.21	0.013	0.016
	lateral posterior	R	0.24	0.018	0.021
	anteroventral	L	0.27	0.004	0.0051
	medial ventral (reuniens)	R	0.34	0.00072	0.0011
	medial ventral (reuniens)	L	0.43	6.2e-05	0.00015
	lateral geniculate	R	0.46	1.8e-06	1.1e-05
hippocampus subregions	fimbria	R	0.31	0.0023	0.0033
	GC ML DG	L	0.36	0.00036	0.00062
	CA4	L	0.37	0.00023	0.00043
	CA1	L	0.38	0.00059	0.00096
	CA4	R	0.39	2.6e-05	7.5e-05
	hippocampal fissure	R	0.39	7.8e-05	0.00017
	GC ML DG	R	0.41	2.7e-05	7.5e-05
	subiculum	L	0.44	2.6e-06	1.3e-05
	molecular layer	L	0.44	1.7e-05	6.1e-05
	subiculum	R	0.44	1.2e-06	1.1e-05
	molecular layer	R	0.47	8.1e-06	3.2e-05
	CA1	R	0.50	6.1e-06	2.7e-05
	hippocampal tail	R	0.56	1.3e-07	1.6e-06
	hippocampal fissure	L	0.60	9.9e-10	2.7e-08
	hippocampal tail	L	0.61	1.5e-09	2.7e-08
amygdala subregions	paralaminar nucleus	R	0.23	0.014	0.016
	basal nucleus	R	0.26	0.0024	0.0033
	paralaminar nucleus	L	0.28	0.0028	0.0037
	basal nucleus	L	0.30	0.0019	0.0029

Table 2-S4. Gene dosage effects in individual hemispheres. Repeat of main analyses without averaging regions bilaterally, showing highly similar effects of gene dosage on regional volume in the left and right hemispheres. Whole structures and subregions with FDR q < 0.05 are listed in this table.

Structure	Region	diff_TD_22qDel	diff_TD_22qDup
whole brain	total ICV		
thalamus	anteroventral		
	laterodorsal		
	medial geniculate		
	medial ventral (reuniens)		
	mediodorsal		
	parafascicular	12.9-23.2|34.3-49.5	
	ventral anterior		
	ventromedial	14.2-20.3|49.3-49.5	
hippocampus	CA1		
	CA2/3	5.5-8.8|14.7-26.1	5.5-10.3|14-27.5|43.1-49.5
	CA4		
	GC ML DG	17.5-20.3	
	hippocampal amygdala transition area		
	hippocampal tail		
	molecular layer	18.5-20.1	
	subiculum		
	whole hippocampus		
amygdala	accessory basal nucleus	13.4-22.5|37.1-49.5	
	basal nucleus	14.1-24|45.2-49.5	
	central nucleus	11.1-18.5|28.8-49.5	
	corticoamygdaloid transition	17.5-21.6	
	lateral nucleus	5.5-9.8|14.5-26.9	15.1-22.6
	whole amygdala	5.5-6.6|13.7-24.7|39.4-49.5	

Table 2-S5. Age ranges with significant differences between CNV carriers and controls. Age periods with group difference based on 95% confidence interval (CI), multiple discontinuous ranges separated with "|". diff_TD_22qDel lists differences between 22qDel and TD curves, diff_TD_22qDup shows the same for 22qDup.

Structure	Region	beta	p	FDR q
whole brain	total ICV	1.09	7.0e-17	2.9e-15
thalamus	ventromedial	0.32	1.2e-02	0.021
	mediodorsal	0.32	1.4e-02	0.025
	anteroventral	0.33	2.6e-02	0.04
	ventral anterior	0.34	3.6e-03	0.0076
	parafascicular	0.36	1.9e-03	0.0045
	ventral lateral	0.38	1.2e-03	0.0032
	centromedian	0.41	1.1e-03	0.0032
	whole thalamus	0.54	2.2e-05	0.00031
	pulvinar	0.60	1.2e-04	0.00073
hippocampus	CA2/3	0.31	2.5e-02	0.04
	subiculum	0.37	5.1e-03	0.01
	parasubiculum	0.38	1.8e-02	0.031
	fimbria	0.44	3.0e-03	0.0067
	molecular layer	0.47	1.2e-03	0.0032
	CA4	0.48	6.4e-04	0.0022
	CA1	0.49	1.5e-03	0.0037
	HATA	0.50	6.4e-04	0.0022
	GC ML DG	0.50	4.0e-04	0.0017
	whole hippocampus	0.52	1.9e-04	0.0009
	presubiculum	0.57	7.4e-05	0.00052
amygdala	accessory basal nucleus	0.39	5.3e-03	0.01
	corticoamygdaloid transition	0.46	7.6e-04	0.0024
	basal nucleus	0.50	1.7e-04	0.0009
	whole amygdala	0.51	6.9e-05	0.00052
	lateral nucleus	0.54	4.3e-05	0.00045
	paralaminar nucleus	0.64	4.3e-06	9e-05

Table 2-S6. Main effects of sex. Regions with an FDR significant main effect of sex in the GAMM used for the primary gene dosage analysis.

Structure	Region	beta	p	FDR q
thalamus	mediodorsal	-0.35	2.6e-05	0.00036
	lateral geniculate	0.37	1.1e-04	0.00076
	medial ventral (reuniens)	0.40	9.1e-05	0.00075
hippocampus	CA4	0.43	1.2e-03	0.0046
	GC ML DG	0.43	1.0e-03	0.0042
	whole hippocampus	0.49	2.9e-04	0.0013
	CA1	0.50	2.1e-04	0.0012
	subiculum	0.52	4.6e-05	0.00048
	molecular layer	0.52	2.8e-04	0.0013
	hippocampal fissure	0.56	5.1e-08	2.1e-06
	hippocampal tail	0.62	3.6e-07	7.3e-06
amygdala	paralaminar nucleus	0.31	3.2e-03	0.01
	basal nucleus	0.34	2.6e-03	0.0089

Table 2-S7. Gene dosage effects controlling for antipsychotic medication. Repeat of gene dosage volume analysis with the addition of a covariate coding whether or not each participant was taking antipsychotic medication at the time of the scan. Regions with FDR q < 0.05 are listed in this table.

CHAPTER TWO SUPPLEMENTAL REFERENCES

1. Ghandour RM, Sherman LJ, Vladutiu CJ, Ali MM, Lynch SE, Bitsko RH, et al. Prevalence and Treatment of Depression, Anxiety, and Conduct Problems in US Children. J Pediatr. 2019;206:256-267.e3.

2. Sayal K, Prasad V, Daley D, Ford T, Coghill D. ADHD in children and young people: prevalence, care pathways, and service provision. Lancet Psychiatry. 2018;5:175–186.

3. Thapar A, Collishaw S, Pine DS, Thapar AK. Depression in adolescence. The Lancet. 2012;379:1056–1067.

4. First MB, Gibbon M. The Structured Clinical Interview for DSM-IV Axis I Disorders (SCID-I) and the Structured Clinical Interview for DSM-IV Axis II Disorders (SCID-II). Compr. Handb. Psychol. Assess. Vol 2 Personal. Assess., Hoboken, NJ, US: John Wiley & Sons, Inc.; 2004. p. 134–143.

5. Miller TJ, McGlashan TH, Rosen JL, Somjee L, Markovich PJ, Stein K, et al. Prospective diagnosis of the initial prodrome for schizophrenia based on the Structured Interview for Prodromal Syndromes: preliminary evidence of interrater reliability and predictive validity. Am J Psychiatry. 2002;159:863–865.

6. Jalbrzikowski M, Carter C, Senturk D, Chow C, Hopkins JM, Green MF, et al. Social Cognition in 22q11.2 Microdeletion Syndrome: Relevance to Psychosis. Schizophr Res. 2012;142:99–107.

7. Jalbrzikowski M, Jonas R, Senturk D, Patel A, Chow C, Green MF, et al. Structural abnormalities in cortical volume, thickness, and surface area in 22q11.2 microdeletion syndrome: Relationship with psychotic symptoms. NeuroImage Clin. 2013;3:405–415.

8. Jalbrzikowski M, Lin A, Vajdi A, Grigoryan V, Kushan L, Ching CRK, et al. Longitudinal trajectories of cortical development in 22q11.2 copy number variants and typically developing controls. Mol Psychiatry. 2022:1–10.

9. Jack Jr. CR, Bernstein MA, Fox NC, Thompson P, Alexander G, Harvey D, et al. The Alzheimer's disease neuroimaging initiative (ADNI): MRI methods. J Magn Reson Imaging. 2008;27:685–691.

10. FreeSurferMethodsCitation. https://surfer.nmr.mgh.harvard.edu/fswiki/FreeSurferMethodsCitation. Accessed 27 February 2023.

11. Fischl B, Salat DH, Busa E, Albert M, Dieterich M, Haselgrove C, et al. Whole brain segmentation: automated labeling of neuroanatomical structures in the human brain. Neuron. 2002;33:341–355.

12. Fischl B, van der Kouwe A, Destrieux C, Halgren E, Ségonne F, Salat DH, et al. Automatically parcellating the human cerebral cortex. Cereb Cortex N Y N 1991. 2004;14:11–22.

13. Reuter M, Schmansky NJ, Rosas HD, Fischl B. Within-subject template estimation for unbiased longitudinal image analysis. Neuroimage. 2012;61:1402–1418.

14. Iglesias JE, Augustinack JC, Nguyen K, Player CM, Player A, Wright M, et al. A computational atlas of the hippocampal formation using ex vivo, ultra-high resolution MRI: Application to adaptive segmentation of in vivo MRI. NeuroImage. 2015;115:117–137.

15. Iglesias JE, Van Leemput K, Augustinack J, Insausti R, Fischl B, Reuter M, et al. Bayesian longitudinal segmentation of hippocampal substructures in brain MRI using subject-specific atlases. NeuroImage. 2016;141:542–555.

16. Iglesias JE, Insausti R, Lerma-Usabiaga G, Bocchetta M, Van Leemput K, Greve DN, et al. A probabilistic atlas of the human thalamic nuclei combining ex vivo MRI and histology. Neuroimage. 2018;183:314–326.

17. Saygin ZM, Kliemann D, Iglesias JE, van der Kouwe AJW, Boyd E, Reuter M, et al. High-resolution magnetic resonance imaging reveals nuclei of the human amygdala: manual segmentation to automatic atlas. NeuroImage. 2017;155:370–382.

18. Sämann PG, Iglesias JE, Gutman B, Grotegerd D, Leenings R, Flint C, et al. FreeSurfer-based segmentation of hippocampal subfields: A review of methods and applications, with a novel quality control procedure for ENIGMA studies and other collaborative efforts. Hum Brain Mapp. 2022;43:207–233.

19. Grace S, Rossetti MG, Allen N, Batalla A, Bellani M, Brambilla P, et al. Sex differences in the neuroanatomy of alcohol dependence: hippocampus and amygdala subregions in a sample of 966 people from the ENIGMA Addiction Working Group. Transl Psychiatry. 2021;11:156.

20. Weeland CJ, Kasprzak S, de Joode NT, Abe Y, Alonso P, Ameis SH, et al. The thalamus and its subnuclei—a gateway to obsessive-compulsive disorder. Transl Psychiatry. 2022;12:70.

21. Huang AS, Rogers BP, Sheffield JM, Jalbrzikowski ME, Anticevic A, Blackford JU, et al. Thalamic Nuclei Volumes in Psychotic Disorders and in Youths With Psychosis Spectrum Symptoms. Am J Psychiatry. 2020;177:1159–1167.

22. Hoang D, Lizano P, Lutz O, Zeng V, Raymond N, Miewald J, et al. Thalamic, Amygdalar, and Hippocampal Nuclei Morphology and their Trajectories in First Episode Psychosis: A Preliminary Longitudinal Study. Psychiatry Res Neuroimaging. 2021;309:111249.

23. Latrèche C, Maeder J, Mancini V, Bortolin K, Schneider M, Eliez S. Altered developmental trajectories of verbal learning skills in 22q11.2DS: associations with hippocampal development and psychosis. Psychol Med. 2022:1–10.

24. Mancini V, Sandini C, Padula MC, Zöller D, Schneider M, Schaer M, et al. Positive psychotic symptoms are associated with divergent developmental trajectories of hippocampal volume during late adolescence in patients with 22q11DS. Mol Psychiatry. 2020;25:2844–2859.

25. Fonov V, Evans AC, Botteron K, Almli CR, McKinstry RC, Collins DL. Unbiased average age-appropriate atlases for pediatric studies. NeuroImage. 2011;54:313–327.

26. Beer JC, Tustison NJ, Cook PA, Davatzikos C, Sheline YI, Shinohara RT, et al. Longitudinal ComBat: A method for harmonizing longitudinal multi-scanner imaging data. NeuroImage. 2020;220:117129.

27. Johnson WE, Li C, Rabinovic A. Adjusting batch effects in microarray expression data using empirical Bayes methods. Biostatistics. 2007;8:118–127.

28. Fortin J-P, Cullen N, Sheline YI, Taylor WD, Aselcioglu I, Cook PA, et al. Harmonization of cortical thickness measurements across scanners and sites. NeuroImage. 2018;167:104–120.

29. Schleifer CH, O'Hora KP, Jalbrzikowski M, Bondy E, Kushan-Wells L, Lin A, et al. Longitudinal development of thalamocortical functional connectivity in 22q11.2 deletion syndrome. 2023:2023.06.22.546178.

30. Larsen B, Bourque J, Moore TM, Adebimpe A, Calkins ME, Elliott MA, et al. Longitudinal Development of Brain Iron Is Linked to Cognition in Youth. J Neurosci. 2020;40:1810–1818.

31. Hastie TJ. Generalized Additive Models. Stat. Models S, Routledge; 1992.

32. Wood SN. Generalized Additive Models: An Introduction with R, Second Edition. 2nd ed. Boca Raton: Chapman and Hall/CRC; 2017.

33. Benjamini Y, Hochberg Y. Controlling the False Discovery Rate: A Practical and Powerful Approach to Multiple Testing. J R Stat Soc Ser B Methodol. 1995;57:289–300.

CHAPTER THREE

Unique functional neuroimaging signatures of genetic versus clinical high risk for psychosis

Charles H. Schleifer[1], Sarah E. Chang[1], Carolyn M. Amir[1], Kathleen P. O'Hora[1], Hoki Fung[1], Jee Won D. Kang[2], Leila Kushan-Wells[1], Eileen Daly[3], Fabio Di Fabio[4], Marianna Frascarelli[4], Maria Gudbrandsen[3,5], Wendy R. Kates[6], Declan Murphy[3], Jean Addington[7], Alan Anticevic[8], Kristin S. Cadenhead[9], Tyrone D. Cannon[8], Barbara A. Cornblatt[10], Matcheri Keshavan[11], Daniel H. Mathalon[12], Diana O. Perkins[13], William Stone[11], Elaine Walker[14], Scott W. Woods[8], Lucina Q. Uddin[1], Kuldeep Kumar[15], Gil D. Hoftman[1], Carrie E. Bearden[1,2*]

1. Department of Psychiatry and Biobehavioral Sciences, Semel Institute for Neuroscience and Human Behavior, University of California, Los Angeles, CA, USA.
2. Department of Psychology, University of California, Los Angeles, CA, USA.
3. Department of Forensic and Neurodevelopmental Sciences, Institute of Psychiatry, Psychology & Neuroscience (IoPPN), King's College London, London, UK.
4. Department of Human Neurosciences, Sapienza University, Rome, Italy.
5. Centre for Psychological Research (CREW), School of Psychology, University of Roehampton, London, UK
6. Department of Psychiatry and Behavioral Sciences, SUNY Upstate Medical University, Syracuse, NY, USA.
7. Department of Psychiatry, Hotchkiss Brain Institute, University of Calgary, Calgary, Alberta, Canada.
8. Departments of Psychology and Psychiatry, Yale University, New Haven, CT, USA.
9. Department of Psychiatry, University of California, San Diego, CA, USA.
10. Department of Psychiatry, Donald and Barbara Zucker School of Medicine at Hofstra/Northwell, Hempstead, NY, USA.
11. Department of Psychiatry, Harvard Medical School at Beth Israel Deaconess Medical Center, Boston, Massachusetts, USA.
12. Department of Psychiatry, University of California, and San Francisco Veterans Affairs Medical Center, San Francisco, CA, USA.
13. Department of Psychiatry, University of North Carolina, Chapel Hill, NC, USA.
14. Departments of Psychology, Emory University, Atlanta, GA, USA.
15. Centre de Recherche du CHU Sainte-Justine, University of Montreal, Montreal, Canada.

ABSTRACT

Background: 22q11.2 Deletion Syndrome (22qDel) is a copy number variant (CNV) associated with psychosis and other neurodevelopmental disorders. Adolescents at clinical high risk for psychosis (CHR) have subthreshold psychosis symptoms without known genetic risk factors. Whether common neural substrates underlie these distinct high-risk populations is unknown. We compared functional brain measures in 22qDel and CHR cohorts and mapped results to biological pathways.

Methods: We analyzed two large multi-site cohorts with resting-state functional MRI (rs-fMRI): 1) 22qDel (n=164, 47% female) and typically developing (TD) controls (n=134, 56% female); 2) CHR individuals (n=244, 41% female) and TD controls (n=151, 46% female) from the North American Prodrome Longitudinal Study-2. We computed global brain connectivity (GBC), local connectivity (LC), and brain signal variability (BSV) across cortical regions, testing case-control differences for 22qDel and CHR separately. Group difference maps were related to published brain maps using autocorrelation-preserving permutation.

Results: BSV, LC, and GBC are significantly disrupted in 22qDel compared with TD controls (False Discovery Rate $q<0.05$). Spatial maps of BSV and LC differences are highly correlated with each other, unlike GBC. In CHR, only LC is significantly altered versus controls, with a different spatial pattern compared to 22qDel. Group differences map onto biological gradients, with 22qDel effects strongest in regions with high predicted blood flow and metabolism.

Conclusion: 22qDel and CHR exhibit divergent effects on fMRI temporal variability and multi-scale functional connectivity. In 22qDel, strong and convergent disruptions in BSV and LC not seen in CHR individuals suggest distinct functional brain alterations.

INTRODUCTION

Multiple lines of evidence suggest that disruptions to local and large-scale neural circuits are a core feature of psychosis spectrum disorders (1–3). This manifests as alterations to the temporal variability and spatial correlations of brain signals, which are detectable with resting-state functional magnetic resonance imaging (rs-fMRI) (4–9). Studying these temporal and network features of brain disruptions in people with clinical and genetic risk factors for psychosis will help us to better understand these important high-risk states and will advance our understanding of the underlying pathophysiology.

Multiple approaches can be taken to identify people at increased risk for psychosis. Schizophrenia and related disorders are highly heritable due to the polygenic effects of common genetic variants (10) as well as rarer highly penetrant mutations that include several copy number variants (CNVs) in which segments of the genome are deleted or duplicated (11). 22q11.2 Deletion Syndrome (22qDel) is one such CNV that strongly increases risk for psychosis, autism, and other neuropsychiatric disorders. This deletion of ~46 protein-coding genes occurs in approximately 1 in 4000 people (12), of whom 10-20% can be expected to develop a psychosis spectrum disorder (13,14). Approximately 30% of 22qDel carriers endorse positive psychosis symptoms of at least moderate intensity (15–17). Highly penetrant genetic risk factors like 22qDel represent important opportunities for characterizing biological pathways underlying psychosis risk in a “genetics-first” approach (18,19). Alternatively, in a “behavior-first” framework, a Clinical High Risk (CHR) state can be defined based on the presence of sub-threshold positive symptoms, without considering specific genetic risk factors (20). Approximately 20-30% of people meeting CHR criteria can be expected to convert to a diagnosable form of psychotic disorder within a three-year follow-up period (20,21).

Substantial research has been done on various functional neuroimaging measures in separate studies of 22qDel and CHR relative to typically developing (TD) controls, with a range of convergent and divergent outcomes (22,23). However, no study to date has directly compared

rs-fMRI correlates of these genetic and clinical high-risk states using the same analytic pipelines. Here, we conduct a mega-analysis of rs-fMRI data from a total of 687 22qDel carriers, CHR individuals, and age- sex- and site-matched TD controls collected at multiple sites and subjected to a harmonized preprocessing and analysis pipeline.

Our aims are to: i) characterize shared and unique effects of 22qDel and CHR on rs-fMRI measures of global brain connectivity (GBC), local connectivity (LC), and brain signal temporal variability (BSV), and ii) gain deeper biological understanding of fMRI phenotypes by relating these findings to other multimodal maps of regional brain features. The three rs-fMRI measures index different spatial and temporal aspects of neurophysiology. GBC reflects connectivity of large-scale functional networks which have been shown to be disrupted in 22qDel, schizophrenia, and CHR (24–26). LC is often measured as the similarity in signal between spatially adjacent voxels, to which alterations have been observed in schizophrenia and in first degree relatives at genetic high risk (6,27–29). BSV is a heritable brain phenotype that relates to hemodynamic physiology, excitation/inhibition balance, and the spatial expression pattern of schizophrenia risk genes (30,31). We chose these three measures to capture functional brain alterations at multiple scales across the same sets of cortical regions. To generate biologically-informed hypotheses from our rs-fMRI findings, we relate spatial maps of case-control group differences to published brain maps from multiple sources, such as metabolic data from positron emission tomography (PET) and gene expression data from the Allen Human Brain Atlas (32–35).

METHODS

Participants

The neuroimaging dataset contains a total of 687 participants from two separate multi-site studies (Table 1): 164 carriers of molecularly confirmed 22qDel along with 134 matched TD controls (Control-22q), and 240 individuals with CHR for psychosis plus 149 matched TD controls (Control-CHR). 22qDel and Control-22q data were shared from five scanners/sites in the United States, Europe, and the United Kingdom. CHR and Control-CHR data came from the North American Prodrome Longitudinal Study 2 (NAPLS2) (36,37), which includes eight sites in the United States and Canada. CHR participants were adolescents and young adults ages 12-35 with subthreshold psychosis symptoms (38). See Supplemental Methods for inclusion/exclusion criteria and a detailed description of participant counts by site. After study procedures were fully explained, adult participants provided written consent, while participants younger than 18 years provided written assent with the written consent of their parent or guardian. The respective Institutional Review Boards at each site approved all study procedures and informed consent documents.

	22qDel	Control22q	p-val-22q	CHR	ControlCHR	p-val-CHR
n	164	134		240	149	
Age, Years, Mean (SD)	19.9 (6.8)	19.4 (6.9)	0.489	18.8 (4.1)	19.5 (4.5)	0.116
Sex, Female, n (%)	77 (47.0)	75 (56.0)	0.152	99 (41.2)	70 (47.0)	0.316
fMRI movement, Mean (SD)	8.1 (11.2)	5.1 (8.0)	0.008	4.9 (7.2)	3.3 (6.2)	0.023
Antipsychotic med, n (%)	23 (14.0)	0 (0.0)	<0.001	46 (19.2)	0 (0.0)	<0.001
Psychosis diagnosis, n (%)	16 (9.8)	0 (0.0)	0.001	26 (10.8)	0 (0.0)	<0.001
Full Scale IQ, Mean (SD)	78.7 (14.1)	110.9 (15.8)	<0.001	105.3 (15.6)	110.9 (14.9)	0.001
Congenital cardiac diagnosis, n (%)	53 (32.3)	0 (0.0)	<0.001	-	-	-

Table 3-1. Demographics. 22q11.2 Deletion Syndrome (22qDel) carriers and matched typically developing controls (Control22q), as well as Clinical High Risk (CHR) patients and matched typically developing controls (ControlCHR). p-val-22q describes difference tests (ANOVA or chi-squared) between 22qDel and Control22q groups. p-val-CHR refers to comparisons between CHR and ControlCHR groups. fMRI movement describes the percentage of frames removed per scan for exceeding displacement/intensity thresholds. Antipsychotic med indicates the proportion of participants taking medication in that drug class. In the 22qDel group, “Psychosis diagnosis”

indicates diagnosis of psychotic disorder (schizophrenia, schizoaffective, or not otherwise specified) at the time of scan. In the CHR group, “Psychosis diagnosis” indicates those who were diagnosed with a psychotic disorder at any point during the two-year study follow-up period (i.e. CHR individuals who eventually “convert” to a psychosis spectrum diagnosis). Psychotic disorder diagnosis was based on Structured Clinical Interview for DSM/SCID-5. Full Scale IQ includes normed scores from multiple scales: Wechsler Adult Intelligence Scale (WAIS), Wechsler Adult Intelligence Scale-Revised (WAIS-R), Standard Progressive Matrices (SPM), Wechsler Intelligence Scale for Children-III (WISC-III), Wechsler Abbreviated Scale of Intelligence-II (WASI-II). Congenital cardiac diagnosis indicates any 22qDel carrier with a documented diagnosis of a congenital heart defect (e.g., septal defect, Tetralogy of Fallot, etc.).

Neuroimaging acquisition and processing

Blood oxygen level dependent (BOLD) resting-state functional magnetic resonance imaging (rs-fMRI) and high-resolution structural images were collected at each study site (see Supplemental Methods). All data from 22qDel, CHR, and TD controls were processed with the same workflow, as described in detail in previous publications (39,40). Functional and structural images were processed with the Quantitative Neuroimaging Environment and Toolbox (41), applying a modified version of the methods developed for the Human Connectome Project (HCP) (42), as well as motion scrubbing, i.e. censoring frames with displacement or intensity change thresholds exceeding those recommended by Power et al. (43–45). Functional connectivity analyses were computed on the residual of the signal after regression of motion time series, the mean signal time series from the ventricles and deep white matter, and the first derivatives of these measures.

fMRI measures

Three rs-fMRI measures were calculated for each scan: global brain connectivity (GBC), local connectivity (LC), and brain signal variability (BSV). All three measures used the same set of 360 cortical regions defined from multi-modal MRI in 210 healthy young adults from the HCP (46). See Supplemental Methods for details on each measure. Computations were performed in R using ciftiTools to manipulate neuroimaging data (47).

GBC is a well-validated measure defined as the average functional connectivity between a given brain region and all other regions (48,49). A high GBC value indicates a region in which signal is similar to many other regions of the brain, whereas a low GBC value represents a region that is dissimilar to the majority of other regions.

LC was calculated as a measure of the cohesiveness or homogeneity of vertex-level BOLD time series within the same set of regions. This approach is based on the network homogeneity method, wherein FC is computed between each pair of voxels in a chosen network (50).

BSV was calculated as the average temporal standard deviation of the BOLD time series in each region. This measure of variability is also referred to as resting state fluctuation amplitude, and represents a heritable brain phenotype that relates to underlying excitation/inhibition balance and hemodynamic physiology (30,31).

To correct for variability related to site/scanner, we used a neuroimaging-optimized implementation of ComBat (51) which uses empirical Bayes methods to correct for batch/site effects, with increased robustness compared to linear model approaches (52). After ComBat, values for each measure were normalized within each region based on the mean and standard deviation for the relevant control group.

Group-level fMRI comparisons

For each fMRI measure, across each region, linear models were used to test the main effect of 22qDel versus matched controls (Control22q), and the main effect of CHR versus matched controls (ControlCHR). 22qDel and CHR groups were compared to their respective control groups but not directly to each other to avoid the confounding effects of scanner/site and demographic differences between the 22qDel and CHR groups. All models controlled for linear and quadratic age, sex, site, and movement (measured as the percentage of frames scrubbed from each scan), and p-values for the main effect of group were adjusted for multiple comparisons

with False Discovery Rate (FDR) $q<0.05$ for each brain map (53). See Supplemental Methods for more details on linear models.

Brain map comparisons

In order to assess similarity of the three fMRI measures within and between clinical groups, we used permutation methods to compare the spatial brain maps for case-control comparisons with significant group main effects. For a given pair of maps, similarity was tested via Pearson's correlations, and two-tailed p-values were computed from a null distribution generated from 10,000 spatial autocorrelation-preserving surrogate brain maps per hemisphere, generated with BrainSMASH (33), see Supplemental Methods.

We next used the same permutation testing procedure to compare the left hemisphere cortical maps from our case-control analyses to a set of 22 left hemisphere cortical maps from previously published datasets, using the neuromaps and abagen toolboxes (35,54), see Supplemental Methods. Maps include metabolic and physiologic data from positron emission tomography (PET), gene expression from post-mortem tissue, and various measures from magnetoencephalography (MEG), structural MRI, and functional MRI; see Table 2 for a description of each map (34,46,55–61). Analyses were restricted to the left hemisphere because some datasets did not include densely sampled right hemisphere data.

Map	Modality	Citation
Glucose metabolism	PET	Vaishnavi et al. 2010
Oxygen metabolism	PET	Vaishnavi et al. 2010
Cerebral blood flow	PET	Vaishnavi et al. 2010
Cerebral blood volume	PET	Vaishnavi et al. 2010
PC1 gene expression	mRNA	Markello et al. 2021
PVALB-SST gradient	mRNA	Markello et al. 2021
fMRI gradient	fMRI	Margulies et al. 2016
Intersubject variability	fMRI	Mueller et al. 2013
PC1 neurosynth	fMRI	Yarkoni et al. 2011
Allometric scaling (PNC)	sMRI	Reardon et al. 2018
Allometric scaling (NIH)	sMRI	Reardon et al. 2018
Developmental expansion	sMRI	Hill et al. 2010
Evolutionary expansion	sMRI	Hill et al. 2010
Cortical thickness	sMRI	Glasser et al. 2016
T1w/T2w ratio	sMRI	Glasser et al. 2016
MEG delta	MEG	Van Essen et al. 2013
MEG theta	MEG	Van Essen et al. 2013
MEG alpha	MEG	Van Essen et al. 2013
MEG beta	MEG	Van Essen et al. 2013
MEG gamma1	MEG	Van Essen et al. 2013
MEG gamma2	MEG	Van Essen et al. 2013
ROI size	sMRI	Glasser et al. 2016

Table 3-2. Reference brain maps. Description of neuroimaging modality and citation for each published brain map (34,46,55–61). PET = positron emission tomography; mRNA = messenger ribonucleic acid; fMRI = functional magnetic resonance imaging; sMRI = structural MRI; MEG = magnetoencephalography; PC1 = first principal component; PVALB-SST = difference in normalized parvalbumin and somatostatin expression; PNC = Philadelphia Neurodevelopmental Cohort; NIH = National Institute of Health; T1w = T1-weighted sMRI; T2w = T2-weighted sMRI.

Clinical and cognitive analyses

The primary CHR fMRI analyses were repeated comparing the 26 CHR individuals who eventually converted to a psychosis diagnosis (CHRc) to the ControlCHR group, and to the subset of the CHR participants who did not convert. All models controlled for age, age2, sex, site, and movement.

The primary 22qDel fMRI analyses were repeated comparing the 54 22qDel carriers with psychosis risk symptoms (PS+) and the 110 22qDel carriers without (PS-), controlling for age, age2, sex, site, and movement. See Supplemental Methods for classification of psychosis risk status based on clinical scales.

In an exploratory analysis of cognition, linear relationships were tested for each measure in each group across all regions between fMRI measures and Full Scale IQ controlling for sex, site, and movement.

For all clinical and cognitive analyses, significance for the relevant main effects were evaluated at FDR $q<0.05$ within each set of tests for a given group and measure.

Secondary analyses

For all regions with a significant main effect of group in the original model, p-values for the main effects of site were investigated.

The primary case-control analyses did not include global signal regression (GSR) as a preprocessing step for consistency with prior NAPLS work (26,62) and due to systemic associations between global signal topography and factors such as age (63). However, case-control comparisons were repeated with the additional inclusion GSR. Within the 22qDel and CHR groups, across all regions, linear models were tested for the relationship between fMRI measures and antipsychotic medication status.

Because congenital heart disorders are common in 22qDel (Table 1), we tested a linear model for fMRI effects of any congenital cardiac diagnosis (e.g. atrial or ventricular septal defect, conotruncal defect, etc.) within the 22qDel group.

For all secondary analyses, significance for the relevant main effects were evaluated at FDR $q<0.05$ within each set of tests for a given group and measure. All models controlled for age, age2, sex, site, and movement.

RESULTS

fMRI analyses

22qDel carriers significantly differ from matched controls with respect to each fMRI measure (GBC, LC, and BSV); Figure 1a-c. GBC is lower in 22qDel for a set of brain regions including bilateral somatomotor, visual, and temporal cortex. No areas of higher GBC in 22qDel survived correction for multiple comparisons. Both LC and BSV show decreases in 22qDel relative to controls across a similar set of frontal and parietal regions, and similar increases in inferior temporal regions. However, LC is decreased in somatomotor cortex, which is not observed for BSV in 22qDel.

In CHR individuals compared to matched controls, there are no significant differences in GBC or BSV. However, local connectivity is significantly decreased in CHR relative to controls in a set of somatomotor and temporal regions (Figure 1d).

Testing correlations between the four threshold-free brain maps with significant group effects (22qDel GBC, LC, and BSV, and CHR LC; Figure 1i), using spatial autocorrelation-preserving permutations, revealed that the effect of 22qDel is similar between LC and BSV (driven by similarity in frontal-parietal and temporal regions; Figure 1b,c), and that the effect of 22qDel on GBC resembles the effect of CHR on LC (driven by somatomotor regions; Figure 1a,d). While the threshold-free maps for group effects on LC are not significantly correlated between 22qDel and CHR, there is a notable overlap of significant effects, in which 6 somatomotor regions show significant effects for both CHR and 22qDel (out of 16 total significant regions in CHR).

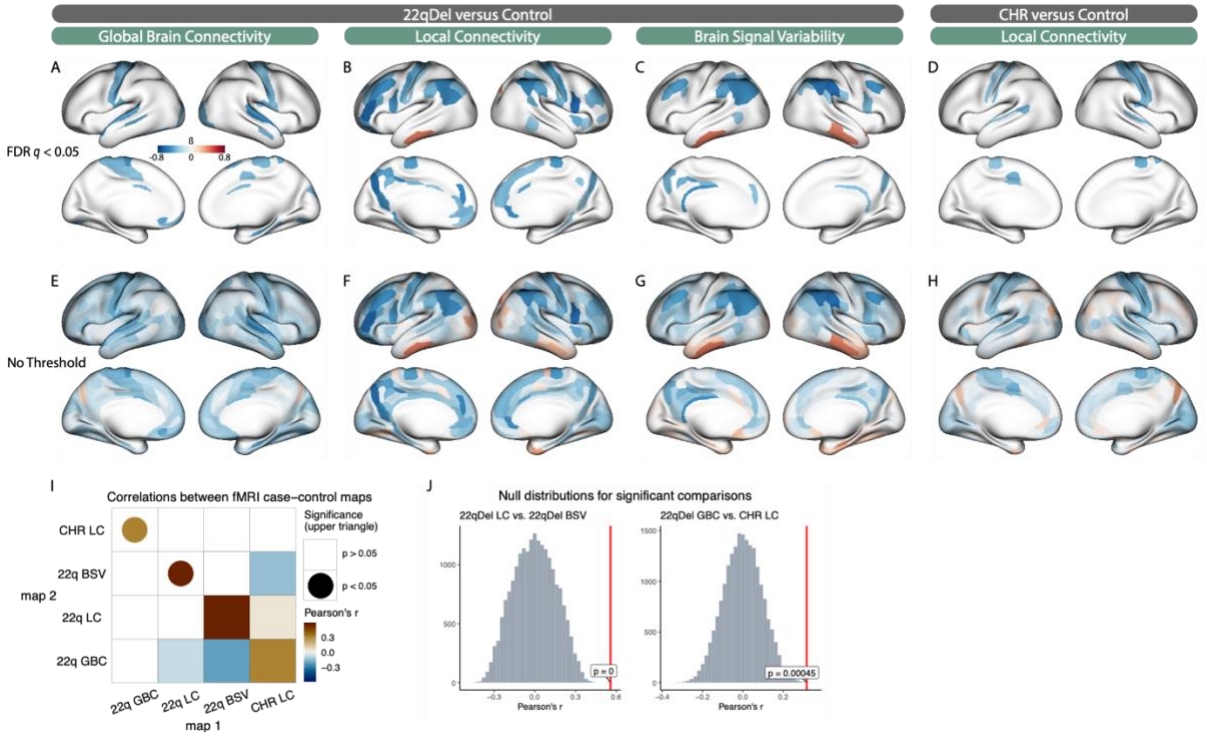

Figure 3-1. Case-control fMRI differences. A-C) Standardized coefficients for significant main effects of 22qDel versus controls for global brain connectivity (GBC), local connectivity (LC), and brain signal variability (BSV), visualizing effect sizes for regions where False Discovery Rate (FDR) corrected q < 0.05. Blue indicates 22qDel < control, red indicates 22qDel > control. D) regions with significantly decreased LC in clinical high risk (CHR) versus controls. No significant differences in GBC or BSV were found between CHR and controls. E-H) Same as A-D visualizing standardized group difference effect sizes for all cortical regions (no significance threshold). I) Correlations between brain maps in E-H. All correlations are shown in the lower triangle; upper triangle shows only those with p<0.05. J) Two-tailed p-values are calculated from the true correlation between brain maps (red line) compared to a null distribution (gray histogram) of correlations to 10,000 spatial autocorrelation-preserving surrogate brain maps per hemisphere.

Multi-modal brain map relationships

The map of 22qDel versus control differences for BSV is significantly related to published PET maps of glucose and oxygen metabolism as well as cerebral blood flow and volume (55), such that decreased BSV in 22qDel is associated with regions of typically high metabolism and blood flow. 22qDel BSV is also significantly correlated with a map of inter-individual variability from an rs-fMRI study of typical adults (57). The map of LC differences in 22qDel versus controls is similarly related to cerebral blood flow and volume (55). LC in 22qDel was also related to the principal sensory/associative gradient extracted from a large rs-fMRI study, highlighting default

mode and frontoparietal regions with low LC in 22qDel (56). The 22qDel LC map is also related to region of interest (ROI) size in the atlas. All relationships had the same direction of effect, in which lower values in the 22qDel effect size map (representing 22qDel < control) are related to higher values in the reference map; see Figure 2. See Table 2 for descriptions of each reference map. Brain map comparisons for the CHR group are shown in Supplementary Figure S1. Similar to 22qDel, ROI size was significantly related to the CHR versus ControlCHR difference map for local connectivity. No other LC brain map relationships were found to be significant in the CHR analysis. The effects of CHR on GBC and BSV were not strong enough to allow interpretable brain map comparisons.

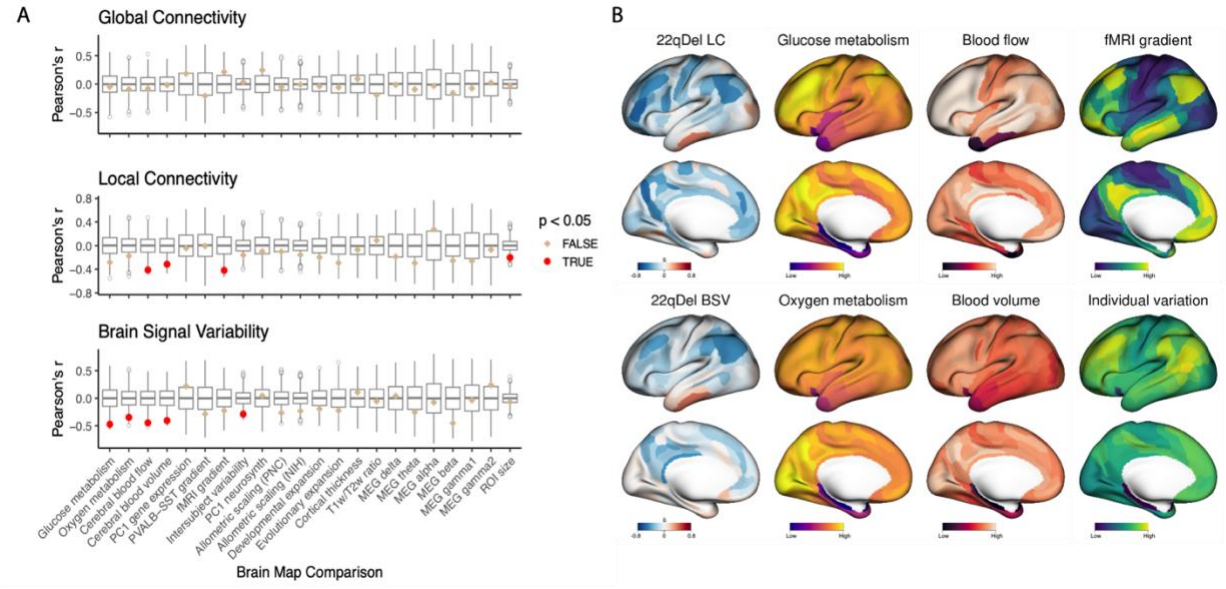

Figure 3-2. Multi-modal brain map comparisons for 22qDel fMRI effects. A) Left hemisphere cortical maps from 22qDel case-control models were tested for spatial similarity to multiple publicly available datasets including metabolic and physiologic data from positron emission tomography (PET), gene expression from post-mortem tissue, and various measures from magnetoencephalography (MEG), structural magnetic resonance imaging (MRI), and functional MRI. Null distributions (gray box plots) were computed from the Pearson correlations between 10,000 spatial autocorrelation-preserving permutations of the target fMRI 22qDel-control map (named in the plot title) and the second map of interest (named on the x-axis). The true correlation values between the two maps of interest are marked by tan or red points, and two-tailed p-values are computed from the proportion of values in the null distribution whose absolute value exceeds the absolute value of the true test statistic. B) Left hemisphere maps for 22qDel-control group differences in local connectivity (LC) and brain signal variability (BSV), as well as example maps for glucose and oxygen metabolism (55), cerebral blood flow and volume (55), and fMRI maps describing a sensory/transmodal gradient (56) and inter-individual variation (57).

Clinical and cognitive analyses

Across all three fMRI measures, there were no regions where we observed a significant main effect of CHRc versus ControlCHR, or CHRc versus CHR. Similarly, in 22qDel there were no regions with a significant effect of PS+ versus PS-.

In an exploratory analysis of cognition, there were no regions with significant linear relationships between Full Scale IQ and any fMRI measure in any group (22qDel, Control22q, CHR, ControlCHR).

Secondary analyses

For all regions with a significant main effect of group, none showed a significant effect of dummy coded site for any measure in the 22qDel and CHR analyses. In fact, the uncorrected p-values for site effects in these regions were all greater than 0.05. This provides reassurance that after ComBat correction site/scanner differences are not driving the observed results.

Within the 22qDel and CHR groups, there were no brain regions with significant main effects of antipsychotic medication status in any of the three measures. This suggests that our measures are more sensitive to case-control differences than medication effects.

Within the 22qDel group, across all three rs-fMRI measures, there were no regions with a significant main effect of congenital heart defect diagnosis.

Across both clinical groups and all three measures, the results of case-control analyses with the inclusion of GSR are highly consistent with our initial findings that did not include GSR (see Supplemental Figure S3).

DISCUSSION

This is the first study to compare patterns of functional brain disruption in the clinical high-risk (CHR) and genetic high-risk (22qDel) conditions. We find robust and significant effects of 22qDel versus matched controls across all three measures: global brain connectivity (GBC), local connectivity (LC), and brain signal variability (BSV) (Figure 1). The CHR group only differs significantly from controls for LC. Overall, the rs-fMRI effects of 22qDel and CHR are mostly dissimilar. Comparison to previously established brain maps suggests that spatial patterns of 22qDel versus control differences in LC and BSV relate to multiple patterns including regional variation in cerebral blood flow and metabolism, measured from PET studies in neurotypical individuals.

Case-control findings

22qDel and CHR both show significantly decreased LC across a set of somatomotor regions, but the overall spatial patterns of LC differences from controls are not significantly correlated between the two groups. Somatomotor LC has not been directly characterized before in 22qDel or CHR, as we did here; however, using other analytic approaches functional connectivity between somatomotor cortex and the thalamus has been found to be increased in both 22qDel youth and in CHR individuals who convert to a psychotic disorder (39,40,64).

In 22qDel, LC and BSV can be seen to converge on a similar pattern of disruptions: a set of frontal and parietal regions show both decreased temporal variability and decreased within-region spatial homogeneity (i.e., LC), with the opposite pattern observed for inferior temporal regions.

We do not find any significant differences between the CHR and control groups in terms of BSV. Prior studies in schizophrenia have found evidence of widespread increases in fMRI signal variance relative to controls (4,5). In CHR, the fractional amplitude of low frequency

fluctuations has been shown to differ from controls (65), suggesting that frequency-specific measures of signal variability may be more sensitive to the CHR phenotype.

Similarly, we do not find significant CHR effects on GBC. Graph theory based approaches have found functional connectivity differences between CHR and control individuals (26,66), which our GBC measure does not capture. In this CHR sample we also do not see the GBC differences in prefrontal cortex and other regions that have been observed in schizophrenia (4,49,67). This suggests that functional connectivity disruptions on smaller spatial scales, or between specific long-range nodes, may be more indicative of the CHR state, but that overall global connectivity of regions is not as strongly impacted.

Multi-modal brain map relationships

For brain-wide case-control fMRI effects, we evaluated relationships to multiple published brain maps (Table 2, Figure 2, Supplemental Figure S2). Regions with significantly decreased LC and BSV in 22qDel relative to controls are both associated with high cerebral blood flow and blood volume from a PET study of typical adults (55). The map of BSV differences in 22qDel was additionally associated with glucose and oxygen metabolism from the same PET study. While these are exploratory findings, they are consistent with the hypothesis that neuronal metabolic pathology and/or vascular and hemodynamic abnormalities in 22qDel underlie some of the observed rs-fMRI differences. 22qDel is associated with high rates of congenital cardiac defects (12) and increased neurovascular anomalies (68,69). In our sample, we did not find a relationship between congenital heart defects and rs-fMRI measures, but there may be neurovascular alterations in 22qDel that are unrelated to categorical cardiac defect status. A recent arterial spin labeling MRI study showed increased cerebral blood flow in 22qDel compared to controls (70). Additionally, animal models of 22qDel and studies of induced pluripotent stem cell-derived neurons from human 22qDel samples provide convergent evidence for neuronal mitochondrial disruption (71–74) and disrupted neurovascular development (75–78) caused by 22q11.2 CNVs.

Neurovascular interactions are fundamental to the BOLD fMRI signal (79,80), and play a key role in neurodevelopmental processes such as cortical expansion (76,81,82), which appears to be strongly impacted in 22qDel given structural MRI findings of markedly reduced cortical surface area (83).

22qDel LC effects were also related to the principal gradient of functional connectivity from a study in typical adults (56), and BSV effects were related to intersubject variability in another study of typical adults (57). This is a reflection of the preferential LC and BSV decreases in 22qDel across a distributed network of highly dynamic association regions in frontal, parietal, and temporal cortex. The disrupted local connectivity and variability of the default mode and related associative networks converge with prior findings of decreased functional and structural connectivity in the default mode network in 22qDel (24,84).

For both 22qDel and CHR, LC was also found to be preferentially decreased in larger regions (e.g. somatomotor regions). No other significant brain map relationships were found for CHR effects on LC. No significant relationships were found for effects of 22qDel or CHR on GBC, and results should not be interpreted for the effect of CHR on BSV because the effect sizes are too small to facilitate comparison (Supplemental Figures S1-S2).

Strengths, limitations, and future directions

A significant strength of this work is that preprocessing and analytic workflows have been harmonized across all data from 22qDel, CHR, and control groups. Our mega-analytic approach leverages data from multiple sites to increase statistical power and generalizability, while minimizing methodological differences as a source of non-biological variation which can obscure true signals. This allows us to compare 22qDel and CHR findings with greater clarity than ever before. Our secondary analyses provide evidence that our findings are not strongly influenced by site/scanner differences or antipsychotic medication status in either group. Encouragingly, we also

find that all case-control rs-fMRI results are highly comparable with and without the inclusion of GSR as an additional denoising step.

Despite our relatively large sample size, we still have limited power to detect effects specific to the subsets of the 22qDel and CHR samples with a psychosis diagnosis. Only 26 of the 240 CHR participants converted to a psychosis diagnosis during follow-up, and only 16 of the 164 22qDel participants in our young cohort had a diagnosis of a psychotic disorder. A larger proportion of the 22qDel group met criteria for subthreshold psychosis risk symptoms (54/164), but this constitutes a heterogeneous group, and they did not show rs-fMRI differences from the 22qDel carriers without psychosis symptoms. While the robust rs-fMRI effects we see are reflective of the CNV broadly, they may not differentiate people with varying psychiatric phenotypes. However, future studies with larger samples may uncover psychosis-specific rs-fMRI effects. We also did not find any significant relationships between Full Scale IQ and rs-fMRI, but future large studies with standardized and detailed cognitive data will be better suited to analyses of brain-behavior relationships.

The brain map comparison analyses are exploratory and intended to generate rather than confirm hypotheses. Our findings of strong relationships between 22qDel-specific disruptions and gradients of brain hemodynamic and metabolic activity warrant further research into the underlying neurophysiology. fMRI studies with additional physiological measurements such as breathing belts or capnography, or tasks such as breath-holding studies in 22qDel could help disentangle fMRI correlates of altered neuronal activity from those relating to altered hemodynamics and blood oxygenation.

Conclusions

We show, for the first time, that 22qDel carriers and individuals at CHR for psychosis exhibit highly distinct alterations in rs-fMRI measures of global brain connectivity, local connectivity, and temporal variability. Compared to controls, 22qDel carriers show marked

disruptions across all three measures, whereas CHR individuals differ only in local connectivity. Comparison to multi-modal brain maps suggests that, uniquely in 22qDel, temporal variability and spatial homogeneity of rs-fMRI signals are preferentially reduced in association cortex regions with high hemodynamic and metabolic activity. Findings motivate future research to characterize points of convergence between CHR and genetic risk syndromes, as well as specific research into the neurovascular and neurometabolic underpinnings of functional brain alterations in 22qDel.

CHAPTER THREE AUTHOR CONTRIBUTIONS

Charles H. Schleifer: Conceptualization, Methodology, Software, Formal Analysis, Data Curation, Writing - Original Draft, Writing - Review & Editing, Visualization
Sarah Chang: Data Curation, Methodology, Writing - Review & Editing
Carolyn Amir: Data Curation, Methodology, Writing - Review & Editing
Kathleen P. O'Hora: Data Curation, Methodology, Writing - Review & Editing
Hoki Fung: Data Curation, Methodology, Writing - Review & Editing
Jee Won D. Kang: Data Curation, Methodology, Writing - Review & Editing
Leila Kushan-Wells: Data Curation, Project Administration
Eileen Daly: Data Curation, Project Administration
Fabio Di Fabio: Data Curation, Project Administration
Marianna Frascarelli: Data Curation, Project Administration
Maria Gudbrandsen: Data Curation, Project Administration
Wendy R. Kates: Data Curation, Project Administration
Declan Murphy: Data Curation, Project Administration
Jean Addington: Data Curation, Project Administration
Alan Anticevic: Data Curation, Project Administration, Software
Kristin S. Cadenhead: Data Curation, Project Administration
Tyrone D. Cannon: Data Curation, Project Administration
Barbara A. Cornblatt: Data Curation, Project Administration
Matcheri Keshavan: Data Curation, Project Administration
Daniel H. Mathalon: Data Curation, Project Administration
Diana O. Perkins: Data Curation, Project Administration
William Stone: Data Curation, Project Administration
Elaine Walker: Data Curation, Project Administration
Scott W. Woods: Data Curation, Project Administration
Lucina Q. Uddin: Data Curation, Methodology, Writing - Review & Editing
Kuldeep Kumar: Data Curation, Methodology, Writing - Review & Editing
Gil Hoftman: Data Curation, Methodology, Writing - Review & Editing
Carrie E. Bearden: Data Curation, Project Administration, Writing - Review & Editing, Supervision

Thank you to Ming Tsuang for contributions to the NAPLS2 project, Zailyn Tamayo for help accessing data, Ross D. Markello, Bratislav Misic et al. for the development of Neuromaps, and many thanks to all of the research participants who made this project possible.

Data availability

Data are publicly available from the National Institute of Mental Health Data Archive:
https://nda.nih.gov/edit_collection.html?id=2414
https://nda.nih.gov/edit_collection.html?id=2275

To facilitate reproducibility and rigor, analysis code is publicly available on GitHub:
https://github.com/charles-schleifer/22q_chr_fmri

Disclosures

Declan Murphy has received payment from Springer for editorial duties and has served on an advisory board for Roche.

Alan Anticevic is a co-founder, CEO and holds a position as a board director for Manifest Technologies, Inc.

All other authors report no biomedical financial interests or potential conflicts of interest.

Funding

This work was supported by the National Institute of Mental Health (Grant Nos. R01MH085953, R01MH085953-S1, R21MH116473-01A1, P50 MH066286 and U01MH101779 [to CEB], F31MH133326 [to CHS], MH64824 and MH65481 [to WRK], U01MH081984 [to JA], U01MH081928, P50MH080272, Commonwealth of Massachusetts SCDMH82101008006 to Dr. Larry Seidman, R01MH60720, U01MH082022 and K24MH76191 [to KSC], U01MH081902 [to TDC], U01MH082004 [to DOP], U01MH081988 [to EW], U01MH082022 [to SW], UO1MH081857-05 [to BAC], DP5OD012109-01, 1U01MH121766, R01MH112746 and 5R01MH108590 [to AA], U54EB020403 for the Big Data to Knowledge (BD2K) Program, UO1-MH191719 for the International Brain and Behavior 22q11.2DS Consortium [IBBC]), EC480/1-1 and EC480/2-1 from the German Research Foundation under the Heisenberg Programme and the Innovative Medicines Initiative 2 Joint Undertaking under grant agreement No 115300 for the project EU-AIMS and No 777394 for the project AIMS-2-TRIALS to Dr. Christine Ecker, Simons Foundation Autism Research Initiative Explorer Award [to CEB], and UCLA Training Program in Neurobehavioral Genetics (Grant No. T32NS048004 [to CHS]).

CHAPTER THREE REFERENCES

1. Dienel SJ, Schoonover KE, Lewis DA (2022): Cognitive Dysfunction and Prefrontal Cortical Circuit Alterations in Schizophrenia: Developmental Trajectories. Biol Psychiatry 92: 450–459.

2. Sigurdsson T (2016): Neural circuit dysfunction in schizophrenia: Insights from animal models. Neuroscience 321: 42–65.

3. van den Heuvel MP, Fornito A (2014): Brain networks in schizophrenia. Neuropsychol Rev 24: 32–48.

4. Yang GJ, Murray JD, Repovs G, Cole MW, Savic A, Glasser MF, et al. (2014): Altered global brain signal in schizophrenia. Proc Natl Acad Sci U S A 111: 7438–7443.

5. Yang GJ, Murray JD, Glasser M, Pearlson GD, Krystal JH, Schleifer C, et al. (2017): Altered Global Signal Topography in Schizophrenia. Cereb Cortex N Y N 1991 27: 5156–5169.

6. Cai M, Wang R, Liu M, Du X, Xue K, Ji Y, et al. (2022): Disrupted local functional connectivity in schizophrenia: An updated and extended meta-analysis. Schizophrenia 8: 93.

7. Baker JT, Holmes AJ, Masters GA, Yeo BTT, Krienen F, Buckner RL, Öngür D (2014): Disruption of cortical association networks in schizophrenia and psychotic bipolar disorder. JAMA Psychiatry 71: 109–118.

8. Satterthwaite TD, Vandekar SN, Wolf DH, Bassett DS, Ruparel K, Shehzad Z, et al. (2015): Connectome-Wide Network Analysis of Youth with Psychosis Spectrum Symptoms. Mol Psychiatry 20: 1508–1515.

9. Voineskos AN, Hawco C, Neufeld NH, Turner JA, Ameis SH, Anticevic A, et al. (2024): Functional magnetic resonance imaging in schizophrenia: current evidence, methodological advances, limitations and future directions. World Psychiatry 23: 26–51.

10. Trubetskoy V, Pardiñas AF, Qi T, Panagiotaropoulou G, Awasthi S, Bigdeli TB, et al. (2022): Mapping genomic loci implicates genes and synaptic biology in schizophrenia [no. 7906]. Nature 604: 502–508.

11. Singh T, Poterba T, Curtis D, Akil H, Al Eissa M, Barchas JD, et al. (2022): Rare coding variants in ten genes confer substantial risk for schizophrenia. Nature 604: 509–516.

12. McDonald-McGinn DM, Sullivan KE, Marino B, Philip N, Swillen A, Vorstman JAS, et al. (2015): 22q11.2 deletion syndrome. Nat Rev Dis Primer 1: 15071.

13. Provenzani U, Damiani S, Bersano I, Singh S, Moschillo A, Accinni T, et al. (2022): Prevalence and incidence of psychotic disorders in 22q11.2 deletion syndrome: a meta-analysis. Int Rev Psychiatry Abingdon Engl 34: 676–688.

14. Schneider M, Debbané M, Bassett AS, Chow EWC, Fung WLA, van den Bree M, et al. (2014): Psychiatric disorders from childhood to adulthood in 22q11.2 deletion syndrome: results from the International Consortium on Brain and Behavior in 22q11.2 Deletion Syndrome. Am J Psychiatry 171: 627–639.

15. Gur RE, McDonald-McGinn DM, Moore TM, Gallagher RS, McClellan E, White L, et al. (2023): Psychosis spectrum features, neurocognition and functioning in a longitudinal study of youth with 22q11.2 deletion syndrome. Psychol Med 53: 1–10.

16. Tang SX, Gur RE (2018): Longitudinal perspectives on the psychosis spectrum in 22q11.2 deletion syndrome. Am J Med Genet A 176: 2192–2202.

17. Jalbrzikowski M (n.d.): Longitudinal trajectories of cortical development in 22q11.2 copy number variants and typically developing controls. Mol Psychiatry 10.

18. Chawner SJRA, Doherty JL, Anney RJL, Antshel KM, Bearden CE, Bernier R, et al. (2021): A Genetics-First Approach to Dissecting the Heterogeneity of Autism: Phenotypic Comparison of Autism Risk Copy Number Variants. Am J Psychiatry 178: 77–86.

19. Moreau CA, Ching CR, Kumar K, Jacquemont S, Bearden CE (2021): Structural and functional brain alterations revealed by neuroimaging in CNV carriers. Curr Opin Genet Dev 68: 88–98.

20. Fusar-Poli P, Borgwardt S, Bechdolf A, Addington J, Riecher-Rössler A, Schultze-Lutter F, et al. (2013): The psychosis high-risk state: a comprehensive state-of-the-art review. JAMA Psychiatry 70: 107–120.

21. Fusar-Poli P, Salazar de Pablo G, Correll CU, Meyer-Lindenberg A, Millan MJ, Borgwardt S, et al. (2020): Prevention of Psychosis: Advances in Detection, Prognosis, and Intervention. JAMA Psychiatry 77: 755–765.

22. Luna LP, Radua J, Fortea L, Sugranyes G, Fortea A, Fusar-Poli P, et al. (2022): A systematic review and meta-analysis of structural and functional brain alterations in individuals with genetic and clinical high-risk for psychosis and bipolar disorder. Prog Neuropsychopharmacol Biol Psychiatry 117: 110540.

23. Scarpazza C, Lattanzi GM, Antoniades M, Di Fabio F, Sartori G, Eickhoff SB, et al. (2019): Systematic review and multi-modal meta-analysis of magnetic resonance imaging findings in 22q11.2 deletion syndrome: Is more evidence needed? Neurosci Biobehav Rev 107: 143–153.

24. Schreiner M, Forsyth JK, Karlsgodt KH, Anderson AE, Hirsh N, Kushan L, et al. (2017): Intrinsic Connectivity Network-Based Classification and Detection of Psychotic Symptoms in Youth With 22q11.2 Deletions. Cereb Cortex N Y N 1991 27: 3294–3306.

25. Cole MW, Anticevic A, Repovs G, Barch D (2011): Variable Global Dysconnectivity and Individual Differences in Schizophrenia. Biol Psychiatry 70: 43–50.

26. Cao H, Chung Y, McEwen SC, Bearden CE, Addington J, Goodyear B, et al. (2020): Progressive reconfiguration of resting-state brain networks as psychosis develops: Preliminary results from the North American Prodrome Longitudinal Study (NAPLS) consortium. Schizophr Res 226: 30–37.

27. Ji L, Meda SA, Tamminga CA, Clementz BA, Keshavan MS, Sweeney JA, et al. (2020): Characterizing functional regional homogeneity (ReHo) as a B-SNIP psychosis biomarker using traditional and machine learning approaches. Schizophr Res 215: 430–438.

28. Fang X, Zhang R, Bao C, Zhou M, Yan W, Lu S, et al. (2021): Abnormal regional homogeneity (ReHo) and fractional amplitude of low frequency fluctuations (fALFF) in first-episode drug-naïve schizophrenia patients comorbid with depression. Brain Imaging Behav 15: 2627–2636.

29. Ma X, Zheng W, Li C, Li Z, Tang J, Yuan L, et al. (2019): Decreased regional homogeneity and increased functional connectivity of default network correlated with neurocognitive deficits in subjects with genetic high-risk for schizophrenia: A resting-state fMRI study. Psychiatry Res 281: 112603.

30. Kannurpatti SS, Biswal BB (2008): Detection and scaling of task-induced fMRI-BOLD response using resting state fluctuations. NeuroImage 40: 1567–1574.

31. Anderson KM, Collins MA, Chin R, Ge T, Rosenberg MD, Holmes AJ (2020): Transcriptional and imaging-genetic association of cortical interneurons, brain function, and schizophrenia risk. Nat Commun 11: 2889.

32. Hawrylycz M, Miller JA, Menon V, Feng D, Dolbeare T, Guillozet-Bongaarts AL, et al. (2015): Canonical genetic signatures of the adult human brain [no. 12]. Nat Neurosci 18: 1832–1844.

33. Burt JB, Helmer M, Shinn M, Anticevic A, Murray JD (2020): Generative modeling of brain maps with spatial autocorrelation. NeuroImage 220: 117038.

34. Markello RD, Arnatkeviciute A, Poline J-B, Fulcher BD, Fornito A, Misic B (2021): Standardizing workflows in imaging transcriptomics with the abagen toolbox ((S. Jbabdi, T. R. Makin, S. Jbabdi, J. Burt, & M. J. Hawrylycz, editors)). eLife 10: e72129.

35. Markello RD, Hansen JY, Liu Z-Q, Bazinet V, Shafiei G, Suárez LE, et al. (2022): neuromaps: structural and functional interpretation of brain maps [no. 11]. Nat Methods 19: 1472–1479.

36. Addington J, Cadenhead KS, Cornblatt BA, Mathalon DH, McGlashan TH, Perkins DO, et al. (2012): North American Prodrome Longitudinal Study (NAPLS 2): overview and recruitment. Schizophr Res 142: 77–82.

37. Noble S, Scheinost D, Finn ES, Shen X, Papademetris X, McEwen SC, et al. (2017): Multisite Reliability of MR-Based Functional Connectivity. NeuroImage 146: 959–970.

38. McGlashan T, Walsh B, Woods S (2010): The Psychosis-Risk Syndrome: Handbook for Diagnosis and Follow-Up. Oxford University Press, USA.

39. Schleifer CH, O'Hora KP, Jalbrzikowski M, Bondy E, Kushan-Wells L, Lin A, et al. (2023): Longitudinal development of thalamocortical functional connectivity in 22q11.2 deletion syndrome. Biol Psychiatry Cogn Neurosci Neuroimaging. https://doi.org/10.1016/j.bpsc.2023.09.001

40. Schleifer C, Lin A, Kushan L, Ji JL, Yang G, Bearden CE, Anticevic A (2019): Dissociable Disruptions in Thalamic and Hippocampal Resting-State Functional Connectivity in Youth with 22q11.2 Deletions. J Neurosci Off J Soc Neurosci 39: 1301–1319.

41. Ji JL, Demšar J, Fonteneau C, Tamayo Z, Pan L, Kraljič A, et al. (2023): QuNex—An integrative platform for reproducible neuroimaging analytics. Front Neuroinformatics 17. Retrieved May 23, 2023, from https://www.frontiersin.org/articles/10.3389/fninf.2023.1104508

42. Glasser MF, Sotiropoulos SN, Wilson JA, Coalson TS, Fischl B, Andersson JL, et al. (2013): The Minimal Preprocessing Pipelines for the Human Connectome Project. NeuroImage 80: 105–124.

43. Power JD, Barnes KA, Snyder AZ, Schlaggar BL, Petersen SE (2012): Spurious but systematic correlations in functional connectivity MRI networks arise from subject motion. Neuroimage 59: 2142–2154.

44. Power JD, Schlaggar BL, Petersen SE (2015): Recent progress and outstanding issues in motion correction in resting state fMRI. NeuroImage 0: 536–551.

45. Power JD, Plitt M, Laumann TO, Martin A (2017): Sources and implications of whole-brain fMRI signals in humans. NeuroImage 146: 609–625.

46. Glasser MF, Coalson TS, Robinson EC, Hacker CD, Harwell J, Yacoub E, et al. (2016): A multi-modal parcellation of human cerebral cortex. Nature 536: 171–178.

47. Pham DD, Muschelli J, Mejia AF (2022): ciftiTools: A package for reading, writing, visualizing, and manipulating CIFTI files in R. NeuroImage 250: 118877.

48. Cole MW, Pathak S, Schneider W (2010): Identifying the brain's most globally connected regions. NeuroImage 49: 3132–3148.

49. Cole MW, Anticevic A, Repovs G, Barch D (2011): Variable Global Dysconnectivity and Individual Differences in Schizophrenia. Biol Psychiatry 70: 43–50.

50. Uddin LQ, Kelly AMC, Biswal BB, Margulies DS, Shehzad Z, Shaw D, et al. (2008): Network homogeneity reveals decreased integrity of default-mode network in ADHD. J Neurosci Methods 169: 249–254.

51. Fortin J-P, Cullen N, Sheline YI, Taylor WD, Aselcioglu I, Cook PA, et al. (2018): Harmonization of cortical thickness measurements across scanners and sites. NeuroImage 167: 104–120.

52. Johnson WE, Li C, Rabinovic A (2007): Adjusting batch effects in microarray expression data using empirical Bayes methods. Biostatistics 8: 118–127.

53. Benjamini Y, Hochberg Y (1995): Controlling the False Discovery Rate: A Practical and Powerful Approach to Multiple Testing. J R Stat Soc Ser B Methodol 57: 289–300.

54. Markello RD, Arnatkeviciute A, Poline J-B, Fulcher BD, Fornito A, Misic B (2021): Standardizing workflows in imaging transcriptomics with the abagen toolbox ((S. Jbabdi, T. R. Makin, S. Jbabdi, J. Burt, & M. J. Hawrylycz, editors)). eLife 10: e72129.

55. Vaishnavi SN, Vlassenko AG, Rundle MM, Snyder AZ, Mintun MA, Raichle ME (2010): Regional aerobic glycolysis in the human brain. Proc Natl Acad Sci 107: 17757–17762.

56. Margulies DS, Ghosh SS, Goulas A, Falkiewicz M, Huntenburg JM, Langs G, et al. (2016): Situating the default-mode network along a principal gradient of macroscale cortical organization. Proc Natl Acad Sci 113: 12574–12579.

57. Mueller S, Wang D, Fox MD, Yeo BTT, Sepulcre J, Sabuncu MR, et al. (2013): Individual variability in functional connectivity architecture of the human brain. Neuron 77: 586–595.

58. Yarkoni T, Poldrack RA, Nichols TE, Van Essen DC, Wager TD (2011): Large-scale automated synthesis of human functional neuroimaging data [no. 8]. Nat Methods 8: 665–670.

59. Reardon PK, Seidlitz J, Vandekar S, Liu S, Patel R, Park MTM, et al. (2018): Normative brain size variation and brain shape diversity in humans. Science 360: 1222–1227.

60. Hill J, Inder T, Neil J, Dierker D, Harwell J, Van Essen D (2010): Similar patterns of cortical expansion during human development and evolution. Proc Natl Acad Sci 107: 13135–13140.

61. Van Essen DC, Smith SM, Barch DM, Behrens TEJ, Yacoub E, Ugurbil K (2013): The WU-Minn Human Connectome Project: An overview. NeuroImage 80: 62–79.

62. Cao H, Chén OY, Chung Y, Forsyth JK, McEwen SC, Gee DG, et al. (2018): Cerebello-thalamo-cortical hyperconnectivity as a state-independent functional neural signature for psychosis prediction and characterization. Nat Commun 9: 3836.

63. Nomi JS, Bzdok D, Li J, Bolt T, Chang C, Kornfeld S, et al. (2024): Systematic cross-sectional age-associations in global fMRI signal topography. Imaging Neurosci 2: 1–13.

64. Anticevic A, Haut K, Murray JD, Repovs G, Yang GJ, Diehl C, et al. (2015): Association of Thalamic Dysconnectivity and Conversion to Psychosis in Youth and Young Adults at Elevated Clinical Risk. JAMA Psychiatry 72: 882–891.

65. Chén OY, Cao H, Phan H, Nagels G, Reinen JM, Gou J, et al. (2021): Identifying neural signatures mediating behavioral symptoms and psychosis onset: High-dimensional whole brain functional mediation analysis. Neuroimage 226: 117508.

66. Wang C, Lee J, Ho NF, Lim JKW, Poh JS, Rekhi G, et al. (2018): Large-Scale Network Topology Reveals Heterogeneity in Individuals With at Risk Mental State for Psychosis: Findings From the Longitudinal Youth-at-Risk Study. Cereb Cortex N Y N 1991 28: 4234–4243.

67. Anticevic A, Hu X, Xiao Y, Hu J, Li F, Bi F, et al. (2015): Early-Course Unmedicated Schizophrenia Patients Exhibit Elevated Prefrontal Connectivity Associated with Longitudinal Change. J Neurosci 35: 267–286.

68. Robin NH, Taylor CJ, McDonald-McGinn DM, Zackai EH, Bingham P, Collins KJ, et al. (2006): Polymicrogyria and deletion 22q11.2 syndrome: window to the etiology of a common cortical malformation. Am J Med Genet A 140: 2416–2425.

69. von Scheibler ENMM, van der Valk Bouman ES, Nuijts MA, Bauer NJC, Berendschot TTJM, Vermeltfoort P, et al. (2022): Ocular findings in 22q11.2 deletion syndrome: A systematic literature review and results of a Dutch multicenter study. Am J Med Genet A 188: 569–578.

70. Pasternak M, Shirzadi Z, Mutsaerts HJMM, Boot E, Butcher NJ, MacIntosh BJ, et al. (2023): Elevated regional cerebral blood flow in adults with 22q11.2 deletion syndrome. World J Biol Psychiatry 24: 260–265.

71. Campbell PD, Lee I, Thyme S, Granato M (2023): Mitochondrial proteins encoded by the 22q11.2 neurodevelopmental locus regulate neural stem and progenitor cell proliferation [no. 9]. Mol Psychiatry 28: 3769–3781.

72. Devaraju P, Yu J, Eddins D, Mellado-Lagarde MM, Earls LR, Westmoreland JJ, et al. (2017): Haploinsufficiency of the 22q11.2 microdeletion gene Mrpl40 disrupts short-term synaptic plasticity and working memory through dysregulation of mitochondrial calcium. Mol Psychiatry 22: 1313–1326.

73. Li J, Ryan SK, Deboer E, Cook K, Fitzgerald S, Lachman HM, et al. (2019): Mitochondrial deficits in human iPSC-derived neurons from patients with 22q11.2 deletion syndrome and schizophrenia. Transl Psychiatry 9: 302.

74. Fernandez A, Meechan DW, Karpinski BA, Paronett EM, Bryan CA, Rutz HL, et al. (2019): Mitochondrial Dysfunction Leads to Cortical Under-connectivity and Cognitive Impairment. Neuron 102: 1127-1142.e3.

75. Cioffi S, Flore G, Martucciello S, Bilio M, Turturo MG, Illingworth E (2022): VEGFR3 modulates brain microvessel branching in a mouse model of 22q11.2 deletion syndrome. Life Sci Alliance 5: e202101308.

76. Cioffi S, Martucciello S, Fulcoli FG, Bilio M, Ferrentino R, Nusco E, Illingworth E (2014): Tbx1 regulates brain vascularization. Hum Mol Genet 23: 78–89.

77. Crockett AM, Ryan SK, Vásquez AH, Canning C, Kanyuch N, Kebir H, et al. (2021): Disruption of the blood-brain barrier in 22q11.2 deletion syndrome. Brain J Neurol 144: 1351–1360.

78. Li Y, Sun Z, Zhu H, Sun Y, Shteyman DB, Markx S, et al. (2023): Inhibition of Abl Kinase by Imatinib Can Rescue the Compromised Barrier Function of 22q11.2DS Patient-iPSC-Derived Blood-Brain Barriers. Cells 12: 422.

79. Biswal BB, Kylen JV, Hyde JS (1997): Simultaneous assessment of flow and BOLD signals in resting-state functional connectivity maps. NMR Biomed 10: 165–170.

80. Wise RG, Ide K, Poulin MJ, Tracey I (2004): Resting fluctuations in arterial carbon dioxide induce significant low frequency variations in BOLD signal. NeuroImage 21: 1652–1664.

81. Paredes I, Himmels P, Ruiz de Almodóvar C (2018): Neurovascular Communication during CNS Development. Dev Cell 45: 10–32.

82. Wälchli T, Wacker A, Frei K, Regli L, Schwab ME, Hoerstrup SP, et al. (2015): Wiring the Vascular Network with Neural Cues: A CNS Perspective. Neuron 87: 271–296.

83. Sun D, Ching CRK, Lin A, Forsyth JK, Kushan L, Vajdi A, et al. (2020): Large-scale mapping of cortical alterations in 22q11.2 deletion syndrome: Convergence with idiopathic psychosis and effects of deletion size [no. 8]. Mol Psychiatry 25: 1822–1834.

84. Padula MC, Schaer M, Scariati E, Schneider M, Van De Ville D, Debbané M, Eliez S (2015): Structural and functional connectivity in the default mode network in 22q11.2 deletion syndrome. J Neurodev Disord 7: 23.

CHAPTER THREE SUPPLEMENTAL MATERIAL

Supplemental Methods

Participants

The neuroimaging dataset contains a total of 687 participants from two multi-site studies: 164 carriers of 22qDel along with 134 matched TD controls (Control-22q), and 240 individuals with CHR for psychosis plus 149 matched TD controls (Control-CHR).

22qDel and Control-22q data were shared from two scanners at UCLA (UCLAtrio and UCLAprisma), as well as the State University of New York in Syracuse, NY, USA, Sapienza University in Rome, Italy, and King's College London Institute of Psychiatry in London, UK. See Schleifer et al., 2023 for a full description of inclusion/exclusion criteria for 22qDel participants and matched controls (1). Briefly, a history of head injury or neurological disorder was exclusionary for all participants, and controls were excluded based on a personal history or first-degree family history of a psychosis spectrum illness. See Supplementary Table S1 for participant counts and demographics by site.

CHR and Control-CHR data came from the North American Prodrome Longitudinal Study 2 (NAPLS2) (2,3), which includes eight sites in the United States and Canada. Study site details and inclusion criteria are described in Addington et al., 2012 (2). CHR status was defined by the Criteria of Psychosis-risk Syndromes based on the Structured Interview for Psychosis-Risk Syndromes (SIPS) (4). See Supplementary Table S2 for participant counts and demographics by site.

Site	Demographics	22qDel	CONTROL	p
UCLAtrio	n	51	38	
	Age, Years, Mean (SD)	17.1 (6.5)	15.1 (4.2)	0.106
	Sex, Female, n (%)	29 (56.9)	19 (50.0)	0.669
UCLAprisma	n	17	13	
	Age, Years, Mean (SD)	19.1 (8.9)	19.9 (10.4)	0.808
	Sex, Female, n (%)	9 (52.9)	11 (84.6)	0.152
SUNY	n	49	28	
	Age, Years, Mean (SD)	21.0 (2.3)	20.8 (1.5)	0.654
	Sex, Female, n (%)	21 (42.9)	13 (46.4)	0.948
Rome	n	19	21	
	Age, Years, Mean (SD)	27.4 (8.1)	27.3 (6.4)	0.970
	Sex, Female, n (%)	5 (26.3)	14 (66.7)	0.025
KCL	n	28	34	
	Age, Years, Mean (SD)	18.5 (6.6)	17.7 (6.2)	0.657
	Sex, Female, n (%)	13 (46.4)	18 (52.9)	0.799

Supplementary Table 3-S1. Participant counts and demographics for all 22qDel sites. Each set of three rows contains the counts for each group and descriptions of the mean age and proportion of female participants for a given site, with p-values for comparisons between patient and control groups based on ANOVA or chi-squared tests, respectively.

Site	Demographics	CHR	CONTROL-N	p
01	n	37	18	
	Age, Years, Mean (SD)	18.9 (4.8)	18.1 (3.6)	0.518
	Sex, Female, n (%)	11 (29.7)	7 (38.9)	0.709
02	n	43	22	
	Age, Years, Mean (SD)	21.1 (5.1)	21.1 (5.2)	0.966
	Sex, Female, n (%)	22 (51.2)	7 (31.8)	0.222
03	n	24	23	
	Age, Years, Mean (SD)	18.7 (3.4)	18.8 (4.5)	0.949
	Sex, Female, n (%)	11 (45.8)	11 (47.8)	1.000
04	n	25	24	
	Age, Years, Mean (SD)	16.0 (1.7)	17.1 (2.5)	0.102
	Sex, Female, n (%)	12 (48.0)	12 (50.0)	1.000
05	n	47	25	
	Age, Years, Mean (SD)	19.5 (2.9)	19.6 (2.9)	0.875
	Sex, Female, n (%)	19 (40.4)	12 (48.0)	0.713
06	n	19	8	
	Age, Years, Mean (SD)	19.4 (4.3)	21.8 (6.2)	0.265
	Sex, Female, n (%)	6 (31.6)	3 (37.5)	1.000
07	n	39	14	
	Age, Years, Mean (SD)	16.7 (2.7)	20.8 (5.3)	<0.001
	Sex, Female, n (%)	17 (43.6)	8 (57.1)	0.576
08	n	6	15	
	Age, Years, Mean (SD)	21.1 (5.2)	21.6 (5.0)	0.851
	Sex, Female, n (%)	1 (16.7)	10 (66.7)	0.112

Supplementary Table 3-S2. Participant counts and demographics for all NAPLS sites. Each set of three rows contains the counts for each group and descriptions of the mean age and proportion of female participants for a given site, with p-values for comparisons between patient and control groups based on ANOVA or chi-squared tests, respectively.

Neuroimaging acquisition

UCLA 22q Prisma data were collected with Human Connectome Project (HCP)-style sequences on a Siemens Prisma 3 Tesla (3T) scanner. Four-hundred-and-twenty volumes (5.6 min) of resting BOLD data were acquired in 72 interleaved slices with multiband-8 acceleration (voxel size = 2 × 2 × 2 mm, TR = 800 ms, TE = 37 ms, flip angle = 52°, FOV = 208 × 208 mm), along with single-band reference images and a pair of spin-echo field maps with phase encoding in the anterior-posterior (AP) and posterior-anterior (PA) directions. T1w MP-RAGE and T2w SPC images were collected in 208 sagittal slices (voxel size = 0.8 × 0.8 × 0.8 mm, FOV = 256 × 256 mm) with (T1w TR = 2400 ms, TE = 2.22 ms) and (T2w TR = 3200 ms, TE = 563 ms).

UCLA and KCL 22q TimTrio resting BOLD data were acquired on a Siemens TimTrio 3T scanner in 34 interleaved axial slices (voxel size = 3 × 3 × 4 mm, TR = 2000 ms, TE = 30 ms, flip angle = 90°, FOV = 192 × 192 mm). Acquisition lasted 5.1 min and produced 152 volumes. High-resolution T1w MP-RAGE images were collected in 160 sagittal slices (voxel size = 1 × 1 × 1 mm, TR = 2300 ms, TE = 2.91 ms, flip angle = 90°, FOV = 240 × 256 mm)

SUNY 22q data were collected on a Siemens TimTrio 3T scanner. BOLD data were acquired in 34 axial slices (voxel size = 4 × 4 × 4 mm, TR = 2000 ms, TE = 30 ms, flip angle = 90°, FOV = 256 × 256 mm). Acquisition lasted 5.1 min and produced 152 volumes. High-resolution T1w MP-RAGE images were collected in 176 sagittal slices (voxel size = 1 × 1 × 1 mm, TR = 2530 ms, TE = 3.31 ms, flip angle = 7°, FOV = 256 × 256 mm).

22q data from Sapienza university in Rome were collected on a Siemens MAGNETOM Verio 3T scanner. (voxel size = 4 × 4 × 3 mm, TR = 3000 ms, TE = 30 ms, flip angle = 90°). 150 BOLD volumes were acquired. High-resolution T1w MP-RAGE (voxel size = 1 × 1 × 1 mm, TR = 2300 ms, TE = 2.98 ms, flip angle = 7°, FOV = 240 × 256 mm).

Details of BOLD acquisition for the NAPLS2 CHR study are described by Noble et al 2017 (3). Briefly, all data were acquired on comparable 3T scanners from either Siemens or General Electric. BOLD data were acquired with 30 4mm axial slices with a 1mm gap (TR = 2000 MS, TE = 30ms, flip angle = 77°, FOV = 220 x 220 mm). Acquisition lasted 5 min and produced 154 volumes. High-resolution 1 x 1 x 1.2 sagittal T1w images were also collected.

Neuroimaging processing

All data from 22qDel, CHR, and TD controls were processed with the same workflow, as described in detail in previous publications (1,5). Functional and structural images were processed with the Quantitative Neuroimaging Environment and Toolbox (6) to apply a modified version of the methods developed for the Human Connectome Project (HCP) (7) as well as motion scrubbing, i.e. censoring frames with displacement or intensity change thresholds exceeding those recommended by Power et al. (8–10). Functional connectivity analyses were computed on the residual of the signal after regression of motion time series, the mean signal time series from the ventricles and deep white matter, and the first derivatives of these measures.

fMRI measures

Three rs-fMRI measures were calculated for each scan: global brain connectivity (GBC), local connectivity (LC), and brain signal variability (BSV). All three measures used the same set of 360 cortical regions defined from multi-modal MRI in 210 healthy young adults from the HCP (11). Computations were performed in R using ciftiTools to manipulate neuroimaging data (12).

GBC is a well-validated measure defined as the average functional connectivity between a given brain region and all other regions (13,14). A high GBC value indicates a region in which signal is similar to many other regions of the brain, whereas a low GBC value represents a region that is dissimilar to the majority of other regions. GBC is sensitive to functional network disruptions in disorders such as schizophrenia (15,16). Here, we calculated this measure by computing functional connectivity (FC) between each region and each of the other 359 regions, followed by averaging the FC values for each region to achieve 360 unique GBC values (one per region). FC was calculated as the Fisher Z-transformed Pearson correlation between the mean BOLD time series in each region.

LC was calculated as a measure of the cohesiveness or homogeneity of vertex-level BOLD time series within each region. This approach is based on the network homogeneity method, wherein FC is computed between each pair of voxels in a chosen region (17). This is

conceptually related to the regional homogeneity approach (18), except here homogeneity is calculated at the parcel level rather than for each voxel and its immediate neighbors. We generated a single average LC value for each of the 360 cortical regions by computing the full functional connectivity matrix between all vertices in a region and then taking the average of that.

BSV was calculated as the average temporal standard deviation of the BOLD time series in each region. This measure of variability is also referred to as resting state fluctuation amplitude.

To correct for variability related to site/scanner, we used neuroComBat (19), a neuroimaging-optimized implementation of the ComBat algorithm (20), which uses empirical Bayes methods to correct for batch/site effects with increased robustness compared to linear model approaches. Site correction was applied separately to the NAPLS2 data and the data from the multi-site 22qDel studies, and each of the three fMRI measures was corrected with a separate model. After ComBat, values for each measure were normalized within each region based on the mean and standard deviation for the relevant control group.

Group-level fMRI comparisons

For each fMRI measure, across each region, linear models were used to test the main effect of 22qDel versus matched controls (Control22q), and the main effect of CHR versus matched controls (ControlCHR). The models tested took the following form:

fMRIij ~ groupk + age + age2 + sex + site + movement

In which the fMRI measure i (GBC, LC or BSV) at region j (1 of 360) is predicted by group k (either 22qDel versus Control22q, or CHR versus ControlCHR), controlling for linear and quadratic age, sex, site, and movement (measured as the percentage of frames scrubbed from each scan). p-values were computed for the main effect of group in each model, and were adjusted for False Discovery Rate (FDR) (21) across the 360 tests within each set of analyses for a given fMRI measure and reference group. Significance was evaluated at a threshold of FDR $q < 0.05$.

Brain map comparisons

In order to assess similarity of the three fMRI measures within and between clinical groups, we used permutation methods to compare the spatial brain maps for case-control comparisons with significant group main effects. For a given pair of maps, “map A” and “map B”, the comparison was conducted as follows: compute the Pearson correlation between the left hemispheres of maps A and B across 180 regions, repeat for the right hemisphere, and average to get the mean bilateral correlation. Next, use BrainSMASH to create 10,000 surrogate brain maps per hemisphere that preserve the original spatial autocorrelation structure of map A, and generate null models by testing the correlations between map B and each of these 10,000 surrogate maps per hemisphere. Two-tailed p-values were computed as the proportion of these 20,000 null-model values with an absolute value greater than the absolute value of the true average bilateral correlation between maps A and B.

We next used the same permutation testing procedure to compare the left hemisphere cortical maps from our case-control analyses to a set of 22 left hemisphere cortical maps from previously published datasets. Maps include metabolic and physiologic data from positron emission tomography (PET), gene expression from post-mortem tissue, and various measures from magnetoencephalography (MEG), structural MRI, and functional MRI; see Table 2 for a description of each map (11,22–29). Analyses were restricted to the left hemisphere because some datasets did not include densely sampled right hemisphere data. All maps were transformed into the same left hemisphere surface-based parcellation.

For the majority of datasets, brain maps were processed with neuromaps, a toolbox containing resources for accessing, transforming, and comparing multi-modal brain datasets (30). With this toolbox, multimodal published maps were transformed into the same coordinate space and re-parcellated based on the HCP multimodal atlas (11). For each threshold-free case-control fMRI left hemisphere map (e.g. the set of 180 coefficients for the effect of 22qDel versus Control22q on BSV), correlations were tested with each of the 22 reference maps, and two-tailed

p-values were computed from 10,000 BrainSMASH permutations and were evaluated at alpha = 0.05.

Spatial maps of gene expression from densely sampled microarray data from six typical adult post-mortem donors from the Allen Human Brain Atlas (31) were resampled to the same MRI atlas using the abagen toolbox (22). Spatial maps of typical parvalbumin (PVALB) and somatostatin (SST) gene expression across the left cortical hemisphere were generated as follows: Regional microarray expression data were obtained from 6 post-mortem brains (1 female, ages 24.0--57.0, 42.50 +/- 13.38) provided by the AHBA (32,33). Data were processed with the abagen toolbox (version 0.1.3; https://github.com/rmarkello/abagen) using a 360-region surface-based atlas in MNI space. First, microarray probes were reannotated using data provided by Arnatkevičiūtė et al. 2019 (34); probes not matched to a valid Entrez ID were discarded. Next, probes were filtered based on their expression intensity relative to background noise (35), such that probes with intensity less than the background in >=50.00% of samples across donors were discarded. When multiple probes indexed the expression of the same gene, we selected and used the probe with the most consistent pattern of regional variation across donors (i.e., differential stability) (32). The MNI coordinates of tissue samples were updated to those generated via non-linear registration using the Advanced Normalization Tools (ANTs; https://github.com/chrisfilo/alleninf). Samples were assigned to brain regions by minimizing the Euclidean distance between the MNI coordinates of each sample and the nearest surface vertex. Samples where the Euclidean distance to the nearest vertex was more than 2 standard deviations above the mean distance for all samples belonging to that donor were excluded. To reduce the potential for misassignment, sample-to-region matching was constrained by hemisphere and gross structural divisions (i.e., cortex, subcortex/brainstem, and cerebellum, such that e.g., a sample in the left cortex could only be assigned to an atlas parcel in the left cortex (34)). All tissue samples not assigned to a brain region in the provided atlas were discarded. Inter-subject variation was addressed by normalizing tissue sample expression values across genes using a

robust sigmoid function (36). Normalized expression values were then rescaled to the unit interval. Gene expression values were then normalized across tissue samples using an identical procedure. Normalization was performed separately for samples in distinct structural classes (i.e., cortex, subcortex/brainstem, cerebellum). Samples assigned to the same brain region were averaged separately for each donor and then across donors, yielding a regional expression matrix. A similar procedure was used to produce the first principal component of gene expression published by Markello et al. 2021 (37) and accessed via neuromaps. A map of regional size was also generated for each of the 180 left hemisphere regions.

Supplemental Results

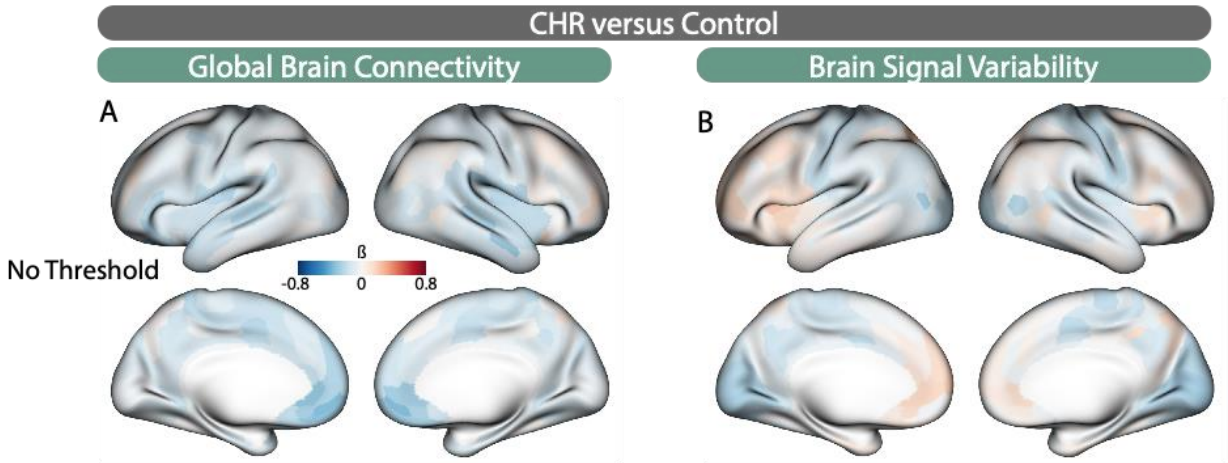

Figure 3-S1. Non-significant effects in CHR. Threshold-free maps for group difference effects (CHR vs ControlCHR) for global brain connectivity and brain signal variability. No regions were significant at False Discovery Rate (FDR) $q<0.05$.

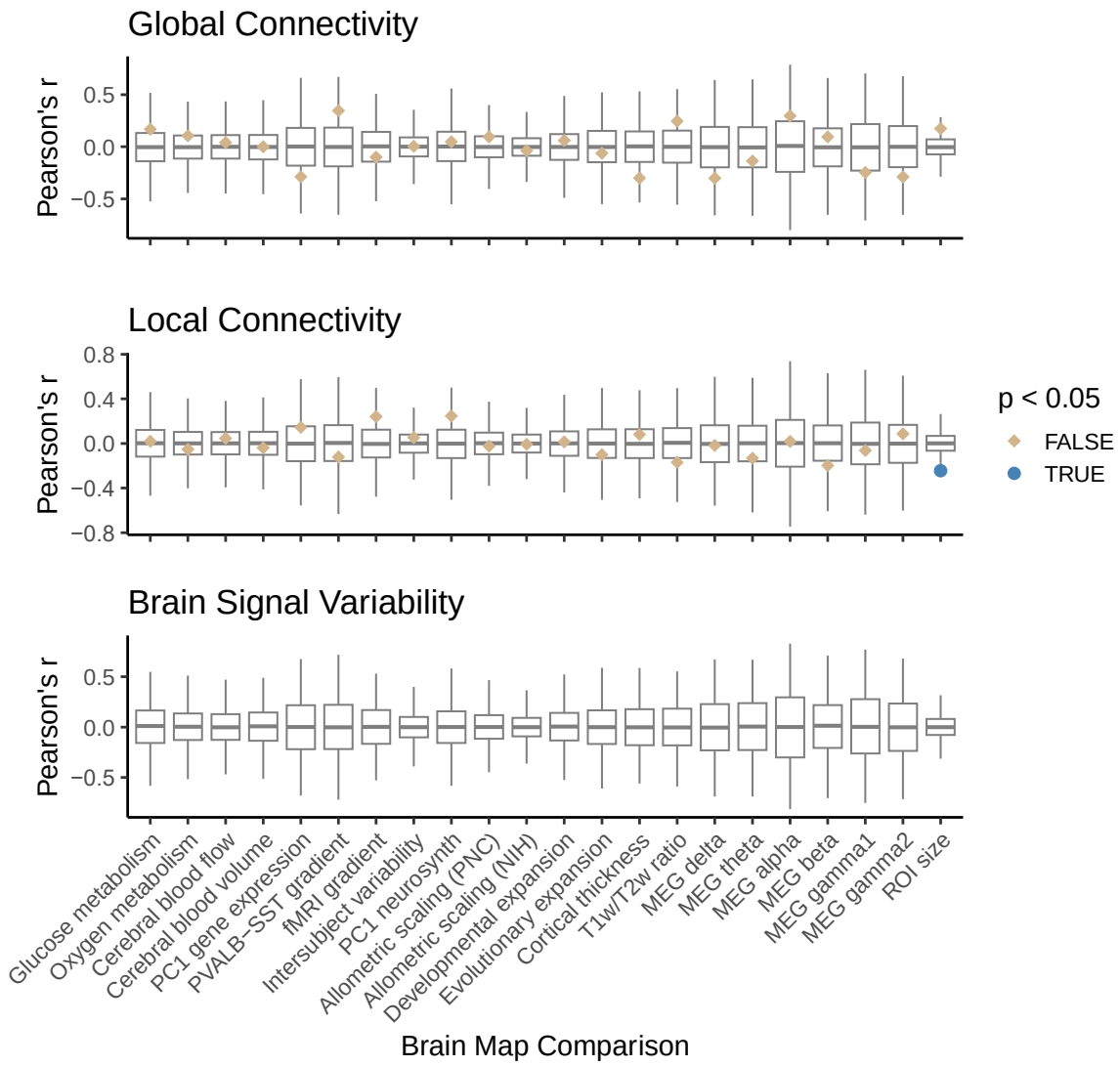

Figure 3-S2. Multi-modal brain map comparisons for CHR. Left hemisphere cortical maps from CHR case-control models were tested for spatial similarity to multiple publicly available datasets including metabolic and physiologic data from positron emission tomography (PET), gene expression from post-mortem tissue, and various measures from magnetoencephalography (MEG), structural MRI, and functional MRI. Null distributions (gray box plots) were computed from the Pearson correlations between 10,000 spatial autocorrelation-preserving permutations of the target fMRI 22qDel-control map (named in the plot title) and the second map of interest (named on the x-axis). The true correlation values between the two maps of interest are marked by tan or blue points, and two-tailed p-values are computed from the proportion of values in the null distribution whose absolute value exceeds the absolute value of the true test statistic. Relationships are visualized for all three measures but should not be interpreted for global brain connectivity or brain signal variability which do not have sufficient effect sizes for CHR vs ControlCHR comparisons.

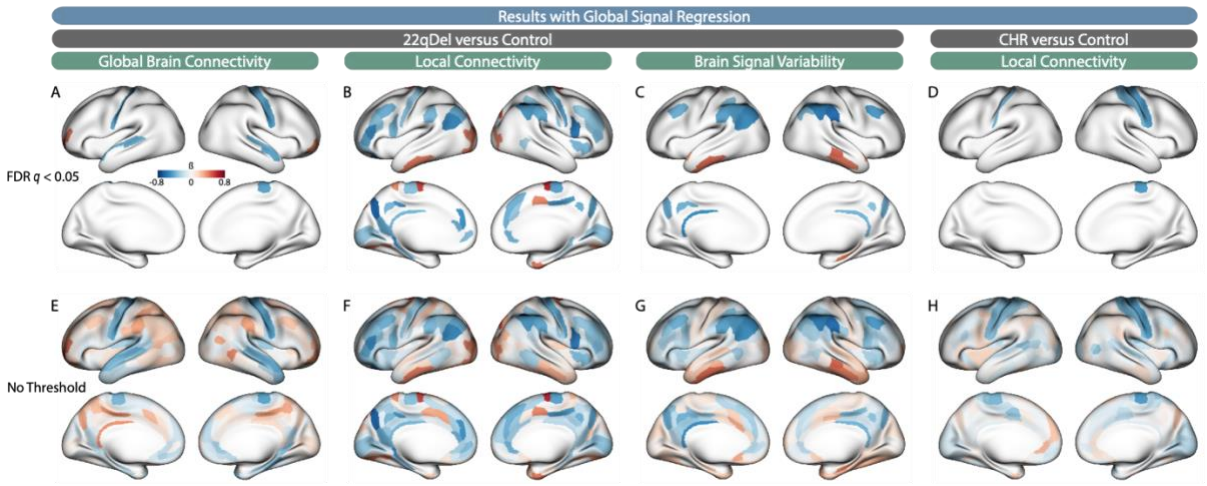

Figure 3-S3. Case-control fMRI results with Global Signal Regression (GSR). Repeat of primary analyses using input fMRI time series that have been residualized based on the average whole-brain signal as well as the average signal from the ventricles and deep white matter, motion parameters, and their first derivatives. Results are highly consistent with our primary findings without GSR.

CHAPTER THREE SUPPLEMENTAL REFERENCES

1. Schleifer CH, O'Hora KP, Jalbrzikowski M, Bondy E, Kushan-Wells L, Lin A, et al. (2023): Longitudinal development of thalamocortical functional connectivity in 22q11.2 deletion syndrome. Biol Psychiatry Cogn Neurosci Neuroimaging. https://doi.org/10.1016/j.bpsc.2023.09.001

2. Addington J, Cadenhead KS, Cornblatt BA, Mathalon DH, McGlashan TH, Perkins DO, et al. (2012): North American Prodrome Longitudinal Study (NAPLS 2): overview and recruitment. Schizophr Res 142: 77–82.

3. Noble S, Scheinost D, Finn ES, Shen X, Papademetris X, McEwen SC, et al. (2017): Multisite Reliability of MR-Based Functional Connectivity. NeuroImage 146: 959–970.

4. McGlashan T, Walsh B, Woods S (2010): The Psychosis-Risk Syndrome: Handbook for Diagnosis and Follow-Up. Oxford University Press, USA.

5. Schleifer C, Lin A, Kushan L, Ji JL, Yang G, Bearden CE, Anticevic A (2019): Dissociable Disruptions in Thalamic and Hippocampal Resting-State Functional Connectivity in Youth with 22q11.2 Deletions. J Neurosci Off J Soc Neurosci 39: 1301–1319.

6. Ji JL, Demšar J, Fonteneau C, Tamayo Z, Pan L, Kraljič A, et al. (2023): QuNex—An integrative platform for reproducible neuroimaging analytics. Front Neuroinformatics 17. Retrieved May 23, 2023, from https://www.frontiersin.org/articles/10.3389/fninf.2023.1104508

7. Glasser MF, Sotiropoulos SN, Wilson JA, Coalson TS, Fischl B, Andersson JL, et al. (2013): The Minimal Preprocessing Pipelines for the Human Connectome Project. NeuroImage 80: 105–124.

8. Power JD, Barnes KA, Snyder AZ, Schlaggar BL, Petersen SE (2012): Spurious but systematic correlations in functional connectivity MRI networks arise from subject motion. Neuroimage 59: 2142–2154.

9. Power JD, Schlaggar BL, Petersen SE (2015): Recent progress and outstanding issues in motion correction in resting state fMRI. NeuroImage 0: 536–551.

10. Power JD, Plitt M, Laumann TO, Martin A (2017): Sources and implications of whole-brain fMRI signals in humans. NeuroImage 146: 609–625.

11. Glasser MF, Coalson TS, Robinson EC, Hacker CD, Harwell J, Yacoub E, et al. (2016): A multi-modal parcellation of human cerebral cortex. Nature 536: 171–178.

12. Pham DD, Muschelli J, Mejia AF (2022): ciftiTools: A package for reading, writing, visualizing, and manipulating CIFTI files in R. NeuroImage 250: 118877.

13. Cole MW, Pathak S, Schneider W (2010): Identifying the brain's most globally connected regions. NeuroImage 49: 3132–3148.

14. Cole MW, Anticevic A, Repovs G, Barch D (2011): Variable Global Dysconnectivity and Individual Differences in Schizophrenia. Biol Psychiatry 70: 43–50.

15. Voineskos AN, Hawco C, Neufeld NH, Turner JA, Ameis SH, Anticevic A, et al. (2024): Functional magnetic resonance imaging in schizophrenia: current evidence, methodological advances, limitations and future directions. World Psychiatry 23: 26–51.

16. Cole MW, Anticevic A, Repovs G, Barch D (2011): Variable Global Dysconnectivity and Individual Differences in Schizophrenia. Biol Psychiatry 70: 43–50.

17. Uddin LQ, Kelly AMC, Biswal BB, Margulies DS, Shehzad Z, Shaw D, et al. (2008): Network homogeneity reveals decreased integrity of default-mode network in ADHD. J Neurosci Methods 169: 249–254.

18. Zang Y, Jiang T, Lu Y, He Y, Tian L (2004): Regional homogeneity approach to fMRI data analysis. NeuroImage 22: 394–400.

19. Fortin J-P, Cullen N, Sheline YI, Taylor WD, Aselcioglu I, Cook PA, et al. (2018): Harmonization of cortical thickness measurements across scanners and sites. NeuroImage 167: 104–120.

20. Johnson WE, Li C, Rabinovic A (2007): Adjusting batch effects in microarray expression data using empirical Bayes methods. Biostatistics 8: 118–127.

21. Benjamini Y, Hochberg Y (1995): Controlling the False Discovery Rate: A Practical and Powerful Approach to Multiple Testing. J R Stat Soc Ser B Methodol 57: 289–300.

22. Markello RD, Arnatkeviciute A, Poline J-B, Fulcher BD, Fornito A, Misic B (2021): Standardizing workflows in imaging transcriptomics with the abagen toolbox ((S. Jbabdi, T. R. Makin, S. Jbabdi, J. Burt, & M. J. Hawrylycz, editors)). eLife 10: e72129.

23. Vaishnavi SN, Vlassenko AG, Rundle MM, Snyder AZ, Mintun MA, Raichle ME (2010): Regional aerobic glycolysis in the human brain. Proc Natl Acad Sci 107: 17757–17762.

24. Margulies DS, Ghosh SS, Goulas A, Falkiewicz M, Huntenburg JM, Langs G, et al. (2016): Situating the default-mode network along a principal gradient of macroscale cortical organization. Proc Natl Acad Sci 113: 12574–12579.

25. Mueller S, Wang D, Fox MD, Yeo BTT, Sepulcre J, Sabuncu MR, et al. (2013): Individual variability in functional connectivity architecture of the human brain. Neuron 77: 586–595.

26. Yarkoni T, Poldrack RA, Nichols TE, Van Essen DC, Wager TD (2011): Large-scale automated synthesis of human functional neuroimaging data [no. 8]. Nat Methods 8: 665–670.

27. Reardon PK, Seidlitz J, Vandekar S, Liu S, Patel R, Park MTM, et al. (2018): Normative brain size variation and brain shape diversity in humans. Science 360: 1222–1227.

28. Hill J, Inder T, Neil J, Dierker D, Harwell J, Van Essen D (2010): Similar patterns of cortical expansion during human development and evolution. Proc Natl Acad Sci 107: 13135–13140.

29. Van Essen DC, Smith SM, Barch DM, Behrens TEJ, Yacoub E, Ugurbil K (2013): The WU-Minn Human Connectome Project: An overview. NeuroImage 80: 62–79.

30. Markello RD, Hansen JY, Liu Z-Q, Bazinet V, Shafiei G, Suárez LE, et al. (2022): neuromaps: structural and functional interpretation of brain maps [no. 11]. Nat Methods 19: 1472–1479.

31. Hawrylycz MJ, Lein ES, Guillozet-Bongaarts AL, Shen EH, Ng L, Miller JA, et al. (2012): An anatomically comprehensive atlas of the adult human brain transcriptome [no. 7416]. Nature 489: 391–399.

32. Hawrylycz M, Miller JA, Menon V, Feng D, Dolbeare T, Guillozet-Bongaarts AL, et al. (2015): Canonical genetic signatures of the adult human brain [no. 12]. Nat Neurosci 18: 1832–1844.

33. Hawrylycz MJ, Lein ES, Guillozet-Bongaarts AL, Shen EH, Ng L, Miller JA, et al. (2012): An anatomically comprehensive atlas of the adult human brain transcriptome [no. 7416]. Nature 489: 391–399.

34. Arnatkeviciute A, Fulcher BD, Fornito A (2019): A practical guide to linking brain-wide gene expression and neuroimaging data. NeuroImage 189: 353–367.

35. Quackenbush J (2002): Microarray data normalization and transformation. Nat Genet 32 Suppl: 496–501.

36. Fulcher BD, Little MA, Jones NS (2013): Highly comparative time-series analysis: the empirical structure of time series and their methods. J R Soc Interface 10: 20130048.

37. Markello RD, Arnatkeviciute A, Poline J-B, Fulcher BD, Fornito A, Misic B (2021): Standardizing workflows in imaging transcriptomics with the abagen toolbox ((S. Jbabdi, T. R. Makin, S. Jbabdi, J. Burt, & M. J. Hawrylycz, editors)). eLife 10: e72129.

CONCLUSIONS

The three studies comprising this dissertation each provide a unique but related perspective on brain development in people with genetic and clinical risk factors for neurodevelopmental and psychiatric illness. Each study asked an important question and provided novel knowledge that will hopefully advance the field. Specifically, this work has shed new light on longitudinal development of thalamocortical functional connectivity in 22q11.2 Deletion Syndrome (22qDel), the effects of deletions and duplications at the 22q11.2 locus on the development of subcortical brain structure volumes, as well as differences in resting-state functional magnetic resonance imaging (rs-fMRI) phenotypes between 22qDel carriers and individuals at Clinical High Risk (CHR) for psychosis and the potential role of hemodynamic and metabolic differences underlying the observed effects of 22qDel.

In the first study, we found that maturation of functional connectivity between the thalamus and cortex is altered in 22qDel carriers, specifically with regards to somatomotor and frontoparietal brain networks. Children with 22qDel exhibited increased thalamocortical connectivity in a somatomotor network, and decreased connectivity in a frontoparietal network relative to neurotypical controls. While significant developmental changes from age 6-23 were not found in the control group across any network, 22qDel carriers showed decreases in somatomotor connectivity and increases in frontoparietal connectivity, such that the 22qDel curve intersected with the control curve in early to mid-adolescence and continued to diverge in past the controls, displaying somatomotor hypoconnectivity and mild frontoparietal hyperconnectivity in early adulthood. Thalamocortical dysconnectivity, specifically increased somatomotor and decreased frontoparietal connectivity, has been found in multiple independent studies of schizophrenia (1–4), and in CHR individuals, especially those who go on to convert to a full psychosis diagnosis (5). Our prior cross-sectional work has replicated this finding in 22qDel carriers (6); however, it was previously unknown if this phenotype was stable across the age range in 22qDel. Our new

findings suggest that children with 22qDel predominantly show this schizophrenia-associated phenotype of somatomotor thalamocortical hyperconnectivity and frontoparietal hypoconnectivity, and that this normalizes through adolescence and even potentially reverses by early adulthood. Whether this developmental change, not seen in neurotypical controls, represents compensatory normalization or pathological development remains to be clarified. Our study highlights the importance of considering maturational trajectories, and the developmental nature of this important psychosis-related biomarker.

In the second study, we expanded upon the findings of the first study and sought to understand the impacts of copy number variation at the 22q11.2 locus on subcortical brain structural phenotypes. We took advantage of a unique and novel longitudinal dataset of structural MRI in individual with 22qDel, neurotypical controls, and individuals with 22q11.2 Duplication Syndrome (22qDup) which involves a duplication of the same set of genes deleted in 22qDel. This allowed us to assess the impact of gene dosage (i.e., 22q11.2 copy number) on cross-sectional and longitudinal regional brain volumes. Prior cross-sectional work from our group in a smaller sample had shown gene dosage effects on the shapes of multiple subcortical structures (7), and recent longitudinal analyses from our group had found an overall pattern of flattened developmental curves in deletion and duplication carriers with regards to cortical thickness and surface area (8). In the current study, we found strong positive gene dosage effects on total intracranial volume (i.e., increasing volume with increasing copy number), and when controlling for total intracranial volume found positive gene dosage effects on whole hippocampal volume but not thalamus or amygdala volumes. By segmenting the thalamus, hippocampus and amygdala into smaller anatomical subregions, we were able to see that 22q11.2 gene dosage had positive effects on specific amygdala nuclei that were not appreciable at the level of the whole structure, and that bi-directional effects were present within the thalamus, with mediodorsal volumes decreasing with gene dosage and several other nuclei increasing with gene dosage. By using nonlinear models to map maturational effects across our three cohorts we were able to discern a

wide range of developmental differences between groups, most notably a flattening of the typical inverted U-shaped developmental curve for hippocampal CA2/3 volumes in 22qDel and 22qDup, and similar flattened trajectories for the amygdala. This study provided important new information on the effects of 22q11.2 genes on subcortical development and is one of the first to systematically investigate development across reciprocal copy number variants.

In the final study, we asked the important question, to what extent do rs-fMRI brain phenotypes converge between 22qDel carriers at high genetic risk for psychosis and CHR individuals with behavioral risk factors for psychosis. Never before have these two high-risk groups been systematically analyzed in the same study such that direct comparisons can be drawn between phenotypes. The most harmonious prior studies of rs-fMRI in 22qDel and CHR involved our replication in 22qDel of the finding of thalamocortical dysconnectivity previously observed in a CHR population (5,6). However, it was previously unknown to what extent other rs-fMRI measures showed similarity between these two groups. To address this, we compiled one of the largest ever multi-site samples of 22qDel and matched control rs-fMRI and processed this with state-of-the-art methods that we also applied to a large multi-site sample of CHR and matched controls from the North American Prodrome Longitudinal Study 2 (NAPLS2). From these two datasets, processed with directly comparable methods, we computed measures of long-range and local functional connectivity and brain signal variability and compared each clinical group to their respective matched controls. We were then able to directly compare these case-control brain difference maps between 22qDel and CHR using spatially informed permutation approaches to test for significant similarities in phenotypes (9). Using these same spatial permutation approaches, we also compared case control maps to a set of previously published brain maps from multiple modalities including positron emission tomography (PET) studies of neurotypical hemodynamics and metabolism, spatial patterns of cortical gene expression from the Allen Human Brain Atlas, structural and functional MRI phenotypes and magnetoencephalography (MEG) to generate hypotheses about the biological pathways underlying the observed differences

(10). We found that, overall, rs-fMRI phenotypes were broadly dissimilar in 22qDel and CHR, with 22qDel showing large scale disruptions in long-range connectivity, local connectivity, and brain signal variability, while CHR only showed disruptions in local connectivity. Comparison to established brain maps did not yield informative relationships for CHR. However, multiple relationships were found for 22qDel, most notable of which were similarities between case-control maps of local connectivity and brain signal variability with PET maps of neurotypical blood flow/volume and glucose/oxygen metabolism. Regions typically high in hemodynamic and metabolic activity in neurotypical individuals showed the strongest decreases in rs-fMRI measures in 22qDel.

All three studies in this dissertation used MRI along with advanced statistical methods to investigate the development of brain structure and function in unique cohorts that can help advance understanding of the biology underlying risk for severe neurodevelopmental and psychiatric illness. The novel findings from these studies give new insights into brain phenotypes in these important conditions and provide a foundation for future work that will continue to parse the relationships between genes, brain systems, and behaviors relevant to neuropsychiatric illness.

CONCLUSION REFERENCES

1. Anticevic A, Cole MW, Repovs G, Murray JD, Brumbaugh MS, Winkler AM, *et al.* (2014): Characterizing Thalamo-Cortical Disturbances in Schizophrenia and Bipolar Illness. *Cereb Cortex N Y NY* 24: 3116–3130.
2. Woodward ND, Karbasforoushan H, Heckers S (2012): Thalamocortical Dysconnectivity in Schizophrenia. *Am J Psychiatry* 169: 1092–1099.
3. Welsh RC, Chen AC, Taylor SF (2010): Low-frequency BOLD fluctuations demonstrate altered thalamocortical connectivity in schizophrenia. *Schizophr Bull* 36: 713–722.
4. Giraldo-Chica M, Woodward ND (2017): Review of thalamocortical resting-state fMRI studies in schizophrenia. *Schizophr Res* 180: 58–63.
5. Anticevic A, Haut K, Murray JD, Repovs G, Yang GJ, Diehl C, *et al.* (2015): Association of Thalamic Dysconnectivity and Conversion to Psychosis in Youth and Young Adults at Elevated Clinical Risk. *JAMA Psychiatry* 72: 882–891.
6. Schleifer C, Lin A, Kushan L, Ji JL, Yang G, Bearden CE, Anticevic A (2019): Dissociable Disruptions in Thalamic and Hippocampal Resting-State Functional Connectivity in Youth with 22q11.2 Deletions. *J Neurosci* 39: 1301–1319.
7. Lin A, Ching CRK, Vajdi A, Sun D, Jonas RK, Jalbrzikowski M, *et al.* (2017): Mapping 22q11.2 Gene Dosage Effects on Brain Morphometry. *J Neurosci* 37: 6183–6199.
8. Jalbrzikowski M (n.d.): Longitudinal trajectories of cortical development in 22q11.2 copy number variants and typically developing controls. *Mol Psychiatry* 10.
9. Burt JB, Helmer M, Shinn M, Anticevic A, Murray JD (2020): Generative modeling of brain maps with spatial autocorrelation. *NeuroImage* 220: 117038.
10. Markello RD, Hansen JY, Liu Z-Q, Bazinet V, Shafiei G, Suárez LE, *et al.* (2022): neuromaps: structural and functional interpretation of brain maps [no. 11]. *Nat Methods* 19: 1472–1479.